Size Characterisation of Liposomes Using Asymmetrical Flow Field-Flow Fractionation

Factors Influencing Fractionation and Size Determination

Stefan Hupfeld

A dissertation for the degree of Philosophiae Doctor

UNIVERSITY OF TROMSØ
Faculty of Medicine
Department of Pharmacy

August 2009

A dissertation for the degree of Philosophiae Doctor

Size Characterisation of Liposomes Using Asymmetrical Flow Field-Flow Fractionation

Factors Influencing Fractionation and Size Determination

Stefan Hupfeld

Tromsø 2009

Pharmaceutics and Biopharmaceutics
Department of Pharmacy
University of Tromsø
Norway

ISBN: 978-82-7589-242-1

To the memory of my mother
And to my family

"If you trust in yourself ... and believe in your dreams ... and follow your star ... you'll still get beaten by people who spent their time working hard and learning things and weren't so lazy."

From "*The Wee Free Men*", Terry Pratchett

TABLE OF CONTENTS

ABSTRACT

Liposomes play an important role in medical and pharmaceutical science as e.g. nanoscale drug carriers. One of their most important features is their size and size distribution, influencing both their biodistribution and passive targeting abilities upon intravenous administration. To this day there is no single method for size characterisation of liposomes that fulfils all following criteria: being fast and easy to perform, covering the whole size range of liposomes from tens of nanometers up to tens of micrometers as well as determining size distributions rather than mean sizes in a non-destructive manner.

In this thesis a method for size characterisation of liposomes by asymmetrical flow field-flow fractionation coupled online with multi-angle light scattering (AF4-MALS) was established. Key factors influencing the fractionation behaviour of various liposome samples such as cross flow rate, focus flow rate, sample load, ionic strength of the carrier liquid and membrane effects were identified and characterised. Finally, size distributions obtained by AF4-MALS were compared to mean particle sizes and size distribution measured with other standard methods such as photon correlation spectroscopy (PCS), size exclusion chromatography in combination with PCS (SEC-PCS) and cryogenetic transmission electron microscopy.

Satisfactory fractionation of liposomes within reasonable experiment time was obtained by the use of programmed cross flow gradients. Both sample load mass and ionic strength of the carrier liquid were shown to extensively influence the elution behaviour of liposomes and may cause overloading of the channel for extreme values. Further, it was demonstrated that ionic strength of the carrier solution different to the ionic strength of the medium used during liposome preparation may change the vesicles in terms of osmotic shrinking/swelling during an AF4 run. The limit of detection was improved by the use of stained liposomes and for fitting of MALS data, the coated sphere model was found to describe liposomes best in terms of quality of fit.

The suitability of AF4-MALS for the size characterisation of liposomes was proven. Size characterization by AF4-MALS gave similar size distributions as the other standard methods tested, yet it was performed in less time and gave a better insight into the whole size distribution of the liposome samples used in this study.

ABBREVIATIONS

A_2	Second virial coefficient
AF4	Asymmetrical flow field-flow fractionation
BSA	Bovine serum albumine
Cryo-TEM	Cryogenic transmission electron microscopy
dn/dc	Differential index of refraction
dRI	Differential refractive index
Egg-PC	Egg-phosphatidylcholine
FFF	Field-flow fractionation
LOD	Limit of detection
LUV	Large unilamellar vesicles
MALS	Multi-angle light scattering
MLV	Multilamellar vesicles
PCS	Photon correlation spectroscopy
PEEK	Poly(ether-ether-ketone)
QELS	Quasi-elastic light scattering
RC	Regenerated cellulose
r_g	Radius of gyration
r_H	Hydrodynamic radius
Rh-PE	18:1 Lissamine Rhodamine phosphoethanoleamine
rms	Root mean square
SdFFF	Sedimentation field-flow fractionation
SEC	Size-exclusion chromatography
SUV	Small unilamellar vesicles
UV-VIS	Ultraviolet-visible spectroscopy
Vc	Channel flow
Vf	Focus flow
Vx	Cross flow

LIST OF PUBLICATIONS

The present thesis is based on the following publications, which are included in the appendix and referred to in the text by the given numeration.

Publication 1

Hupfeld S., Holsæter A. M., Skar M., Frantzen C. B. & Brandl M. (2006) Liposome size analysis by dynamic/static light scattering upon size exclusion-/field flow-fractionation. *Journal of Nanoscience and Nanotechnology*, 6, 3025 – 3031.

Publication 2

Hupfeld S., Ausbacher D. & Brandl M. (2009) Asymmetric flow field-flow fractionation of liposomes: optimization of fractionation variables. *Journal of Separation Science*, 32, 1465 – 1470.

Publication 3

Hupfeld S., Ausbacher D. & Brandl M. (2009) Asymmetric flow field-flow fractionation of liposomes: 2. concentration-detection and adsorptive loss phenomena, *Journal of Separation Science*, in press.

Publication 4

Hupfeld S., Moen H. H., Ausbacher D., Haas H. & Brandl M. (2009) Liposome fractionation and size analysis by asymmetrical flow field-flow fractionation/multi-angle light scattering: influence of ionic strength and osmotic pressure of the carrier liquid, submitted manuscript.

1 INTRODUCTION

1.1 Liposomes

Liposomes or phospholipid vesicles are composed of one or several phospholipid bilayers surrounding an aqueous core (Bangham et al., 1965). They form spontaneously upon contact of phospholipids with aqueous medium and mechanical agitation. Liposome sizes may range from about tens of nanometers to tens of micrometers for giant uni- and oligolamellar liposomes (New, 1990). It is a common practice to roughly categorise them according to particle size and lamellarity into small unilamellar vesicles (SUV) up to 100 nm, large unilamellar vesicles (LUV) between 100 and 800 nm and multilamellar vesicles (MLV) (Woodle and Papahadjopoulos, 1989). There is a variety of preparation techniques that results in liposomes of different sizes and lamellarity. Dispersions of MLVs can be obtained from the rehydration of lipid films. Starting from MLV dispersions SUVs can be prepared by e.g. sonication of the dispersion (Papahadjopoulos and Watkins, 1967), extrusion through membrane filters by high pressure (Olson et al., 1979, Hope et al., 1985) or by high pressure homogenisation (Mayhew et al., 1987). LUVs can be prepared by e.g. detergent removal techniques from mixed micelles (Milsmann et al., 1978) and LUVs and MLVs can be obtained from reverse-phase evaporation (Szoka and Papahadjopoulos, 1978).

Liposomes can both encapsulate hydrophilic compounds in their core and incorporate amphiphilic or lipophilic compounds in their bilayer membrane (Gregoriadis, 1978). Due to their membrane-like structure liposomes are well tolerated and have the advantage of being bio-degradable. Through the choice of phospholipid composition or additives to the bilayer membrane such as cholesterol, charged or ligand-carrying phospholipids, the versatility of liposomes can further be increased by e.g. liposomes with charged surfaces or long circulating pegylated liposomes. During the last decades liposomes have gained increasing interest as drug carriers (Gregoriadis, 1978, Lasic, 1993) and a number of liposomal formulations are under FDA approved clinical studies or have been approved such as AmBisome® (amphothericin B), Doxil®/Caelyx® (doxorubicin) and DaunoXome® (daunorubicin).

1.2 Importance of particle size characterisation of liposomes

1.2.1 Physical aspects

The particle size is one of the key issues during the manufacturing process of liposomes. It gives important information about the control of the preparation technique and can be utilised for process optimisation. Particle size measurement is performed on routine base for batch to batch comparison and plays an important role in scaling-up processes. During storage of liposome dispersions the control over particle size is an important variable in terms of physical stability. Very small liposomes (smaller than 40 nm) are prone to fusion processes due to the high curvature of their bilayer membrane (New, 1990). For larger, electro-neutral liposomes aggregation through van der Waals forces due to the greater area of membrane contact is described (New, 1990). Particle size influences the ability of liposomes to incorporate/encapsulate drug compounds. Whereas for lipophilic and amphiphilic compounds a high lipid to core ratio, namely SUVs or MLVs is preferred, a bigger aqueous core volume, as for LUVs, is desired for the encapsulation of hydrophilic compounds.

1.2.2 Physiological aspects for liposomes used as drug carriers

Formulation of chemotherapeutic agents in form of liposomes is one of the main applications of liposomes as drug carriers. The advantages of this type of formulation are: the agents are better protected from metabolism and degradation during circulation in the blood stream, formulation of poorly-soluble agents is enabled and administration of higher doses of less toxic formulation is possible (Mayer et al., 1989). The volume of distribution for the application of free chemotherapeutic agents often is very large. Formulation of the agents in liposomal drug carriers reduces the volume of distribution drastically and higher concentrations at the site of action can be achieved (Allen and Stuart, 1999). For liposomes without surface modifications the circulation time in the blood stream is limited by uptake through the reticuloendothelial system (RES). It has been shown that small liposomes (smaller than 70 nm) are taken up from the blood stream by liver parenchymal cells while large liposomes (larger than 300 nm) accumulate in the spleen. An optimum size range of 70 to 200 nm has been identified to give highest blood concentration of ganglioside GM_1-containing liposomes in mice (Liu et al., 1992, Abra and Hunt, 1981). In another study it was demonstrated that biodistribution of liposomes depends not only on the mean particle size but also on the size distribution. Of two liposome samples with nearly identical mean diameters the more heterogeneous sam-

ple shows less distribution to the RES because of a larger fraction of small liposomes (Liu and Huang, 1992).

The endothelium of most healthy tissues represents a size selective barrier with tight junctions being impermeable to particles larger than 1.8 to 2 nm (Seymour, 1992). In tumours the microvascular permeability is increased drastically for larger particles. A cut-off size between 400 and 600 nm has been found for liposomes penetrating through tumour vessels (Yuan et al., 1995). The combination of a leaky endothelium for tumour vessels and no lymphatic clearance, the so called enhanced permeation and retention (EPR) effect, have been found to be responsible for the accumulation of large macromolecules in tumour tissue (Matsumura and Maeda, 1986). Thus for small liposomes passive targeting of liposomal drug carriers into tumours can be achieved and higher doses can be administered with less systemic toxic effects.

1.3 Methods for size characterisation of liposomes

1.3.1 Limitations of commonly used methods

Techniques used for the size characterisation of liposomes comprise freeze fracture electron microscopy ffEM, negative stain electron microscopy, atomic force microscopy and size exclusion chromatography (SEC). The most direct way of size determination of particle sizes down to one nanometer is by looking at the particles via electron microscope techniques.

For analysis of liposomes by ffEM samples are first frozen quickly in order to prevent structural damage before they are fractured. The fractures are shadowed by deposition of platinum and carbon at an angle of 45 degrees before being visualised by TEM. The fracture plane usually runs through the bilayer membrane in case of small liposomes such that a correction of half the thickness of a bilayer has to be performed. For larger liposomes the problem is that the fracture plane not always runs through the liposomes at its equatorial section such that wrong particle sizes are determined. In addition large liposomes are more likely to be fractured than small liposomes so that large liposomes are overestimated in the size distribution (Egelhaaf et al., 1996).

Another TEM based technique is negative stain electron microscopy. Here, liposomes are placed on a grid and treated with a heavy metal salt solution for staining. A thin electron-dense film of stain will form around the liposomes. In the electron micrographs the liposomes will thus be visible as dark spots (New, 1990). During the

treatment with the stain flattening of the liposomes occurs and must be corrected for in the size analysis. Variability of identical samples treated in the same manner is described (New, 1990). However, for both techniques similar limitations exist as seen for cryo-TEM. Only a small fraction of the sample is investigated and particle sizes from a large number of independent pictures have to be measured. Also instruments are costly, measurements have to be performed under vacuum and sample preparation is relatively time consuming.

Atomic force microscopy (AFM) is a relatively new scanning probe microscopy technique. Mainly a method for characterisation of surfaces at the nanoscale, it can also be used for the direct measurement of liposome sizes at room temperature in both water and air (Kanno et al., 2002). The liposomes are immobilised onto very smooth surfaces and thus scanned by the AFM tip. A laser beam measures the deflection of the tip while it passes over the sample. Measurements should be performed in the so-called tapping mode in order to minimise deformation of the liposomes during measurements. AFM covers the whole range of liposome particle sizes. Sample preparation is easier than for the aforementioned electron microscope techniques, and visualisation is performed under physiological conditions. However, liposomes might be destroyed due to adhesion to the surface such that planar bilayers are formed (Edwards and Baeumner, 2006). A size-selective adsorption behaviour has been reported: small liposomes remain intact when adsorbed to the surface, while large liposomes rupture and adsorb to the surface as bilayer discs which might even fuse into each other (Reviakine and Brisson, 2000).

SEC or gel exclusion chromatography is a widespread method for size characterisation of liposomes. Particles are separated according to their hydrodynamic radii via interaction with pores in the gel. Large particles will penetrate pores to a lesser extent and elute earlier than smaller particles. For direct determination of particle sizes from retention times, size standards are required. SEC is a quick and convenient method for size characterisation of small liposomes. Liposomes above a size of approximately 300 nm, however, will elute from the column mainly unfractionated (Nozaki et al., 1982). Careful pre-saturation of the column with liposomes is required in order to prevent reduced recovery rates due to the adsorption of liposomes to the gel material which might result in wrong size distributions (Ruysschaert et al., 2005). A further bias of the size distribution can occur from large liposomes of low rigidity entering pores and thus eluting too late (Edwards and Baeumner, 2006). The need of size standards is a drawback and should be avoided by combining SEC with e.g. light scattering detectors online, or collection of fractions with subsequent size characteri-

sation, however, shear forces are exerted onto sample material in tight packed columns that are required for such combination.

1.3.2 Cryogenic transmission electron microscopy

For the sub-technique cryogenic transmission electron microscopy (Cryo-TEM) specimens are prepared without chemical treatment such as fixation, dehydration and resin embedding which can potentially cause artefacts. Samples are immersed quickly into liquid ethane at its freezing point. Due to the fast cooling rates occurring during this process the water in the sample is vitrified. Through the vitrification, supramolecular structures such as liposomes are better preserved because the rearrangement of water molecules during formation of ice crystals is mostly prevented (Vinson et al., 1991). The technique has demonstrated its suitability for the direct imaging of morphological changes of liposomes during exposure to osmotic pressure, although it only creates two-dimensional projections (Mui et al., 1993). Size determination can be performed by manual measurement of a sufficient number ($n > 500$) of liposome diameters in enlargements of the electron micrographs as described by Olsen for negative stain electron microscopy (Olson et al., 1979). Cryo-TEM gives an insight into the size distribution of the liposome sample, however, still only a small fraction of the sample is analysed. In addition cryo-TEM is a relatively costly method, the sample preparation is complex and requires a lot of experience in order to prevent artefacts or destruction of the sample.

1.3.3 Photon correlation spectroscopy

Photon correlation spectroscopy (PCS), also known as dynamic light scattering or quasi-elastic light scattering, is a widely used method for the determination of particle sizes in nano-scale. The method is based on measuring time dependent fluctuations of light scattering from a particle. These fluctuations are caused by random movements of the particle in the suspending medium as described by the Stokes-Einstein equation:

$$D_T = \frac{kT}{6\pi\eta r_H} \qquad (1)$$

where T is the absolute temperature, k is the Boltzmann constant, η is the viscosity of the suspending liquid and r_H is the hydrodynamic radius.

The scattering intensity collected at time points t is multiplied with the scattering intensity collected at time points slightly earlier $(t - t')$, resulting in the so-called

auto-correlation function C(t′). The plot of the auto-correlation function against values of t′ shows a characteristic exponential decay. The decay time constant τ is obtained from this plot and correlates directly to the translational diffusion coefficient by:

$$\frac{1}{\tau} = 2q^2 D_T \tag{2}$$

where q is the scattering vector given by:

$$q = \frac{4\pi n}{\lambda} \sin(\frac{\theta}{2}) \tag{3}$$

where n is the refractive index of the medium, λ the wavelength of the incident light, θ the scattering angle.

Mean hydrodynamic radii can thus be determined from the translational diffusion coefficient using equation 1. PCS is a fast, direct and non-invasive method for the size determination of small sample volumes of narrow size distribution. However, there are certain limitations for more heterogeneous samples. The light scattering intensity is proportional to the sixth power of the particle size in the range up to 100 nm. When small particles are measured in the presence of e.g. a few large particles the mean particle diameter, therefore, will overestimate the large particles. Also the relatively high sensitivity of PCS towards contamination with dust can be explained by this behaviour. There are different approaches for distribution analysis of polydisperse samples such as linear and quadratic fitting to the correlation function. However, such determined size distributions do not represent the real situation well and the resolution remains relatively poor.

One attempt for improving the performance of PCS analysis of liposomes is to fractionate the sample by size exclusion chromatography prior to the size determination. From the lipid concentration and particle sizes of the fractions a size distribution plot can be constructed. However, the approach is time-consuming and technically demanding.

1.3.4 Field-flow fractionation

Field-flow fractionation (FFF) is a family of separation techniques developed by Giddings in 1966 (Giddings, 1966). The sub-families have a common principle of separation. Analytes are transported through a thin channel in a laminar flow (hereafter called channel flow) with longitudinal direction. Separation takes place through the application of a field of force, applied in perpendicular direction, which

drives the analyte into different heights over the lower channel wall (hereafter called accumulation wall). A steady state concentration profile is established as given by:

$$c = c_0 e^{-\frac{x}{l}} \tag{4}$$

where c is the concentration at height x, c_0 is the maximum concentration over the accumulation wall, and the mean layer thickness l is given by the relation as:

$$l = \frac{D}{|U|} \tag{5}$$

where D is the diffusion coefficient of the analyte and U the drift velocity of the analyte towards the accumulation wall.

Due to the parabolic flow profile of the channel flow, analytes having different values of l will occupy different heights over the accumulation wall and thus be separated. It can be seen from equation 5 that both the strength and the type of the applied field and/or the diffusion coefficient influence the mean layer thickness.

A wide range of different fields exist such that analytes of various physical properties can be separated, which makes FFF to a very versatile method. Gravitational-FFF employs Earth's gravity for driving analytes into different laminae. Sedimentation-FFF uses a similar principle with the channel being arranged in a centrifuge-like manner such that particles are separated by the exertion of acceleration forces. Gradients of heat in thermal-FFF, electrical fields in electrical FFF and magnetic fields in magnetic-FFF are only a selection of further fields that can be applied. A second flow of solvent as field of force was first introduced in 1976 (Giddings et al., 1976). Flow-FFF is probably the most versatile sub-technique of the FFF-family due to its non-specific, hydrodynamic field (Kowalkowski et al., 2006). A constant evolution of the method has taken place with the development of various channel shapes and dimensions. Further presentation of the sub-families is given in reviews written about this technique, e.g. (Giddings, 1993, Colfen and Antonietti, 2000) or in the Field Flow Fractionation Handbook (Schimpf et al., 2000).

1.3.4.1 Asymmetrical flow field-flow fractionation

The sub-technique of flow-FFF introduced by Wahlund and Giddings in 1987 is called asymmetrical flow field-flow fractionation (AF4) (Wahlund and Giddings, 1987). In case of AF4 the separation channel consists of an impermeable top block and a bottom block holding a semipermeable ultrafiltration membrane (the accumu-

lation wall) on top of a porous frit (Figure 1.1). The perpendicular field is caused by restricting the channel flow at the outlet. This restriction will force portions of the carrier liquid to leave the channel through the bottom block and thus cause the cross flow.

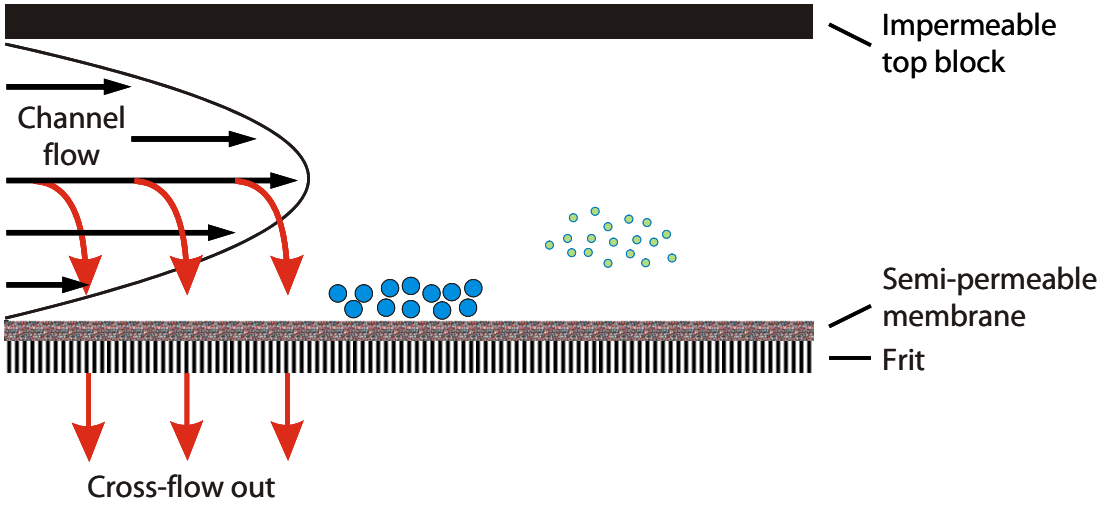

Figure 1.1: *Cross section through an AF4 channel.*

Prior to elution the analyte will be concentrated at a position close to the injection port during a focussing step. Equilibrium heights over the accumulation wall in AF4 depend on the diffusion coefficient of the analyte and the applied cross flow rate with larger particles being driven closer to the accumulation wall. Retention times are dependent on the equilibrium height at which the analyte travels in the parabolic flow profile of the channel flow and can be expressed by:

$$t_r = \frac{\pi \cdot \eta \cdot d \cdot \omega^2}{2 \cdot kT} \cdot \frac{\dot{V}_{Cross}}{\dot{V}_{Channel}} \qquad (6)$$

where t_r is the retention time of the analyte; η the viscosity; d the stokes diameter; ω the channel thickness; k the Boltzmann constant; T the absolute temperature; $\dot{V}_{Cross}$ the cross flow rate and $\dot{V}_{Channel}$ the channel flow rate.

From equation 6 the calculation of hydrodynamic diameters can be performed directly from retention times for known channel dimensions at a constant channel - to cross flow ratio. For such conditions the hydrodynamic diameters should linearly increase with retention time. In cases where cross flow gradients are used, however, the relation is not so straightforward. Furthermore, the elution behaviour of analytes

may show aberrations from the aforementioned relation, induced by e.g. electrostatic forces, non-parabolic flow or steric exclusion(Giddings, 1997). For such cases a combination with an independent method of size determination is desirable such as light scattering (Giddings, 1993, Roessner and Kulicke, 1994).

1.3.4.2 AF4 in combination with static light scattering

Static light scattering measures the intensity of scattered light at different angles around a particle causing scattering, a so-called scatterer. The detection method is called multi-angle light scattering (MALS). The MALS detector contains a flow cell surrounded by a set of 18 photo diodes that measure the intensity of scattered light at different angles. For fractionations with water as solvent, 16 out of the 18 photo cells are used at effective scattering angles between 14.44 and 163.28 degrees. Each detector measures the excess light scattering of the solution, R_θ (also called Rayleigh ratio) relative to the scattering caused by the solvent, as expressed in equation 7.

$$R_\theta = \frac{(I_\theta - I_{\theta,\,\mathrm{solvent}})r^2}{I_0 V} \tag{7}$$

where θ is the scattering angle, R_θ is the Rayleigh ratio, I_θ the scattered intensity of the analyte, $I_{\theta,\,\mathrm{solvent}}$ the scattered intensity of the solvent, I_0 intensity of the incident laser light, r the distance between the scattered volume and the photo cell, and V is the scattering volume.

With the knowledge of the Rayleigh ratio and the concentration of a scatterer a direct determination of weight average molar masses M_w and z-average mean square radius $\langle r_g^2 \rangle_z$ of solute molecules is possible by equation 8 developed by Zimm in 1948 (Zimm, 1948).

$$\frac{R_\theta}{Kc} = M_W P(q) - 2A_2 c M_W^{\,2} P^2(q) \tag{8}$$

$$\text{and } K = 4\pi^2 n_0^{\,2} (dn/dc)^2 \lambda_0^{\,-4} N_A^{\,-1} \tag{9}$$

where c is the mass concentration of the analyte; M_w the weight average molar mass; P(q) the theoretically-derived form factor; A_2 the second virial coefficient, n_0 the refractive index of the solvent, dn/dc the refractive index increment of the analyte in solvent, λ_0 the wavelength of the light and N_A Avogadro's number.

The classical way of solving the Zimm equation is constructing a plot of the scattering intensity at the different angles and at different concentrations and

extrapolating against both a scattering angle and a concentration of zero. From the resulting extrapolation one can determine the molar mass M, the second virial coefficient A_2 and the root mean square radius $\langle r_g^2 \rangle_z$ from the intercept with the ordinate and the initial slopes, respectively.

The MALS detector is coupled online to the AF4 system. Software collects sets of data points (so called slices) at each second. For each of those slices the Rayleigh ratios at the different angles are calculated and thus elugrams can be constructed. In a fractionation setup like the AF4-MALS the concentration of the eluting analyte is very low and, therefore, the term A_2 in equation 8 can be neglected. There are different fit methods for deriving M_w and $\langle r_g^2 \rangle_z$ assuming arbitrary particle shapes. For the Zimm fit method a plot of $K \cdot c \cdot R_\theta^{-1}$ on the ordinate vs. $\sin^2(\theta/2)$ on the abscissa is constructed and by polynomial fitting M_w and $\langle r_g^2 \rangle_z$ can be determined. The Zimm fit method works best for radii smaller than 50 nm. For the Debye fit method a plot from the inverse of the ordinate of Zimm fit method ($R_\theta \cdot K^{-1} \cdot c^{-1}$) vs. $\sin^2(\theta/2)$ is constructed (Debye, 1947). This method suits for a wider range of particle sizes (~100 nm). For the Berry fit method the square root of the ordinate of the Zimm fit method $K^{0.5} \cdot c^{0.5} \cdot R_\theta^{-0.5}$ is plotted against $\sin^2(\theta/2)$ (Berry, 1966). The Berry fit method is mainly used for large molecules larger than 50 nm. In case of successful separation it is assumed that each slice of the eluting sample contains molecules of very narrow distribution of molecular weight. The z-average weighted mean square radius can be calculated over the whole peak from equation 10 (Wyatt, 1993):

$$\left\langle r^2 \right\rangle_z = \frac{\sum \left\langle r_g^2 \right\rangle_t c_t M_t}{\sum c_t M_t} \tag{10}$$

where $\langle r^2 \rangle_z$ is the z-average weighted mean square radius and c_t, M_t and $\langle r_g^2 \rangle_t$ are the concentration, molar mass and mean square radii for the t^{th} slice, respectively.

Instead of polynomial fitting particle sizes can also be derived using a theoretical form factor P(q) that describes the angular dependence of the scattered light from the shape of the eluting particles. For polystyrene latex standards it was shown that using a sphere model as form factor led to smaller errors than the traditional polynomial fitting (Shortt et al., 1996). For the liposomes in our study we tried to apply the form factor of a hollow sphere that was found to describe light scattering of vesicles well (Pecora and Aragon, 1974, van Zanten, 1996).

The hollow sphere model is defined by:

$$P(q) = \left[\frac{3}{q^3 (r_o^3 - r_i^3)} (\sin qr_o - qr_o \cos qr_o - \sin qr_i + qr_i \cos qr_i) \right]^2 \quad (11)$$

$$\text{where } q = |q| = \frac{4\pi n_s}{\lambda_0} \sin(\frac{\theta}{2}) \quad (12)$$

where q is the scattering vector, n_s the refractive index of the suspending medium, λ_0 the in-vacuo wavelength, r_o the outer radius and r_i the inner radius.

When the hollow sphere model is used, the coating thickness and the core and coating refractive indices are to be specified. The resulting radius when using the hollow sphere model is a geometric radius. The relation between rms-radii (or radii of gyration) and geometric radii for coated/hollow spheres is given by equation 13 (van Zanten and Monbouquette, 1991).

$$r_g^2 = \frac{3}{5} r_o^2 \frac{1 - (\frac{r_i}{r_o})^5}{1 - (\frac{r_i}{r_o})^3} \quad (13)$$

where r_g is the radius of gyration, and r_i and r_o the inner and outer radius, respectively.

1.3.5 Why size characterisation of liposomes by AF4-MALS?

No single method for size characterisation of liposomes is capable of determining size distributions in an accurate and reliable manner alone. Besides electron microscopy, none of the methods covers the whole range of liposome particle sizes from 10 nm up to several micrometers (Woodle and Papahadjopoulos, 1989). AF4-MALS has experienced its commercial breakthrough during the last decade. User-friendly, fully-automated systems can be purchased from different vendors and the separation range from a few nanometers up to micrometers covers most of the size spectrum of liposomes. According to producers it is a robust and easy to use method which exerts less shear forces onto the analyte than e.g. SEC. In combination with MALS absolute particle size distributions can be plotted without the use of standards. AF4 has shown its applicability for the analysis of e.g. proteins (Litzen and Wahlund, 1989, Wahlund and Litzen, 1989, Yohannes et al., 2006b), plasmids (Wahlund and Litzen, 1989), polysaccharides (Wahlund and Litzen, 1989, Wittgren and Wahlund, 1997b), viruses (Litzen and Wahlund, 1989, Litzen and Wahlund, 1991b, Litzen and

Wahlund, 1991a), virus-like particles (Wei et al., 2007, Chuan et al., 2008) and cells (Wahlund and Litzen, 1989, Lee et al., 2003a) and has shown the potential of being a standard analytical tool for the measurement of liposomes (Arifin and Palmer, 2003, Yohannes et al., 2006a, Setala Niko et al., 2007).

The method is expected to be fast, requires small sample volumes and has a high fractionation power (Colfen and Antonietti, 2000). It gives an insight into the size distribution rather than mean particle sizes of a liposome sample. However, the number of publications about AF4-MALS of liposomes is limited compared to other applications and the technique has still not found wide-spread use. AF4 of nanoparticles is governed by a number of interdependent parameters rendering method-development a rather complex task. There are several potential sources of errors influencing retention times such as steric exclusion, van der Waals and electrostatic forces among analyte and between analyte and accumulation wall or errors in the measurement of experimental parameters (Giddings, 1997), which are not expressed in the standard equation of retention time. The following thesis describes a practical approach for the method development for AF4 of liposomes.

2 AIMS OF THE THESIS

The aims of this thesis were to establish a working and reproducible method for size characterisation of liposomes by AF4-MALS.

More specific aims have been:

- To identify and characterise the primary factors governing the fractionation and size determination of liposomes by AF4-MALS.
- To investigate the performance of the instrumental setup such as adsorption of sample to the separation channel, detector sensitivity and accuracy of different methods for analysing MALS data.
- To compare the results from AF4-MALS with other, well-established methods of size determination of liposomes in terms of resulting size and size distribution as well as to define limitations of the chosen methods.

3 MATERIALS AND METHODS

3.1 Materials

Egg-phosphatidylcholine (Lipoid E80®) was a kind gift of Lipoid (Lipoid GmbH Ludwigshafen, Germany). Soy-phosphatidylcholine liposomes produced by detergent removal using soy-phosphatidylcholine (Lipoid S75®) were provided by the Department of Pharmaceutical Technology, University of Freiburg. Lissamine Rhodamine PE (1,2-dioleoyl-*sn*-glycero-3-phosphoethanolamine-N-(lissamine rhodamine B sulfonyl)) (ammonium salt) (Rh-PE) was purchased from Avanti Polar Lipids (Avanti Polar Lipids, Alabaster, AL, USA). Sudan Red G (reagent for Ph. Eur.) and bovine serum albumine (BSA) (lyophilised powder, ~98%) was purchased from Fluka (Sigma-Aldrich Chemie GmbH, Steinheim, Germany). Sodium nitrate ($NaNO_3$, 99.5%), sucrose ($C_{12}H_{22}O_{11}$, for biochem. Reag., Ph. Eur.), Tris-HCl ($C_4H_{12}ClNO_3$, p.a.) and Triton X-100 ($C_{14}H_{22}O(C_2H_4O)_n$, p.a.) were purchased from Merck (Merck KGaA, Darmstadt, Germany). Calcium chloride hexahydrate ($CaCl_2 \cdot 6H_2O$, p.a.) was purchased from Kebolab (Kebo lab AS, Oslo, Norway). Nanosphere size standards were purchased from Duke Scientific (Duke Scientific Corp., Palo Alto, CA, USA). All carrier liquids for AF4 runs and dilution media for PCS measurements were prepared from ultrapure water (Millipak 20 Express, Millipore S.A., Molsheim, France) and further filtrated with 0.1 µm membrane filters (Vacucap 90 filter units with 0.1 µm supor membranes, Pall Life Sciences, Ann Arbor, MI, USA). For filter extrusion polycarbonate membranes with defined pore sizes were used (Isopore membrane filters, Millipore Ireland B.V., Cork, Ireland and SPI pore filters, SPI supplies, West Chester, PA, USA). Phospholipids B enzymatic test kit was purchased from Wako Chemicals (Wako Chemicals, Neuss, Germany) and Phospholipides enzymatique PAP 150 was purchased from Biomerieux (bioMérieux sa, Marcy-l'Etoile, France). Sephacryl™ S-1000 superfine was purchased from Amersham Biosciences (Amersham Biosciences AB, Uppsala, Sweden).

3.2 Methods

3.2.1 Preparation of liposomes

3.2.1.1 Preparation of lipid dispersion

Liposomes containing dye were produced as follows: egg-PC, Rh-PE or Sudan Red in molar ratio 1:20 and 1:200 respectively were dissolved in chloroform. A thin film

was formed by removing chloroform by rotary evaporation and drying of the film at 5 kPa for additional 2 hours. Subsequently the film was rehydrated using 10 mM sodium nitrate.

Liposomes without dye (called native Liposomes for the rest of this thesis) were produced by mixing egg-PC with 10 mM sodium nitrate to a concentration of 100 $mg \cdot mL^{-1}$ and stirring the mixture by a magnet stirrer for 45 minutes at room temperature.

Some native liposome dispersions were treated with freeze thaw cycles. The dispersion was shock frozen in liquid nitrogen and completely thawed in a water bath at 50 degrees Celsius. This procedure was repeated five times.

3.2.1.2 High-pressure filter extrusion

The resulting lipid dispersions were sequentially extruded through polycarbonate membrane filters (Millipore, Billerica, USA) of decreasing pore sizes from 800 nm down to 30 nm (pore size of the final extrusion step will be specified in results and discussion chapter). Depending on the sample volume different extrusion devices were employed: for up to 1 mL a hand-driven syringe extruder (LiposoFast™, Avestin, Inc. Ottawa, ON, Canada) was used, for sample volumes between 1 and 15 mL a Lipex extruder (Lipex Biomembranes Inc., Vancouver, BC, Canada) operated at a pressure of 1 MPa was used and for larger sample volumes a custom-made high pressure filter extruder driven by a membrane pump as described by Schneider (Schneider et al., 1995) was used. The samples passed each filter pore size ten times.

3.2.1.3 High-pressure homogenisation

Lipid dispersions were homogenised using a non-continuous APV Gaulin Micron lab 40 homogeniser (APV Gaulin GmbH, Lübeck, Germany) as described in (Brandl et al., 1990). Each sample was processed ten times at a pressure of 70 MPa at room temperature. After homogenisation the liposome dispersions were autoclaved to ensure forced healing of membrane defects and fusion of small vesicles of unfavourable curvature (Tardi et al., 2001).

3.2.1.4 Detergent removal

Large single bilayer liposomes can be prepared by detergent removal from mixed micelles by dialysis (Milsmann et al., 1978). The liposomes were produced by Christian Schifter, Department of Pharmaceutical Technology, University of Freiburg (Schifter, 2008). In brief: mixed micelles were prepared by film method from mixtures

of soy-PC and *n*-Octyl-*β*-D-glucopyranoside in molar ratio 1:6. Dialysis was performed in a custom-made dialysis chamber using Diachema very high permeability membranes with a cut-off of 5 and 10 kDa (Dianorm GmbH, Munich, Germany). Dialysis was performed at a flow rate of 15 mL·min^{-1} for one hour and then at 7 mL·min^{-1} for at least 20 hours.

3.2.2 Quantification of liposomes

For the determination of recovery of AF4 experiments the accurate amount of phospholipid had to be known.

3.2.2.1 Determination of lipid concentration by enzymatic test kit

Quantification of phospholipids was performed using an enzymatic kit (Phospholipid B enzymatic colorimetric method, Wako or Phospholipides enzymatique PAP 150, biomerieux) according to the protocol developed by (Grohganz et al., 2003). The kits consist of Phospholipase D, Choline oxidase and Peroxidase which hydrolyze phospholipids to free choline, oxidise choline to betaine and hydrogen peroxide and couple hydrogen peroxide to 4-aminoantipyrine yielding a chromophore, respectively. The chromophore was then measured in a 96-well plate reader at 492 nm against standards of known amounts of egg-PC dissolved in dissolution of Tris-HCl, Triton X-100 and calcium chloride hexahydrate.

3.2.2.2 Determination of values of dn/dc and absorptivity

Online quantification of liposomes using a differential refractive index (dRI) detector requires knowledge of the refractive index increment (dn/dc) of the respective sample. The dn/dc value was determined using the same differential refractive index detector as used in the AF4 measurements (Optilab rEX, Wyatt Technology Corp., Santa Barbara, CA, USA). Distinct dilutions of liposome sample of known phosphatidylcholine content were flushed through the detector at 0.50 mL·min^{-1} using an HPLC pump and a manual injector equipped with a sample loop of 2.0 mL. The resulting differential refractive index values (measured against 10 mM sodium nitrate solution in the reference cell as blank) were measured and plotted against the concentrations of the liposome dilutions. From the steepness of the curve the value of dn/dc was derived to be 1.4636 (± 0.0001) mL·g^{-1} (n = 3).

For recovery determination from absorbance detected by UV-VIS, knowledge of the absorptivity is required. Distinct concentrations of the respective liposome dispersion were injected offline into the UV-VIS detector that is used online for AF4

experiments, absorbance was measured and from the slope of the plot of absorbance vs. concentration the absorptivity was determined. In case of Sudan Red liposomes absorbance was calculated to be 89430 $mL \cdot g^{-1} \cdot cm^{-1}$.

3.2.3 Particle size analysis

3.2.3.1 Photon correlation spectroscopy

PCS measurements were performed on Submicron Particle Sizer Model 380 (Nicomp Particle Sizing Systems, Santa Barbara, CA, USA) as described in (Ingebrigtsen and Brandl, 2002). In brief: samples were diluted with freshly filtrated medium yielding a count rate between 250 and 350 kHz and measured ten times with at least 10^6 counts to assure statistical reliability. For each individual replicate the distribution type was chosen independently as described in (Frantzen et al., 2003). Mean values of the hydrodynamic radii were calculated.

For accurate determination of particle sizes by PCS the values of viscosity and refractive index of the solvent were necessary for the experiments where aqueous media containing sucrose was used. The viscosity of the sodium nitrate/sucrose solution, determined by a capillary viscometer (Ubbelohde viscometer, capillary type 0c, Schott-Geräte GmbH, Hofheim, Germany) at 25 degrees Celsius, was 0.9898 mPa·s. The absolute refractive index determined by batch measurements in a refractive index detector (Optilab rEX, Wyatt Technology) was 1.339. Both values were checked measuring nanosphere size standards in sodium nitrate/sucrose using the determined values and comparing the resulting sizes with measurements performed with the same standards in sodium nitrate solutions.

3.2.3.2 Size exclusion chromatography

Dispersions of liposomes were fractionated by size exclusion chromatography. In a glass tube a column of approximately 23 cm height was packed with Sephacryl S-1000 Superfine. Fractionation was performed at a flow rate of approximately 1.6 $mL \cdot min^{-1}$ and took about 60 minutes for a sample volume of 2 mL liposome dispersion. Fractions were collected following the extent of turbidity. Lipid concentration of the fractions was determined by the enzyme test, size determination was performed by PCS.

3.2.3.3 Measuring of zeta potential values

Zeta potentials of liposome dispersions were measured at the Pharmaceutical Institute, University of Oslo with help by Tove Larsen. Measurements were performed on a Malvern Zetasizer 2000 (Malvern Ltd, Malvern, UK). The liposome dispersions were diluted with pure water and 5, 10, 20, and 50 mM sodium nitrate solutions in triplicates. Each dilution was measured five times.

3.2.3.4 Cryogenic transmission electron microscopy

Cryo-TEM was performed by Dr. Markus Drechsler, Macromolecular Chemistry II, University of Bayreuth, Germany as described in e.g. (Wittemann et al., 2005): a drop of the sample (2 µl) was put on an hydrophilised lacey carbon filmed copper TEM grid (Science Services GmbH, Munich, Germany), where most of the liquid was removed with blotting paper, leaving a thin film stretched over the carbon film lace. Hydrophilisation was done in a Gatan Solarus™ (Model 950) plasma cleaning system (Gatan GmbH, Munich, Germany). For the preparation at 70 degrees Celsius a semi-automatic driven custom-made environmental chamber device was used. The specimens were instantly shock-vitrified by rapid immersion into liquid ethane and cooled to approximately 90 K by liquid nitrogen in a temperature-controlled freezing unit (Zeiss Cryobox, Zeiss SMT GmbH, Oberkochen, Germany). The temperature was monitored and kept constant in the chamber during all the sample preparation steps. After freezing the specimens, the remaining ethane was removed using blotting paper. The specimen was inserted into a cryo-transfer holder (CT3500, Gatan GmbH, Munich, Germany) and transferred to a Zeiss EM922 Omega EF-TEM. Examinations were carried out at temperatures around 90 K at an acceleration voltage of 200 kV. Zero-loss filtered images (E = 0 eV) were taken under reduced dose conditions (100–1000 electrons·nm^{-2}). All images were registered digitally by a bottom-mounted CCD camera system (Ultrascan 1000, Gatan GmbH, Munich, Germany) combined and processed with a digital imaging processing system (Gatan Microscopy Suite 1.8). Enlargements of the electron micrographs were printed and diameters of the liposomes (n > 1000) were measured manually.

3.2.3.5 Asymmetrical flow field-flow fractionation

The bottom block of the 29 cm long AF4 channel (Wyatt Technology Europe GmbH, Dernbach, Germany) was made from PEEK. It was holding a permeable frit through which the carrier liquid exits from the channel, the so-called cross flow

outlet. The upper block was made of a transparent polycarbonate inlay in an aluminium block, and had drills for channel inlet, injection inlet and channel outlet. The permeable frit supported a pre-cut membrane which served as accumulation wall. Regenerated cellulose (RC) ultrafiltration membranes with a 10 kDa cut-off were used as membrane materials during this study. Between the two blocks a spacer was fitted which defined the trapezoidal channel dimensions. The channel had a length of 26.5 cm, a width near inlet and outlet of 2.2 and 0.6 cm, respectively, and a thickness of 250 µm unless stated otherwise.

The various flow settings which are used during an AF4 experiment were controlled by Eclipse 2 separations system (Wyatt Technology Europe). The Eclipse 2 was connected to a standard Agilent HPLC system 1100 series (Agilent Technologies, Santa Clara, CA, USA) consisting of an micro vacuum degasser G1379A, an isocratic pump G1310A and an autosampler G1313A.

The system was coupled online with a variable wavelength UV-VIS detector (G1314A VWD detector, Agilent Technologies), an 18-angle static light scattering detector (Dawn EOS, Wyatt Technology Corp., Santa Barbara, CA, USA) and a dRI detector (Optilab rEX, Wyatt Technology USA). The system was controlled by Eclipse software version 2.5 (Wyatt Technology Europe). Data acquisition and procession were performed using Astra 5.3.2.17 (Wyatt Technology USA). The geometric radii of the liposomes were calculated using the data from 15 angles from the MALS detector applying the coated sphere model.

Table 3.1 displays a typical separation method for AF4 of liposomes consisting of the three basic flow settings focusing, elution and washing of the channel. During all settings a constant flow rate of 1.00 $mL \cdot min^{-1}$ was kept through the detectors to reduce pressure fluctuations. Focusing of the sample is performed during steps two to four (Table 3.1).

Table 3.1: A typical separation protocol for AF4 of liposomes.

	delta t	Time	Mode	X start	X end	Focus Flow
1	2.00	2.00	Elu.	0.00	1.00	-
2	1.00	3.00	Focus	-	-	1.00
3	5.00	8.00	Foc+Inj	-	-	1.00
4	2.00	10.00	Focus	-	-	1.00
5	35.00	45.00	Elu.	1.00	0.10	-
6	10.00	55.00	Elu.	0.00	0.00	-
7	10.00	65.00	Elu+Inj	0.00	0.00	-

During focusing the carrier liquid enters the AF4 channel both from its inlet and outlet and meets at a position close to the injection point. At that position

accumulation of the analyte within a narrow band is achieved (Wahlund and Giddings, 1987). The analyte is pressed towards the accumulation wall, which increases the concentration of the analyte and diffusion towards a steady state position will start. According to its diffusion coefficient the analyte is aligning at a certain height over the accumulation wall. During elution (step five) the carrier liquid enters the channel only from the inlet. By restricting the flow at the channel outlet the carrier liquid partially has to exit the channel through the bottom block which causes a cross flow perpendicular to the main flow direction. In the example from Table 3.1 a cross flow gradient ramping from 1.00 to 0.10 $mL \cdot min^{-1}$ was applied. Finally, the cross flow is turned off and both the channel and the injection loop are flushed with carrier liquid (step six and seven). During this project various separation protocols were applied, with cross flow gradients reaching from 0.80 to 0.15 $mL \cdot min^{-1}$ up to 2.00 to 0.15 $mL \cdot min^{-1}$. The applied conditions will be specified in the results part.

3.2.3.6 Multi-angle light scattering

The photo diodes at the different angles of the MALS detector need to be normalised against the diode at the 90 degree angle for correction of their different distances and refraction angles towards the sample cell and production-related differences among the photo diodes. A mass of 25 µg of BSA was fractionated by AF4 and normalisation was performed with the peak of the BSA monomer.

For the coated sphere model used in this study the coat thickness, refractive index of the coat, refractive index of the medium and the dn/dc need to be specified. Coat thickness was specified with 3.7 nm (van Zanten and Monbouquette, 1991), the refractive index of the coat was 1.45, namely the refractive index of egg-PC (Blessing et al., 1998). The refractive index of the medium was specified with 1.333 and the dn/dc was 1.464, as determined experimentally.

Geometric radii were obtained directly from Astra using the so-called *particle template*. For known particle shapes size determination is possible from MALS data only, without information on the concentration of the eluting sample. For known refractive indices an amount of eluting particles, the number density, can be calculated. The *number density template* calculates the amount of particles from the MALS data. The calculation is based on the light scattering intensity of each slice and the chosen form factor, i.e. coated sphere and gives a number of particles per mL.

4 RESULTS AND DISCUSSION

4.1 Method development

4.1.1 Influence of the focus flow rate

A typical AF4 method includes an injection/focusing step prior to the elution step (see Table 3.1). Focusing improves the resolution of the fractionation and reduces band broadening and premature elution of analytes (Schimpf and Wahlund, 1997). On the other hand, during focusing an concentration of the analyte occurs which may lead to analyte/analyte- and analyte/accumulation wall-interactions (Litzen, 1993, Schimpf and Wahlund, 1997). Obviously, this is undesired and focusing conditions should thus be chosen carefully. In order to investigate the impact of focusing conditions on the outcome of AF4 of liposomes, soy-PC LUVs were fractionated using identical elution conditions and varying the focus flow rate systematically (1.00, 2.00 or 3.00 mL·min^{-1} for 7 minutes) (publication 2).

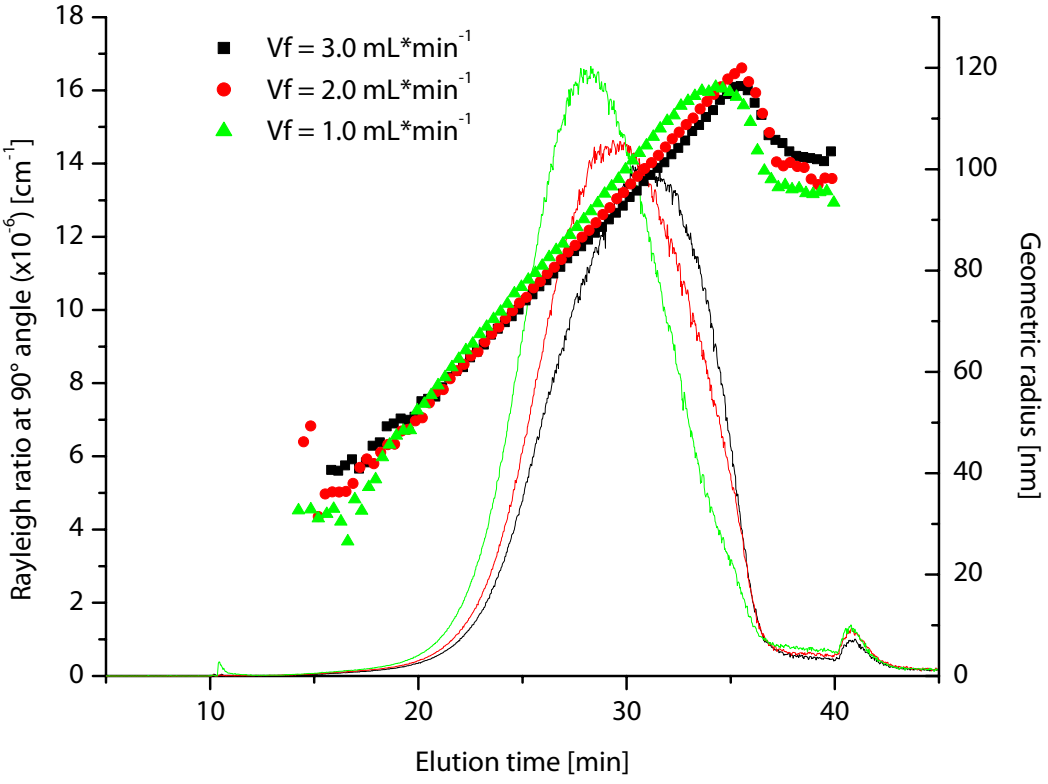

Figure 4.1: *AF4-MALS elugrams of soy-PV LUVs for different focus flow rates. Lines show Rayleigh ratios, scattered symbols the geometric radii.*

Figure 4.1 displays the elugrams of the MALS detector obtained from fractionations with the three different focus flow conditions (Rayleigh ratio vs. elution time along with the geometric radii derived from MALS). With increasing focus flow rates the top of the peak shifts to later retention times and the peak shape changes from steep to the left (1.00 mL·min^{-1} focus flow rate) to steep to the right (3.00 mL·min^{-1}). This shift to later elution times can be explained by the analyte approaching the accumulation wall closer with increasing focus flow rates. As argued in publication 2 a focus flow rate of 2.00 mL·min^{-1} seems preferable since the shape of the fractionation curve obtained under these conditions is most symmetrical. A plot of number density (particles per mL, determined from the light scattering intensity) vs. geometric radii (Figure 4.2) showed a slight shift towards smaller particle sizes with smaller focus flow rates, however, the MALS derived mean radii remained unchanged.

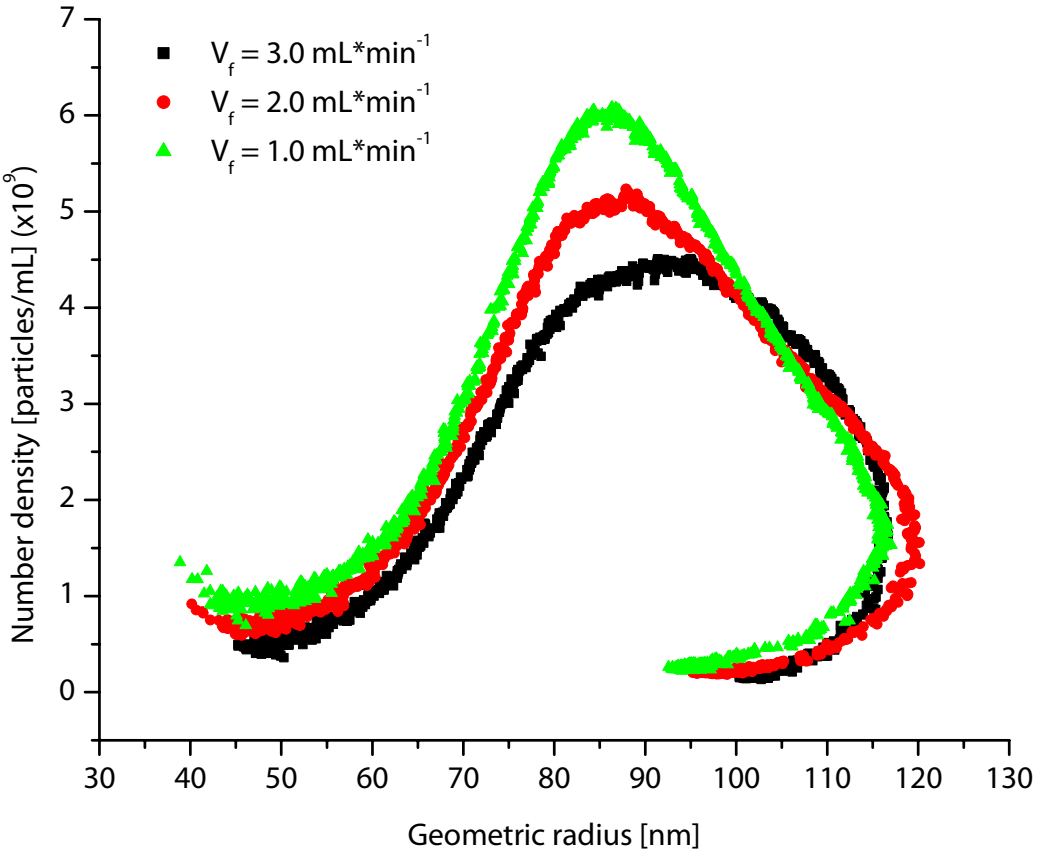

Figure 4.2: *Size distribution plots of soy-PC LUVs for different focus flow rates.*

One would expect that particle size determination by the combination of AF4-MALS yields better results than retention time dependent particle size determination. In the latter case the calculated particle sizes might be subject to variations that are not described by the theoretical retention model (equation 6) such as seen here for the focus flow and thus be incorrect.

When varying the focus flow conditions within the chosen limits aggregation artefacts could not be observed in contrast to literature reports for other analytes (Schimpf and Wahlund, 1997). For virus-like particles no aggregation sensitivity was found which is in accordance with our results (Chuan et al., 2008). In order to evaluate the total amount of particles eluting from the channel at different focus flow conditions the AUC of the UV-VIS signal was calculated. The observed reduction in AUC was marginal (data not shown) and much less pronounced than that reported from other analytes, e.g. humic acid macromolecules (Schimpf and Wahlund, 1997). Sample losses induced by enhanced focusing are generally regarded as an effect of adsorption to the accumulation wall due to enhanced interaction between analyte and membrane at higher focus flow. For the setup in this study adsorption does not seem to play a major role.

It has been reported for cow pea mosaic viruses that changing the focus flow rate did not significantly influence the performance of the fractionation because a secondary relaxation of the analyte occurs at the beginning of the elution step (Litzen and Wahlund, 1991a). Since the focus flow rates studied here showed satisfying fractionation, they were all used throughout this study.

4.1.2 Determination of optimum cross flow rate

The equilibrium height of a sample over the accumulation wall is determined by the equilibrium of the strength of the applied cross flow and the back-diffusion of the analyte according to its diffusion coefficient. Finding appropriate cross flow rates, therefore, is the pivotal step in the development of a fractionation method since it directly influences the quality of fractionation. Elution within a reasonable experimental time and sufficient resolution of the sample fractionation are the two main requirements. In order to investigate the influence of cross flow rate on liposome fractionation behaviour two liposome samples were fractionated using varying cross flow rates (publication 2). Soy-PC liposomes produced by detergent removal with a size of around 200 nm were used as well as egg-PC liposomes coloured with Sudan Red produced by filter extrusion through 100 nm filter pore size.

For the separation of the 100 nm liposomes constant channel flow rates of 1.00 $mL \cdot min^{-1}$ as well as varying isocratic cross flow rates between 0.40 and

1.20 mL·min^{-1} were applied. In Figure 4.3 the Rayleigh ratio at the 90 degree angle and the MALS-derived geometric radii are displayed for all elugrams.

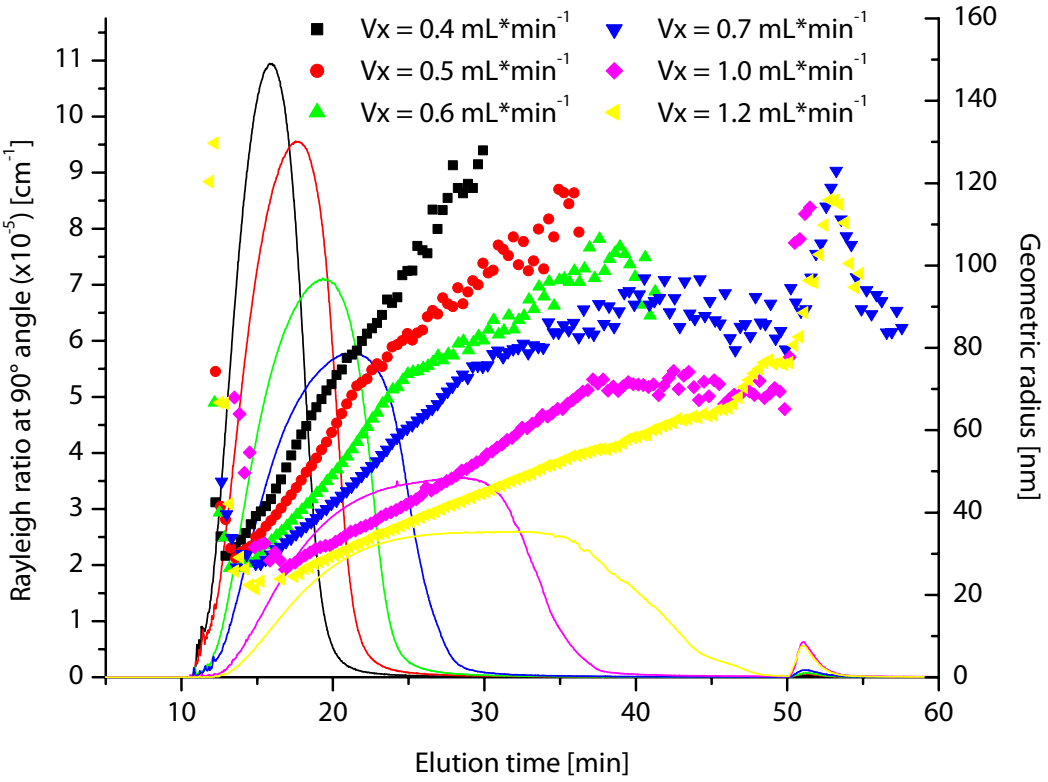

Figure 4.3: *AF4-MALS elugrams of 100 nm Sudan Red liposomes at different isocratic cross flow rates. Lines show Rayleigh ratios, scattered symbols the geometric radii.*

With increasing cross flow rates a shift towards later retention times could be observed as it was expected from the AF4 theory. For high cross flow rates the equilibration height over the accumulation wall is reduced and particles will be eluted later. It could be seen that for low cross flow rates between 0.40 mL·min^{-1} and 0.70 mL·min^{-1} separation from the void peak at the beginning of the separation was poor i.e. peaks starting directly at ten minutes. The curves for particle sizes first show a rapid drop before they increase steadily. An explanation may be that at the beginning of the fractionation larger particles are not yet driven towards their equilibrium height and thus elute too early. This explanation appeared plausible since the phenomenon of dropping radius curves at the beginning of fractionations is also seen for runs with higher cross flow rates. The drop in calculated radii might also be explained from the switching from the focus - to the elution step which is causing

fluctuations in pressure disturbing the detectors at the beginning of the fractionation. In another study those effects were reported for modified celluloses (Wittgren and Wahlund, 1997a) and natural colloids (Baalousha et al., 2006). To prevent the effects of switching between focus - and elution mode sufficient separation from the void peak is desired.

For cross flow rates of 1.00 mL·min^{-1} and above, better separation from the void peak was observed. However, peak broadening increased and elution of particles from the channel was not completed when the cross flow was turned off after 50 minutes. A possible explanation is that for higher cross flow rates the particles are driven very close towards the accumulation wall. Attractive interactions between the liposomes and the accumulation wall may become stronger and cause delayed elution of the sample as also described for cationic potato amylopectin (Lee et al., 2003b) and for ferritin and cow pea mosaic virus (Litzen, 1993). A plot of the UV-VIS signal versus geometric radii (Figure 4.4) is supporting this theory because it shows decreasing AUCs for increasing cross flow rates. At the same time, however, resolution at the lower end of the size distribution was improved as smaller particle sizes were resolved.

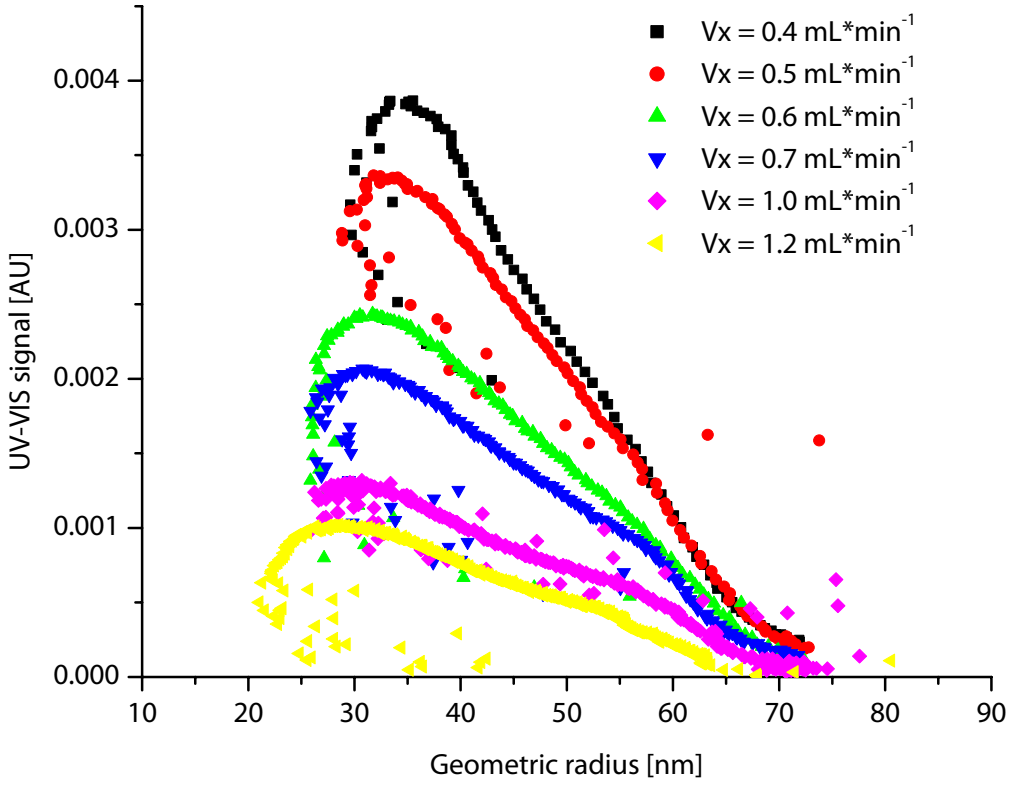

Figure 4.4: *Size distribution plots of 100 nm Sudan Red liposomes for different cross flow rates.*

In summary, none of the isocratic methods could satisfactorily fractionate the 100 nm liposome dispersion. Therefore, a cross flow gradient with decreasing cross flow rates from 1.00 to 0.15 mL·min^{-1} over 30 minutes was applied. The resulting elugram (Figure 4.5) showed both separation from the void peak and elution of the whole sample within the elution step.

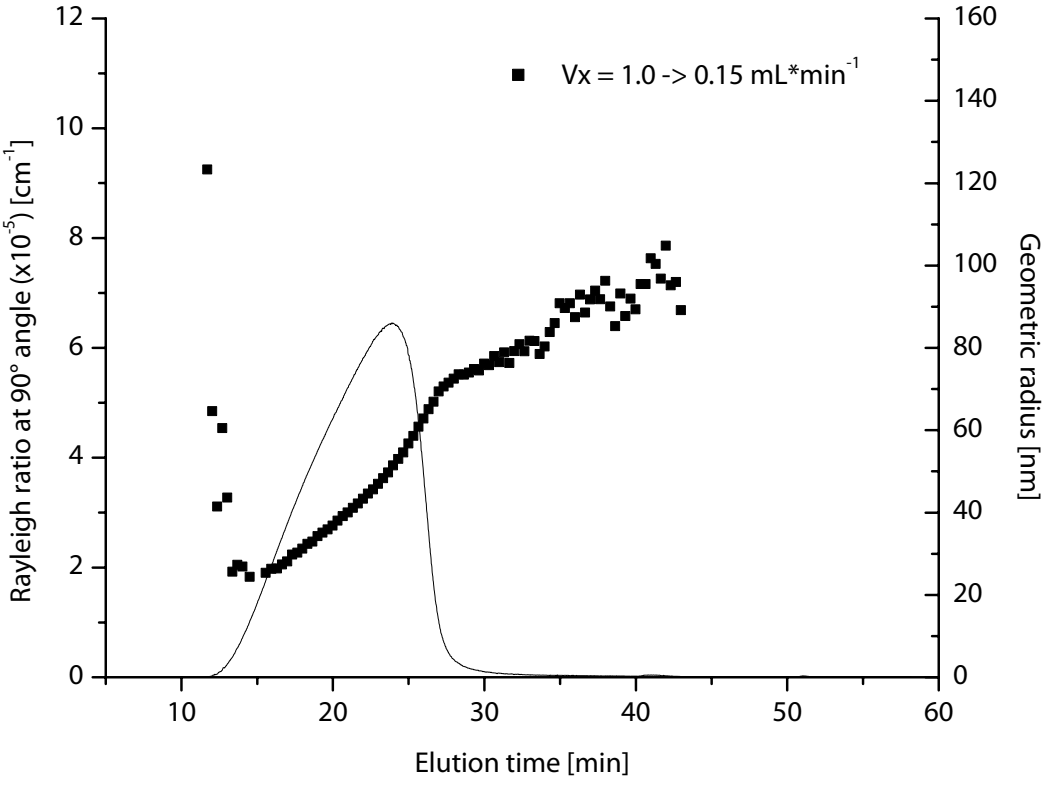

Figure 4.5: *AF4-MALS elugram of 100 nm Sudan Red liposomes with cross flow gradient. Line shows Rayleigh ratio, scattered symbols the geometric radius.*

For the separation of 200 nm liposomes similar behaviour could be observed as described in publication 2. Isocratic cross flow rates were varied between 0.10 mL·min^{-1} and 0.40 mL·min^{-1} with constant channel flow rates of 1.00 mL·min^{-1} (Figure 4.6). Again, poor separation from the void peak for low cross flow rates and peak broadening for higher cross flow rates appeared. Both effects were observed at lower cross flow rates than for the extruded liposomes. This can be explained by the larger size of the liposomes produced by detergent removal and their narrower size distribution compared to the extruded liposomes.

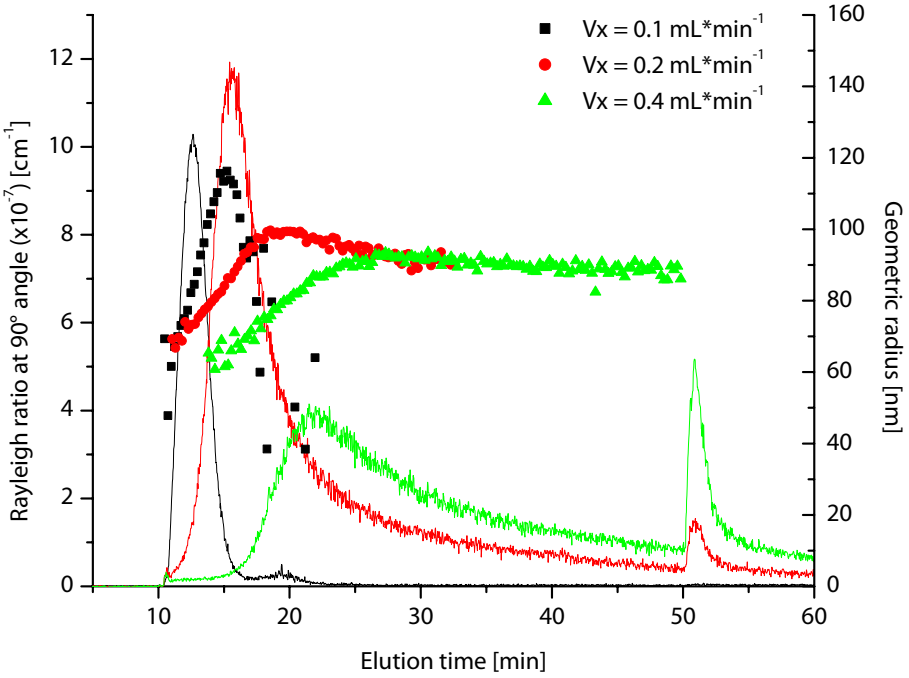

Figure 4.6: *AF4-MALS elugrams of 200 nm liposomes at different isocratic cross flow rates. Lines show Rayleigh ratios, scattered symbols the geometric radii.*

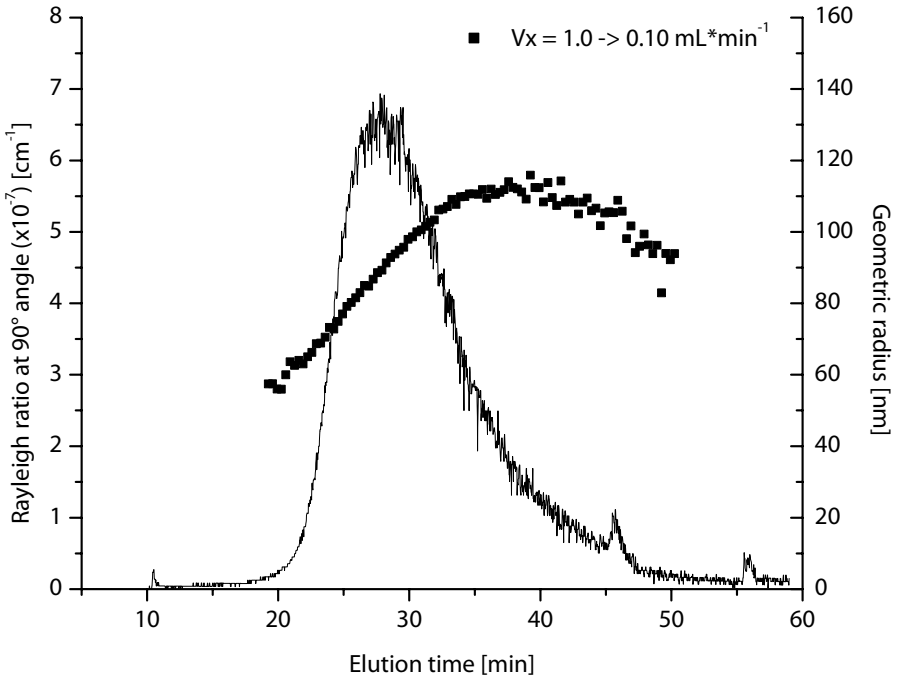

Figure 4.7: *AF4-MALS elugram of 200 nm liposomes with cross flow gradient. Line shows Rayleigh ratio, scattered symbols the geometric radius.*

Again, the use of a cross flow gradient of 1.00 to 0.10 mL·min^{-1} over 35 min resulted in satisfying fractionation, even though a small part of the sample did not elute within the elution step before the cross flow was turned off (Figure 4.7). Throughout this project cross flow gradients were applied for fractionating liposome dispersions. A cross flow rate gradient of 1.00 to 0.10 mL·min^{-1} was used as a universal method for most samples, however, gradients starting with stronger cross flow rates had to be applied for e.g. smaller liposomes.

4.1.3 Elution behaviour for different sample load masses

To our knowledge there is no information in literature regarding the influence of sample load on AF4 of liposomes. For symmetrical channels of varying dimensions liposome sample loads between 20/40 µg (Moon and Giddings, 1993) and 200 µg (Korgel et al., 1998) are reported. In another study using an AF4 system comparable to ours the sample load of virus-like particles was varied in the range between 2 and 20 µg without observing overload phenomena (Chuan et al., 2008).

Three different sample loads of soy-PC LUVs were fractionated, as shown in Table 4.1, using a channel flow rate of 1.00 mL·min^{-1} and a cross flow gradient of 1.00 to 0.10 mL·min^{-1} over 35 minutes (publication 2). In Figure 4.8–Figure 4.10 the elugrams from the Rayleigh ratio at the 90 degree angle along with the MALS-derived geometric radii are displayed over elution time.

Table 4.1: Sample load masses injected into the AF4 channel.

Sample	Concentration [mg·mL^{-1}]	Injection volume [µL]	Sample load mass [µg]
1	2.0	50	100
2	0.2	50	10
3	0.2	5	1

For the first and second injection of sample load mass of 1 µg (Figure 4.8) the liposomes elute at delayed elution times and mainly after the cross flow rate was turned off. Values calculated for the geometric radii derived from MALS were unstable and not increasing steadily. For the third and fourth injection more reproducible elution behaviour appeared and the geometric radii curves became very similar. In addition, sample load masses of 1 µg showed an unfavourable signal to noise ratio and were close to the lower limit of detection. Saturation effects became more significant as can be seen from the clear shift in retention time and increasing AUCs for following injections (see also chapter 4.1.6).

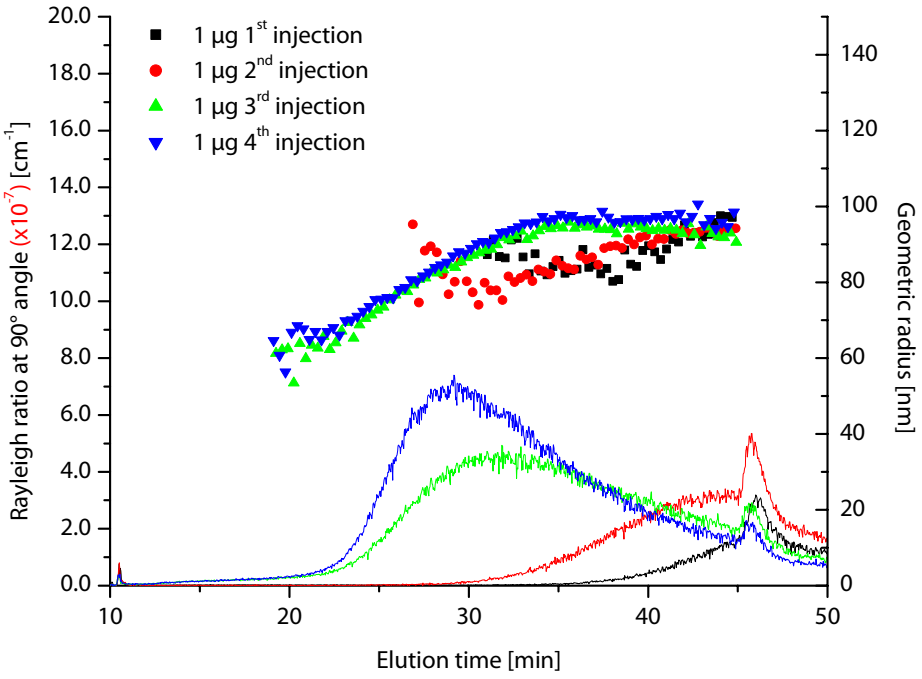

Figure 4.8: *AF4-MALS elugrams of a sequence of injections of soy PC LUVs at a sample load mass of 1 µg. Lines show Rayleigh ratios, scattered symbols the geometric radii.*

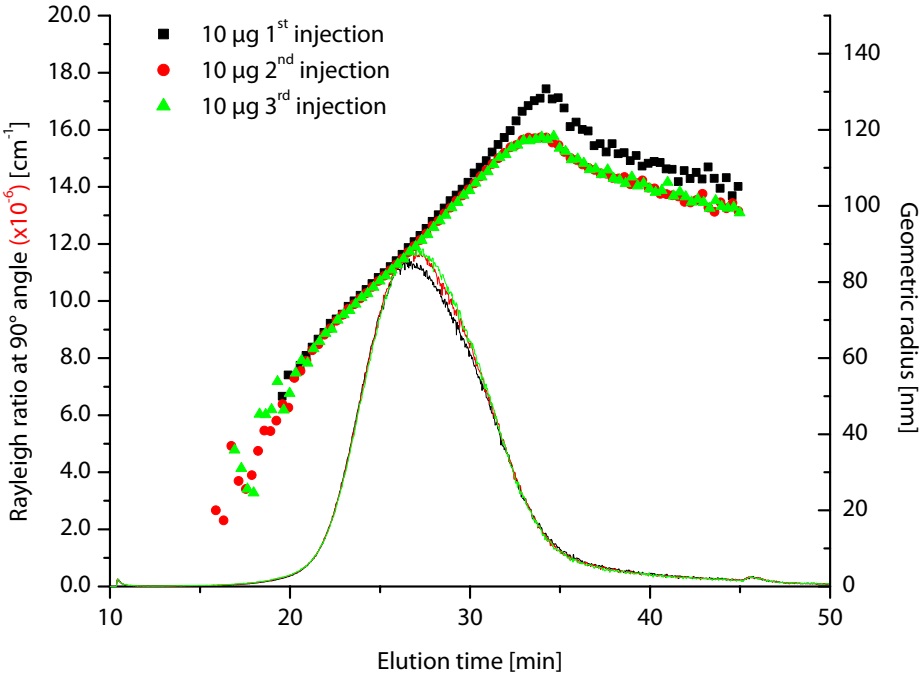

Figure 4.9: *AF4-MALS elugrams of a sequence of injections of soy PC LUVs at a sample load mass of 10 µg. Lines show Rayleigh ratios, scattered symbols the geometric radii.*

For the sample load mass of 10 µg (Figure 4.9) the curves of the Rayleigh ratio appeared smooth and close to symmetrical. Compared to the 1 µg sample load mass a shift to earlier retention times was observed. The calculated geometric radii more or less followed a straight line, in accordance with the FFF theory. For both the 1 µg and 10 µg sample load masses the calculated radii curve of the first injection deviate from the following injections. Therefore, the first run should always be discarded.

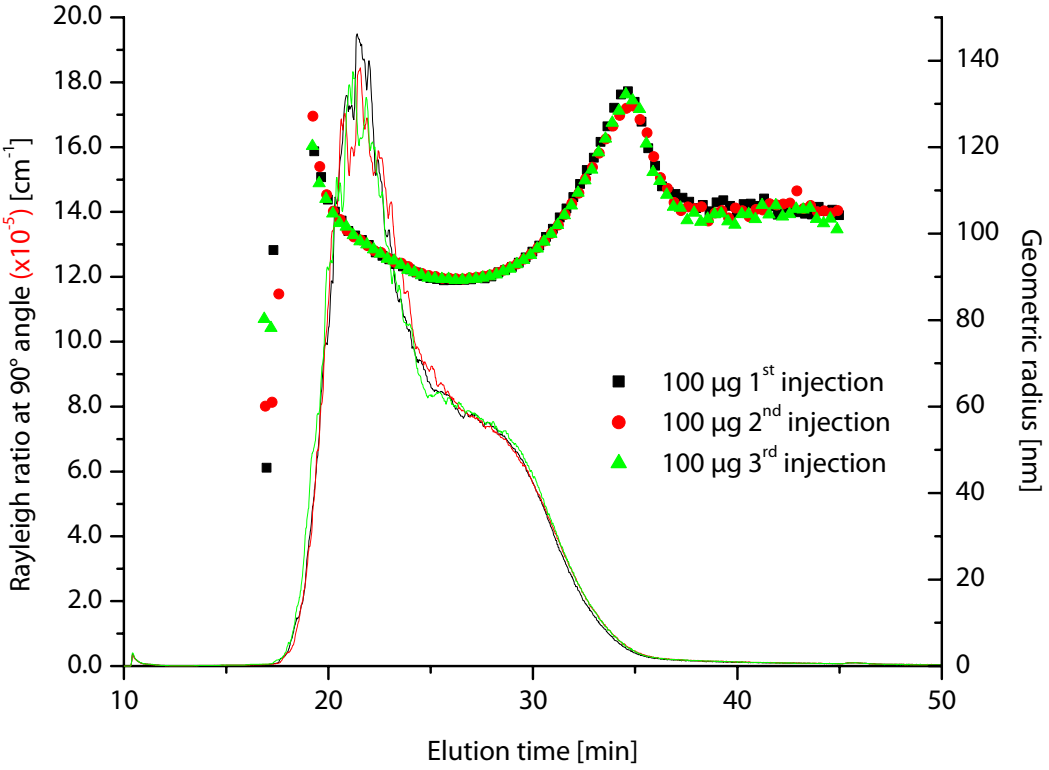

Figure 4.10: *AF4-MALS elugrams of a sequence of injections of soy PC LUVs at a sample load mass of 100 µg. Lines show Rayleigh ratios, scattered symbols the geometric radii.*

The 100 µg sample load mass resulted in a very distorted light scattering signal which was steep to the left (Figure 4.10). The geometric radius curve was deviating strongly from linearity showing a decrease first and then an increase. The phenomena seen for this sample load mass are typical for overloading of the channel. At high particle concentrations two effects will influence the fractionation: first, during focusing, a portion of the particles may be hindered from reaching its steady-state relaxation position with respect to the distance from the accumulation wall. And second, the particle concentration in the height over the accumulation where the

sample migrates will become too high. As consequence from both effects, some particles will end up in a layer which migrates at a higher velocity within the parabolic flow profile due to repulsion between the particles, and elute earlier. The overloading phenomenon is expected to be more pronounced for particles of narrow size distribution such as detergent removal liposomes in this study. A similar explanation was given for monodisperse polystyrene latex beads, separated by sedimentation field-flow fractionation (Hansen et al., 1989).

In summary, retention times were decreasing with increasing sample load masses. Similar observations have been reported for wheat protein glutenin with sodium phosphate buffer as carrier (Arfvidsson and Wahlund, 2003) and for humic substances in distilled water (Benincasa et al., 2002).

In summary, for optimisation sample loads of 10 µg appear ideal for the chosen setup because they allow complete relaxation and good signal to noise ratio.

A validation procedure of the autoinjector revealed that the injected volume was approximately 0.45 µL too high for all injection volumes. That means that injection volumes of at least 5 µL should be used and the desired sample load mass should rather be adjusted by dilution of the analyte than by changing injection volumes.

4.1.4 Influence of the ionic strength of the carrier liquid

Influences of the sample load and the ionic strength of the carrier liquid are strongly related and have to be discussed in close context. For investigating the influence of ionic strength on fractionation behaviour, three liposome samples were prepared by filter extrusion through 200 nm membrane filters: Rh-PE liposomes in 1 mM sodium nitrate (publication 4), Rh-PE liposomes in 10 mM sodium nitrate (publication 4) and native egg-PC liposomes in 10 mM sodium nitrate (publication 2). Fractionation was performed using a cross flow gradient of 1.00 to 0.15 $mL \cdot min^{-1}$ for 30 minutes. A low sample load mass of 2 µg was injected onto the channel in order to prevent overloading. For dilution and as carrier liquid water and sodium nitrate solutions of increasing concentration (5 to 50 mM) were used.

The elugrams displayed in Figure 4.11 represent the progression of the light scattering signals (Rayleigh ratio) along with the MALS-derived geometric radii for the different carrier liquids. In water the liposomes begin to elute at 10 minutes immediately after the void peak and the elugram shows a distorted elution profile with a sharp rise at the beginning followed by a shoulder. At the same time, for the first half of the peak the progression of geometric radii with elution time does not show a steady increase as expected from AF4 theory. Both the irregular peak shape

and the unexpected progression of measured geometric radii point towards a sub-optimal size fractionation of the particles and overloading of the channel.

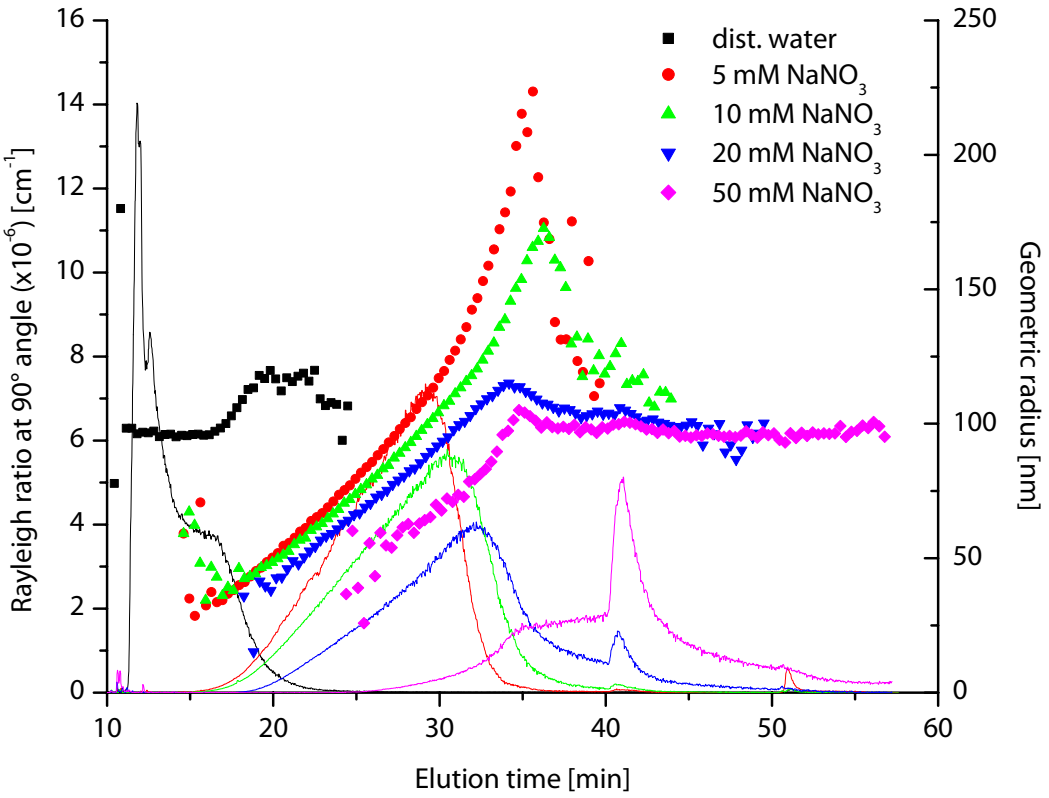

Figure 4.11: *AF4-MALS elugrams of Rh-PE liposomes prepared in 1 mM sodium nitrate with carrier solutions of different salt concentrations. Lines show Rayleigh ratios, scattered symbols the geometric radii.*

Salt concentrations as low as 5 mM sodium nitrate solution already cause a major change in elution profile towards a broad, non-distorted peak occurring at later elution times (15 to 35 minutes). The Rayleigh ratio signal returns to baseline level indicating a complete fractionation of the liposomes within the time frame of the chosen method. The geometric radius curve is rising steadily as expected from AF4 theory. With further increased salt concentrations of the carrier liquid (10 to 50 mM) the peak shape becomes more and more unsymmetrical and liposomes elute over an even longer period of time. The observed shift towards later retention times and broader peaks goes in parallel with a change of the slope of the geometric radius curves.

For 20 and 50 mM sodium nitrate solution retention on the channel is that much enhanced that separation is not completed within the elution step, causing an artefact peak at 40 minutes when the cross flow is turned off. This is an indication that under the chosen conditions a certain fraction of the liposomes has not left the channel until the cross flow is reduced to zero.

Furthermore, at around 35 minutes the calculated particle size curves approach a maximum, deviating from the expected continuously increasing radii. Obviously, the size fractionation is incomplete for such relatively high salt concentration and small cross flow rates, at least within the chosen time-frame.

The experiment was repeated using Rh-PE liposomes prepared in 10 mM sodium nitrate. Zeta potential values were measured upon dilution in water and sodium nitrate solutions of varying concentration between 5 and 50 mM. Figure 4.12 displays the zeta potential values of the Rh-PE-liposomes in the different media. With increasing salt concentration the strongly negative zeta potential value was found to decrease more and more, approaching a value of -15 mV in 50 mM sodium nitrate solution.

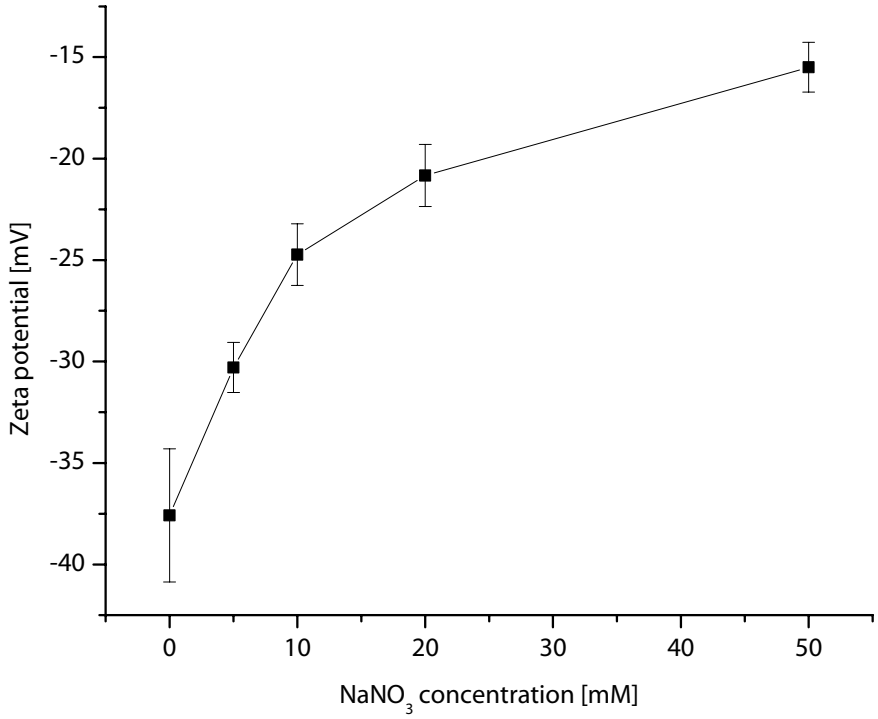

Figure 4.12: *Zeta potential values of Rh-PE liposomes prepared in 10 mM sodium nitrate, measured upon dilution with sodium nitrate solutions of different concentrations.*

These liposomes were fractionated by AF4 using the same set of salt solutions as carrier liquid. Elugrams from the MALS detector and geometric radii are given in Figure 4.13. Surprisingly, all elugrams looked very similar in terms of elution time and peak shape, apart from that obtained from fractionation in water. At the same time the geometric radius traces became superimposable for 5, 10 and 20 mM sodium nitrate carrier solution. Only in 50 mM sodium nitrate solution a moderate decline of the trace towards smaller radii at the end of the run appeared.

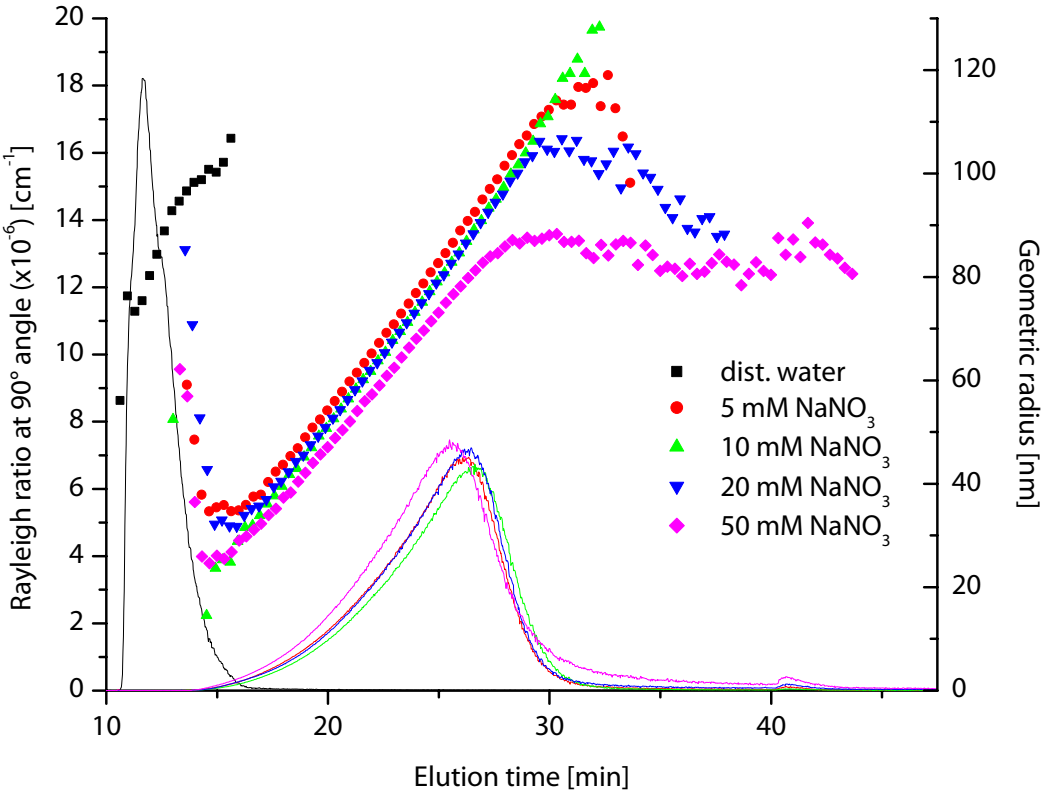

Figure 4.13: *AF4-MALS elugrams of Rh-PE liposomes prepared in 10 mM sodium nitrate with carrier solutions of different salt concentrations. Lines show Rayleigh ratios, scattered symbols the geometric radii.*

Other than in the previous set of experiments (Figure 4.11), the differences in retention time and peak shape became negligible for all salt solutions (except for the sample in water). Despite the fact that the liposomes had shown significantly different zeta potential values, no considerable differences in retention occurred with increasing salt concentration.

The Rh-PE liposomes are bearing a negative net charge on their surface because Rh-PE is negatively charged. In order to exclude charge effects the same experiment was performed using electroneutral egg-PC liposomes without dye. Figure 4.14 shows the Rayleigh ratio at the 90 degree angle along with the derived geometric radii.

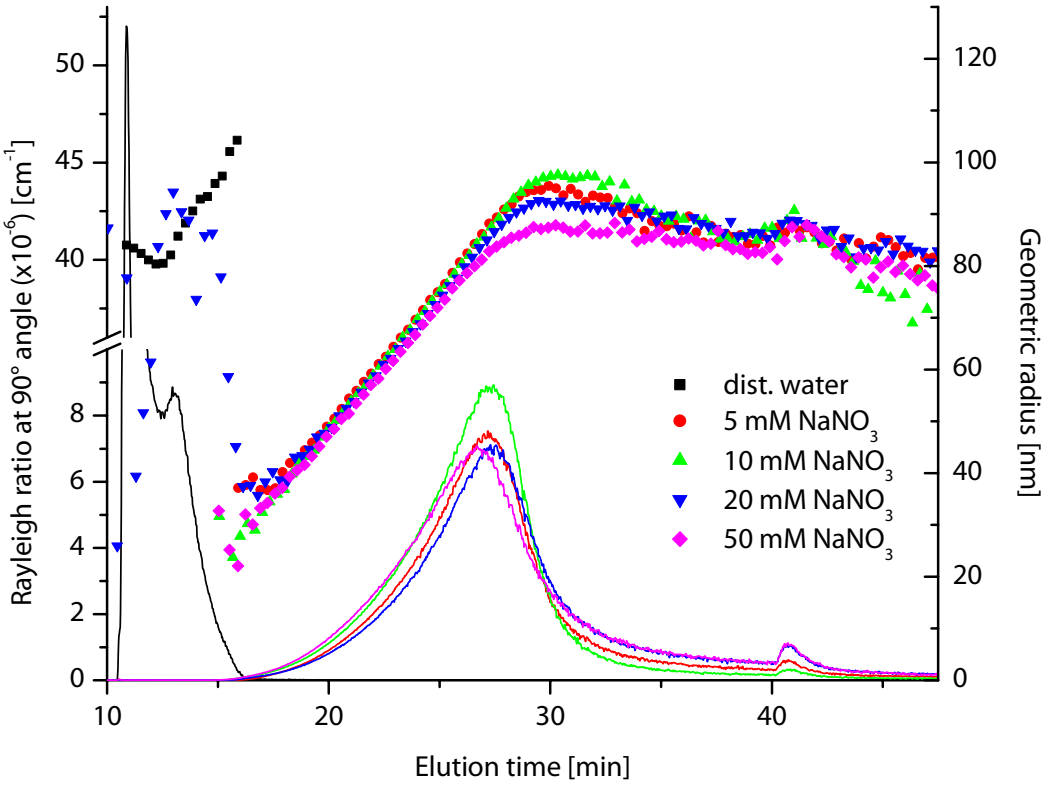

Figure 4.14: *AF4-MALS elugrams of egg-PC liposomes prepared in 10 mM sodium nitrate with carrier solutions of different salt concentrations. Lines show Rayleigh ratios, scattered symbols the geometric radii.*

Again, the elugram obtained with distilled water is very different from the others. An early and narrow peak is observed with considerable indication of overloading. For all sodium nitrate solutions the sample eluted much later as compared to distilled water and showed reasonable fractionation with linearly increasing radii within the given elution time. For the 20 and 50 mM sodium nitrate carrier liquid, a slightly larger fraction of particles was eluting towards the end of the gradient at 40 minutes, and smaller radii were calculated within the main peak. The zeta potential values measured in the different carrier liquids are displayed in Figure 4.15. Despite the fact that egg-PC liposomes do not bear a net charge, all samples showed negative zeta potential values. The liposomes diluted with water had an increased negative zeta potential value compared to the dilutions in sodium nitrate solution and a plateau was reached at an concentration of about 10 mM sodium nitrate. An explanation for this was reported: at low ionic strengths, the negatively charged phosphatidyl groups are located at the outer end of the head group region. As the ionic strength increases,

the choline group approaches the outer region of the bilayer surface while the phosphatidyl group hides behind the surface (Makino et al., 1991).

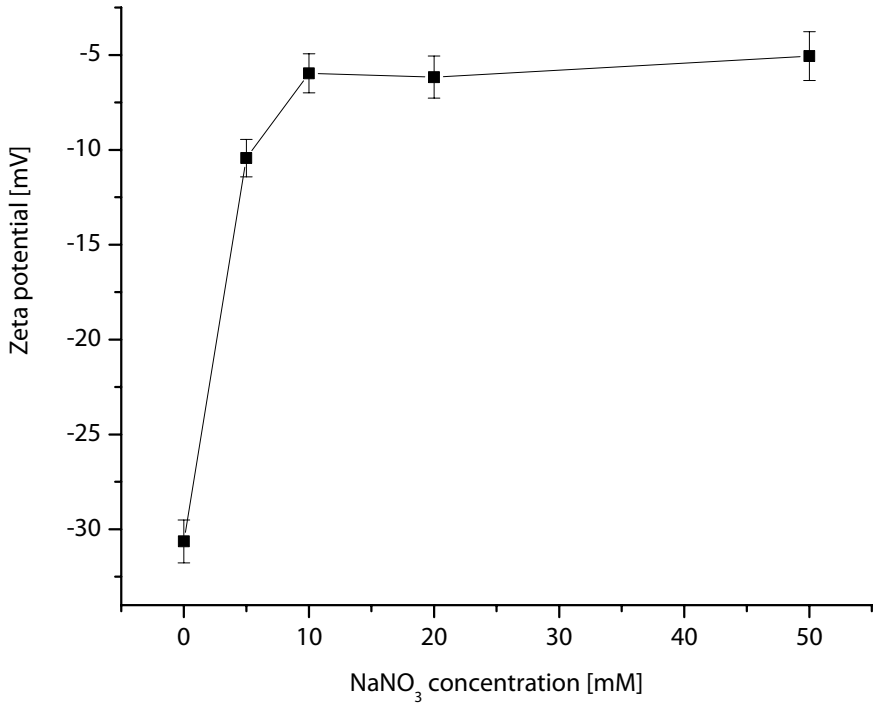

Figure 4.15: *Zeta potential values of native liposomes prepared in 10 mM sodium nitrate, measured upon dilution with sodium nitrate solutions of different concentrations.*

Changes in elution behaviour with carrier liquids of different ionic strengths as seen for the Rh-PE liposomes in 1 mM sodium nitrate have earlier been observed for various nanoparticles (Litzen and Wahlund, 1991a, Moon et al., 1998, Arfvidsson and Wahlund, 2003). Moon et al. examined the influence of both Tris and PBS buffers of different ionic strengths (8–160 mM) on the retention of negatively charged liposomes using a symmetrical field-flow fractionation system and measuring particle size by PCS offline. They found that retention of charged liposomes may deviate from FFF theory both at low and high ionic strength and thus FFF requires establishment of proper ionic conditions of the carrier liquid.

At low ionic strengths there is a significant zone without analyte in close vicinity to the accumulation wall. Strong electrostatic interaction (repulsive) between particles and the accumulation wall and particles themselves give easily rise to overloading effects (Martin, 1998) as it is seen for all fractionations of the liposome samples in water. The increased effective volume of the particles due to an enhanced electrical

bilayer, and exclusion effects from the layer closest to the accumulation wall lead to a displacement of the analyte to higher distances and thus premature elution (Hansen et al., 1989). Already for sodium nitrate concentration of 5 mM the elution behaviour changed drastically and it seems that no overloading effects occurred for any of the fractionations with carrier liquids containing salt.

However, the decrease in calculated geometric radii with increasing ionic strengths cannot be explained by this theory. Therefore, the experiment was repeated with liposomes (with and without Rh-PE) prepared with ionic strengths closer to those of the carrier liquids (10 mM sodium nitrate) and zeta potential values were measured. Independently from their surface charge the elution behaviour of both liposome preparations for all sodium nitrate solutions was very similar and geometric radii were almost identical. Even though dilution with sodium nitrate solutions of increasing concentrations led to different zeta potential values, no such difference was observed from the AF4 experiments. Mori et al. described the influence of particle-wall and particle-particle interaction on retention behaviour in SdFFF and found that perturbations due to electrostatic repulsive and van der Waals attractive forces were not significant at ionic strengths above 10^{-3} M (Mori et al., 1990). Obviously, a salt concentration of 5 mM sodium nitrate is appropriate for successful fractionation of liposomes and preventing channel overloading.

The change in fractionation behaviour of liposomes with carrier liquids of increasing salt concentration is large if, at the same time, the difference in salt concentration between liposome interior and carrier liquid is big (first set of experiments), but rather marginal when the difference in salt concentration is moderate (second and third set of experiments). This suggests that two different phenomena are involved: changes of the elution behaviour due to (1) electrostatic repulsion and (2) actual changes in vesicle size due to osmotic stress. For the investigation of the second phenomenon the following study was performed.

4.1.5 Osmotic pressure influencing the fractionation behaviour of liposomes

In order to study osmotic effects independently of electrostatic interactions, the osmotic pressure was varied by keeping the sodium nitrate concentration constant at 10 mM and varying the osmotic pressure by addition of sucrose (publication 4). Sucrose is uncharged, has a molecular weight of 342 and will not penetrate through the phospholipid bilayer (Bangham et al., 1967). Hyperosmotic conditions were achieved by diluting liposomes prepared in 10 mM sodium nitrate with solutions containing 10 mM sodium nitrate and an aliquot of sucrose imposing the same osmotic pressure as 90 mM sodium nitrate. Egg-PC Liposomes prepared by filter extrusion through membrane filters of 100 nm pore size were used. PCS measurements were performed prior to fractionation with AF4. Upon dilution in the hypertonic medium a significant decrease in hydrodynamic diameter (number weighted) from 90.5 nm (± 3.3 nm) to 73.8 nm (± 2.7 nm) could be seen after one hour which indicated osmotic shrinking of the vesicles. Both after 24 and 48 hours no further change in diameter had occurred indicating that the observed osmotic shrinking was taking place within less than an hour.

AF4 fractionations were performed applying a channel flow rate of 1.00 $mL \cdot min^{-1}$ and a cross flow gradient ramping from 1.00 to 0.15 $mL \cdot min^{-1}$ for 30 minutes. Figure 4.16 shows the elugram from the MALS detector and MALS-derived geometric radii of the liposome sample fractionated both under hyper- and isoosmotic conditions. Under hyperosmotic conditions a shift towards earlier elution times and smaller particle sizes occurs. The size distribution plot (Figure 4.17) indicates a parallel shift of the whole size distribution towards smaller particles. Apparently osmotic shrinking of the whole liposome population occurred. Osmotic shrinking appears to be the reason for the observed shift to earlier elution times.

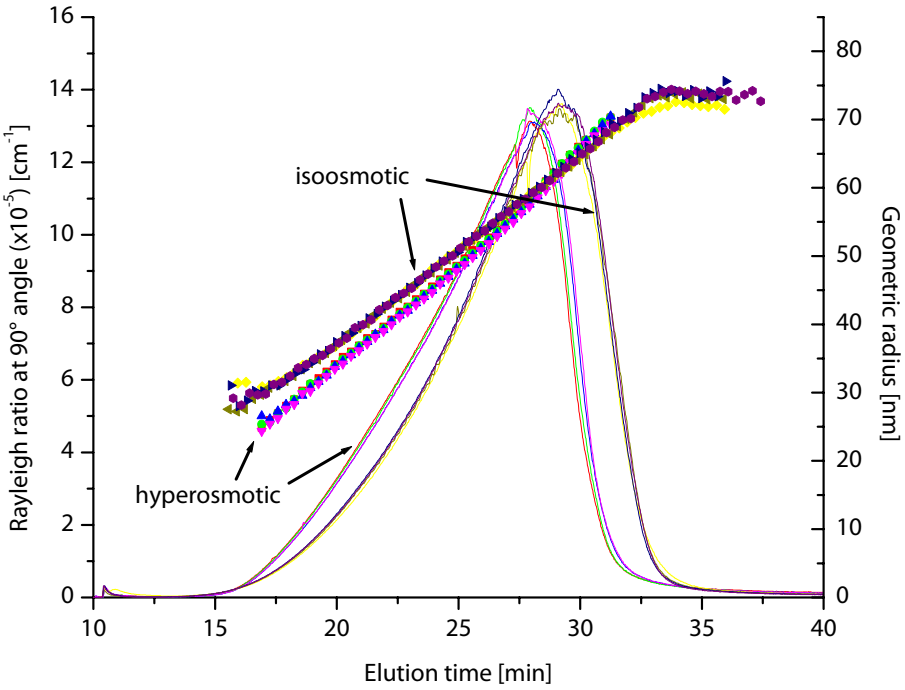

Figure 4.16: *AF4-MALS elugrams of egg-PC liposomes prepared in 10 mM sodium nitrate solution and fractionated with iso- and hyperosmotic carrier liquid.*

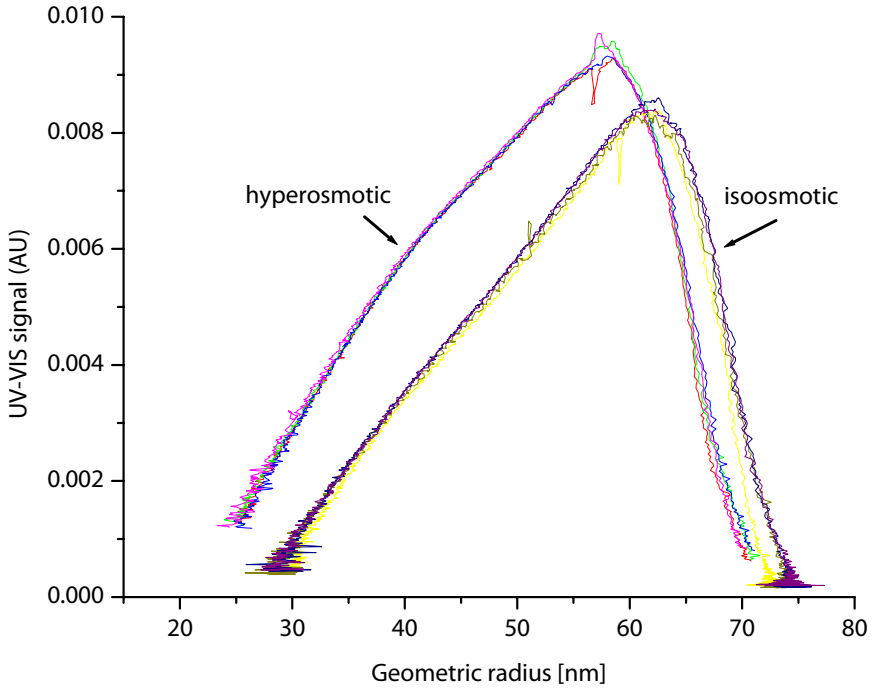

Figure 4.17: *Size distribution plot of egg-PC liposomes prepared in 10 mM sodium nitrate solution and fractionated with iso- and hyperosmotic carrier liquid.*

Hypoosmotic conditions were achieved by preparing liposomes in sucrose supplemented sodium nitrate solution and diluting them in solutions containing 10 mM sodium nitrate, only. Upon exposure to hypoosmotic medium the liposomes showed increasing particle sizes within one hour (85.4 ± 3.9 nm to 96.1 ± 5.5 nm) measured by PCS. Again, no further change was seen up to 48 hours after dilution.

AF4 experiments were performed using 10 mM sodium nitrate as carrier liquid and the same fractionation method as for the previous experiment. The geometric radius trace of the vesicles diluted in hypoosmotical medium indicates a shift towards larger particle sizes (Figure 4.18). Unexpectedly, the peak under hypoosmotic conditions was shifted towards earlier elution times and, at the same time, the peak shape changed. From the size distribution plot (Figure 4.19) it can be seen that a shift towards larger particles occurred only for the larger fraction of the liposome population. An explanation for this fact may be that only the larger particles undergo osmotic swelling.

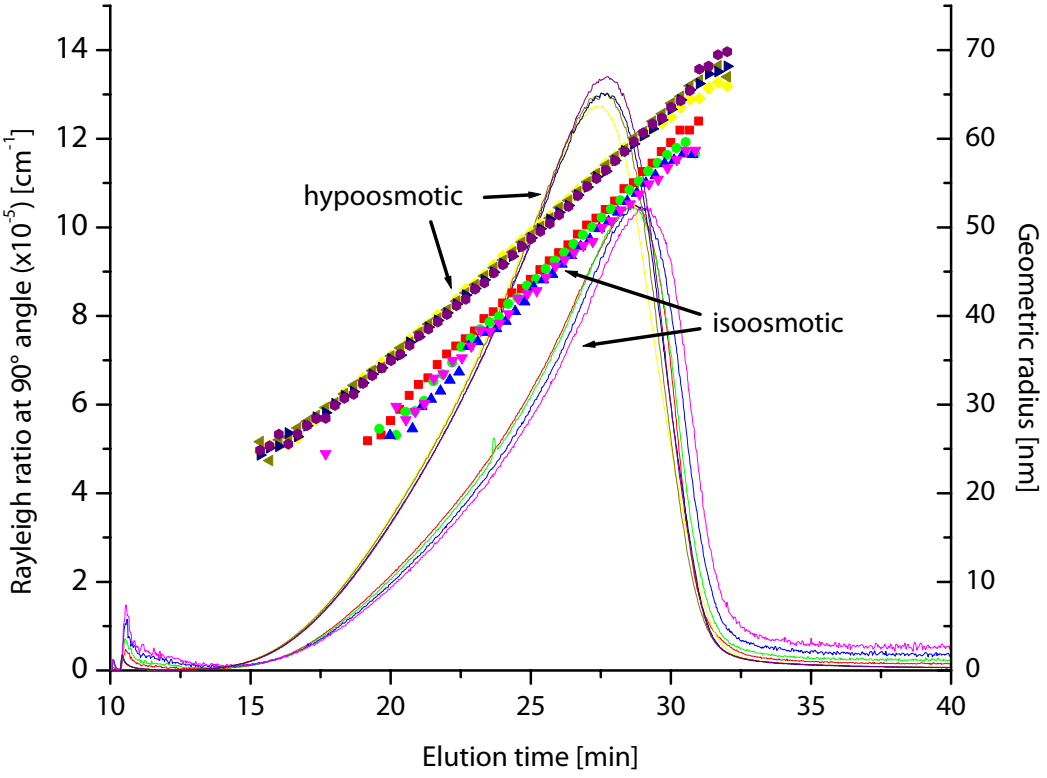

Figure 4.18: *AF4-MALS elugrams of egg-PC liposomes prepared in sucrose supplemented 10 mM sodium nitrate and fractionated with iso- and hypoosmotic carrier liquid. Lines show Rayleigh ratios, scattered symbols the geometric radii.*

These observations indicate that liposomes which have been extruded through 100 nm pore size membranes do undergo osmotic shrinking irrespective of their particle size whereas osmotic swelling appears to occur only within the fraction of larger particles. In literature the occurrence of irregularly shaped (non-spherical) vesicles prepared by filter extrusion was described from Cryo-TEM reports (Mui et al., 1993, Almgren et al., 2000, Berger et al., 2001). Another group was using a combination of dynamic and static light scattering for the investigation of liposomes shape changes upon dialysation with hypo- and hyperosmotic media (Jin et al., 1999). Calculations of elongation factors showed liposomes of non-spherical conformation after filter extrusion which turned spherical in hypotonic media and more elongated in hypertonic media.

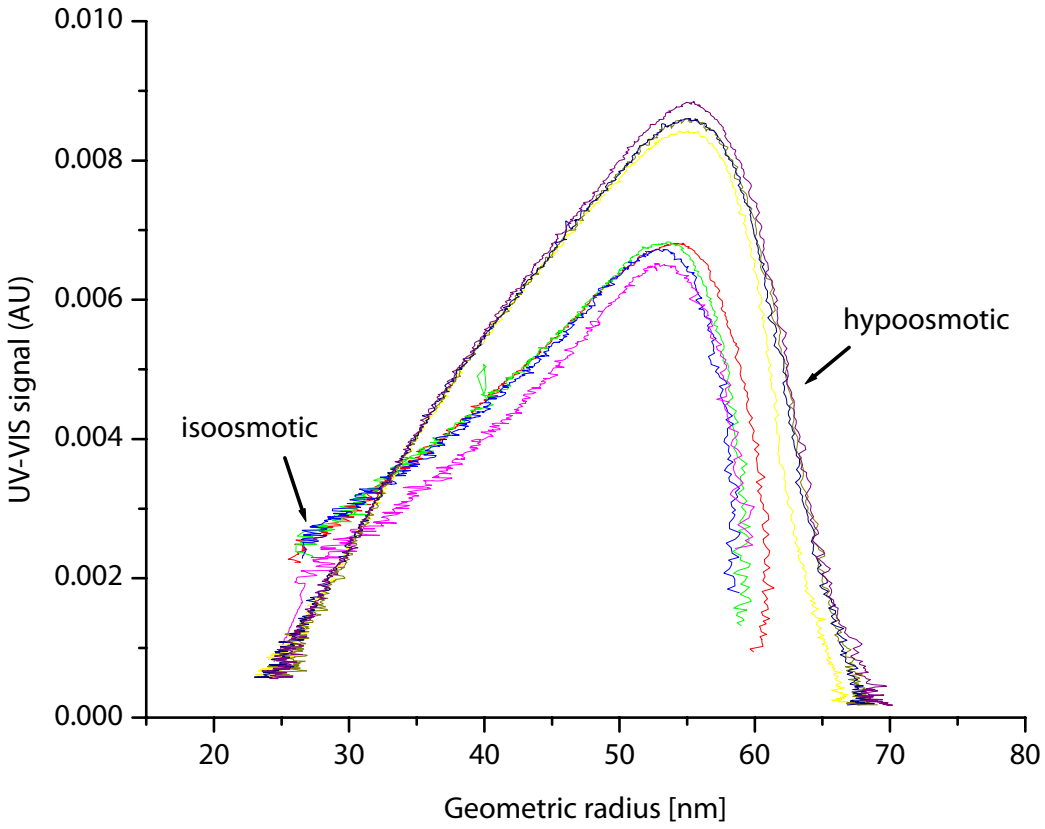

Figure 4.19: *Size distribution plot of egg-PC liposomes prepared in sucrose supplemented 10 mM sodium nitrate solution and fractionated with iso- and hypoosmotic carrier liquid.*

Based on those reports and on our observations following hypothesis was drawn: liposomes small enough to pass the filter pores of the membrane do not undergo

deformation during filter extrusion and adopt spherical shapes. Such spherical vesicles may shrink with response to hyperosmolar stimulus but their ability to swell in hypotonic environment is rather limited since they already have adopted the maximum volume-to-surface ratio. Larger vesicles may not pass the membrane pores without deformation. Such deformed (non-spherical) vesicles may both shrink and swell in hyper- or hypoosmolar environment, respectively. For illustration see the schematic drawing in publication 4. Elugrams obtained from fractionation with identical carrier liquid for liposomes prepared in the two different media cannot be compared with each other, because it can not be expected that the two batches have exactly the same size.

4.1.6 Choice of concentration detection method

For the direct derivation of molar masses of analytes eluting from AF4 experiments, simultaneous detection of the concentration and light scattering intensity is required for constructing a Debye plot. Therefore, a combination of MALS and dRI detectors is often used. Geometric radii on the other hand, can directly be derived from the MALS signal without knowledge of concentration using the particle template in Astra. However, for the construction of quantitative particle size distribution profiles, as well as for sample recovery analysis, concentration detection is necessary. The aim of the following set of experiments was to study the performance of UV-VIS - and dRI detection in terms of their applicability for quantifying the amount of liposomes eluting from the AF4 channel (publication 3).

Besides the established methods of differential refractive index detection and unspecific UV-VIS absorbance (turbidity-) measurement, UV-VIS-detection of coloured liposomes containing amphiphilic or lipophilic dyes was employed, and the specific absorbance signal at the absorbance maximum of the dye was followed. A channel flow rate of 1.00 $mL \cdot min^{-1}$ and cross flow rate gradients of 1.00 to 0.15 $mL \cdot min^{-1}$ for 30 minutes were applied, in case of the Rh-PE liposomes a cross flow gradient of 2.00 to 0.15 $mL \cdot min^{-1}$ for 30 minutes was used. Turbidity originating from liposomes without dye was detected at a wavelength of 280 nm, absorbance of Sudan Red and Rh-PE liposomes was measured at wavelengths of 501 nm and 571 nm, respectively. Figure 4.20 shows the UV-VIS and Figure 4.21 the dRI traces of native (without dye) and coloured liposomes at two different sample load masses, 2 µg lipid and 100 µg lipid.

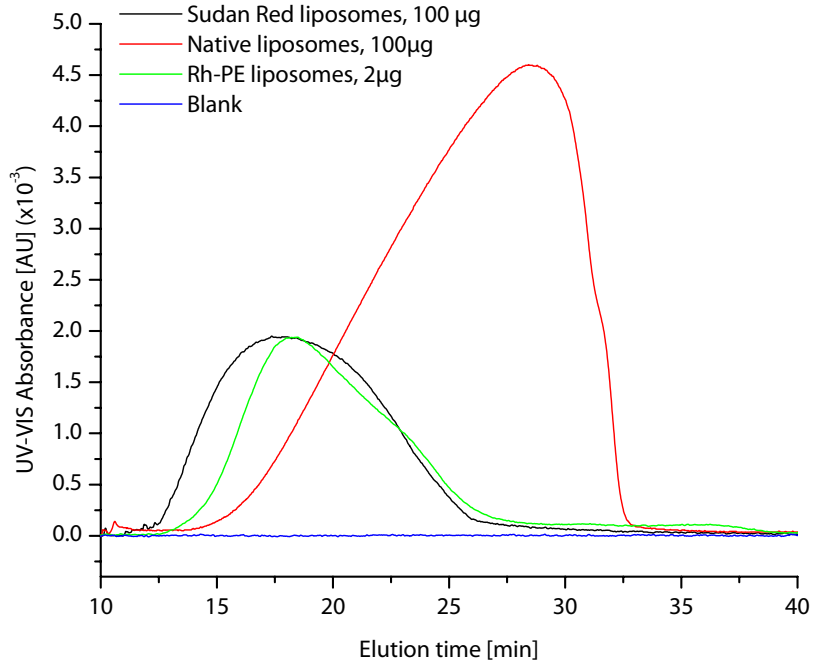

Figure 4.20: *AF4 elugrams obtained by UV-VIS detection of fractionations of Sudan Red liposomes, native liposomes and Rh-PE liposomes at different sample loads and blank.*

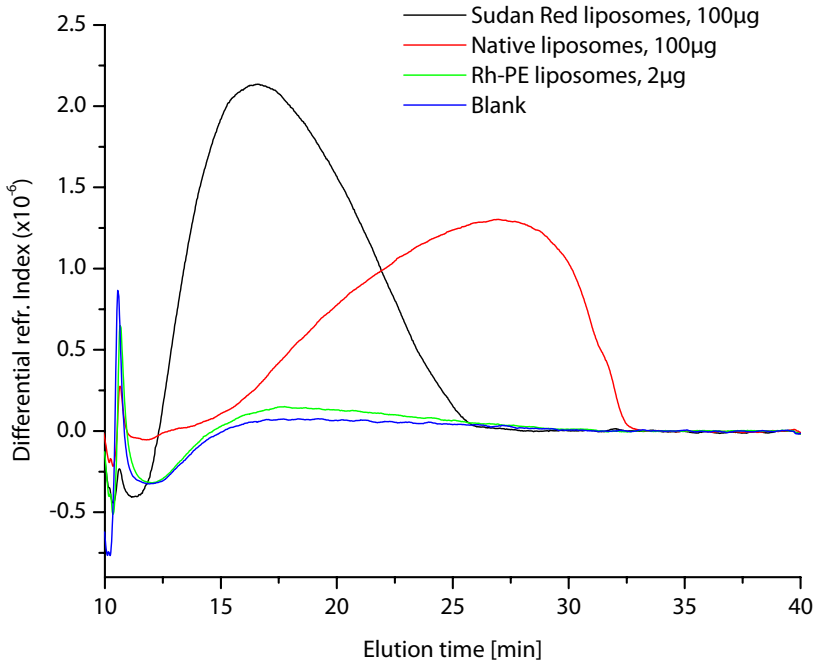

Figure 4.21: *AF4 elugrams obtained by dRI detection of fractionations of Sudan Red liposomes, native liposomes and Rh-PE liposomes at different sample loads and blank.*

AUC determination was straightforward in case of UV-VIS detection of the unspecific absorbance of native liposomes as well as the specific absorbance for both the high (100 µg) and the low (2 µg) sample load mass of coloured liposomes (Figure 4.20). In contrast, the dRI-signal could hardly be discerned from the blank in case of the 2 µg sample load mass of Rh-PE liposomes, while AUC determination was easily done in case of the higher sample load masses (Figure 4.21). Regarding the unspecific UV-VIS absorbance (turbidity) one has to take into account that the signal is not only dependent on concentration but also on particle size as illustrated in Figure 4.22. Native liposomes were sequentially extruded through polycarbonate membranes of decreasing pore sizes, and UV-VIS spectra were taken after each extrusion step. The reduction in absorbance over the whole spectra suggests liposomes of decreasing sizes as expected. Figure 4.23 displays the UV-VIS spectra of Sudan Red liposomes treated in the same way, showing a decrease in absorbance and at the same time a relatively stable level of absorbance at the maximum of the dye at 501 nm. The relative difference of absorbance between the smallest and the largest liposomes measured at a wavelength of 280 nm was 38.7 % in case of the native liposomes. The aberration was smaller (3.2 %) for the absorbance measured at the maxima of the dye in case of the coloured liposomes. The turbidity signal is thus regarded inappropriate for quantitatively measuring liposome concentration, unless liposomes of a certain, uniform size are employed, a prerequisite which is in contradiction to the purpose of particle size fractionation/analysis of liposomes by AF4. Obviously, both dRI- and specific absorbance-detection are well suited for concentration detection in an AF4 setting as long as sample loads in the magnitude of 100 µg are feasible. However, for substantially smaller sample loads, the dye method appears superior due to its better sensitivity compared to dRI-detection. A low LOD by dRI detection of particulate matter was also described for the study of gelatine nanoparticle drug carrier systems (Zillies et al., 2007). Instrumental factors as well as a relative high absorptivity of Sudan Red (89430 $mL \cdot g^{-1} \cdot cm^{-1}$) make UV-VIS detection to the superior alternative for concentration detection. However, the dye method is restricted to cases where staining of the liposomes can be achieved either by insertion of the dye during liposome preparation or by subsequent addition of the dye to an existing liposome sample as described in (Claassen, 1992). No stable values for absorptivity could be achieved for liposomes stained with Rh-PE, possibly due to losses of dye or reallocation of the dye due to flip-flop movements over the bilayer membrane.

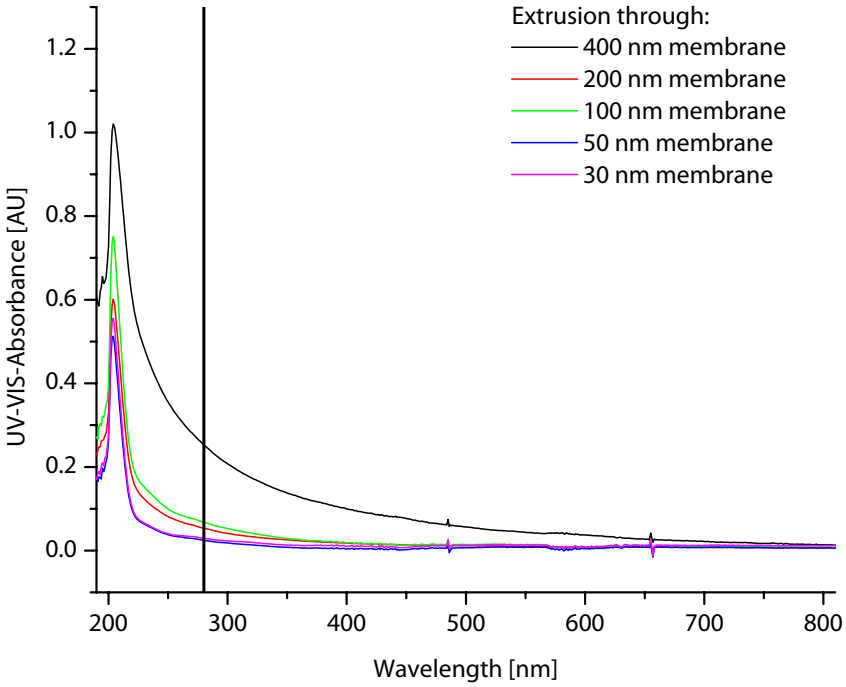

Figure 4.22: *UV-VIS-spectra of native liposomes after extrusion through membrane filters with the designated pore sizes.*

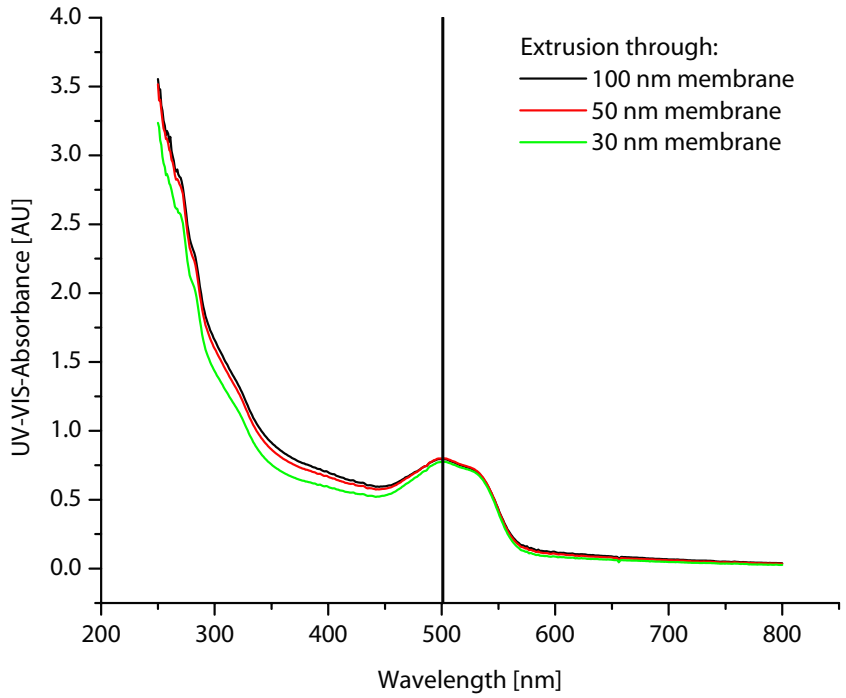

Figure 4.23: *UV-VIS spectra of Sudan Red liposomes after extrusion through membrane filters with the designated pore sizes*

4.1.7 Adsorption/carry-over phenomena at the accumulation wall

In chapter 4.1.2 decreasing recovery rates with increasing cross flow rates were seen for liposomes fractionated by AF4 and in chapter 4.1.3 a change of elution behaviour for the first injections of very small sample load masses was described. It remained open if those two effects are caused by adsorption effects of liposomes onto the accumulation wall used in AF4. Therefore, a study on the performance of the ultrafiltration membranes was done which is described in publication 3. The aim was to determine how the AF4 behaviour of liposomes is developing in subsequent runs of liposome samples in order to check for potential adsorption and carry-over phenomena. Ten injections of a very small sample load (0.5 µg) of native liposomes (filter extruded, 200 nm pore size) were performed with a channel equipped with a new RC membrane. The experiment was repeated two times with freshly mounted membranes, each. As fractionation method a channel flow rate of 1.00 $mL \cdot min^{-1}$ and a cross flow gradient of 1.00 to 0.10 $mL \cdot min^{-1}$ over 35 minutes were used. A mild focus flow rate of 1.00 $mL \cdot min^{-1}$ for seven minutes was chosen. The resulting Rayleigh ratios at the 90 degree angle for the injection sequences are displayed in Figure 4.24. Under the chosen conditions a strong deviation from the expected elution profile was observed for the first injections. The elution of the liposomes appeared in a delayed manner and a significant proportion of the sample eluted not before the cross flow was turned off after 45 minutes. This delayed elution was pronounced to a minor degree during the following injections. The AUC of the injections was constantly increasing during the sequence of injections. The changes in elution times and increasing AUCs did not appear in a reproducible manner for the three different injection sequences.

As accumulation wall a RC membrane with a cut-off of 10 kDa was used throughout this study. The RC membrane has a porous hydrophilic surface which, in principle, is expected to be prone to interaction with hydrophilic analytes like liposomes. During the focusing procedure analytes are forced into a position in close vicinity to the accumulation wall. During subsequent injections of the same sample the delayed elution was less pronounced and approached a more reproducible elution order. Assumingly, a certain amount of liposomes was necessary to saturate the membrane in order to achieve reliable elution behaviour. The required amount was not constant as the experiments with the three membranes showed. The decreased AUCs seen for the first injections may possibly be explained by different phenomena: losses of smaller particles through the membrane, adsorption onto the surface of the membrane or the swelling of the membrane into the channel interior and thus reduction of the void volume (Benincasa and Giddings, 1997).

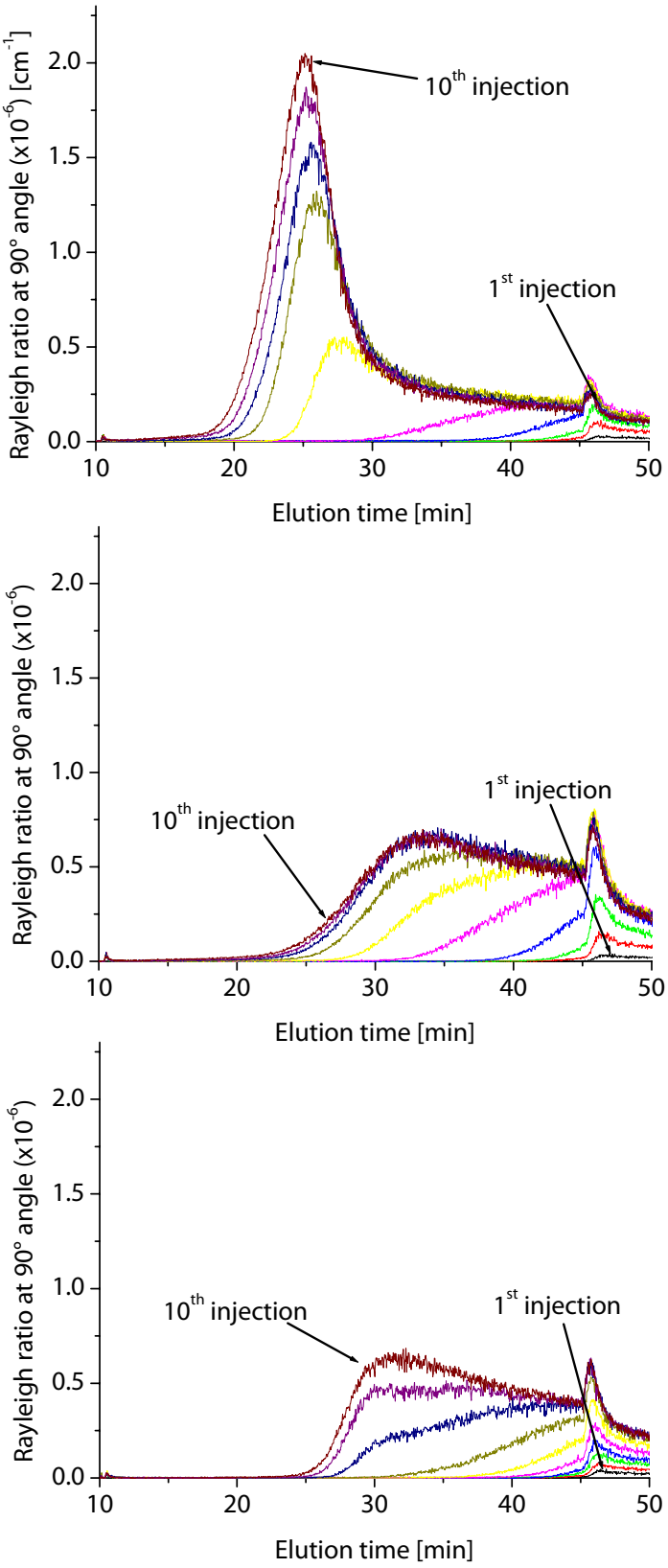

Figure 4.24: *AF4-MALS elugrams of the Rayleigh ratio from sequences of ten injections of 0.5 µg of native liposomes onto three different, freshly mounted membranes.*

Losses through the membrane were shown to be dependent on the membrane composition and its cut-off as described for the separation of human lipoproteins with flow field-flow fractionation (Li et al., 1997). However, losses through the membrane are unlikely in case of liposomes since the apparent molar mass of the liposomes is several orders of magnitude larger than the cut-off of the ultrafiltration membrane (Stauch et al., 2002). Photographs of the RC membrane were taken of a run of 100 µg Rh-PE liposomes, 6 minutes after the elution step began (Figure 4.25). The pictures show a cloud of coloured liposomes travelling over the accumulation wall. It can be seen that the sample is not distributed in an even manner over the membrane. The picture reveals the relatively strong surface texture of the cellulose membrane that could cause areas where the membrane is extending into the channel to a higher degree and delay sample elution. This may explain that at some parts of the membrane the elution of the sample is delayed while most of the sample has moved downstream of the channel.

Figure 4.25: *Photograph taken of the AF4 channel, six minutes after the elution step began for a fractionation of 100 µg Rh-PE liposomes.*

For investigation whether runs with sample load masses of 10 µg lead to carry-over of liposomes to the subsequent fractionation run, another set of experiments was performed: alternating runs with injection of pure buffer (blank) and of native

liposomes were performed, beginning with blank. Figure 4.26 shows the blank traces for the different detectors (Rayleigh ratio at 90 degree angle, UV-VIS and dRI) of the injections before and in-between the liposome runs.

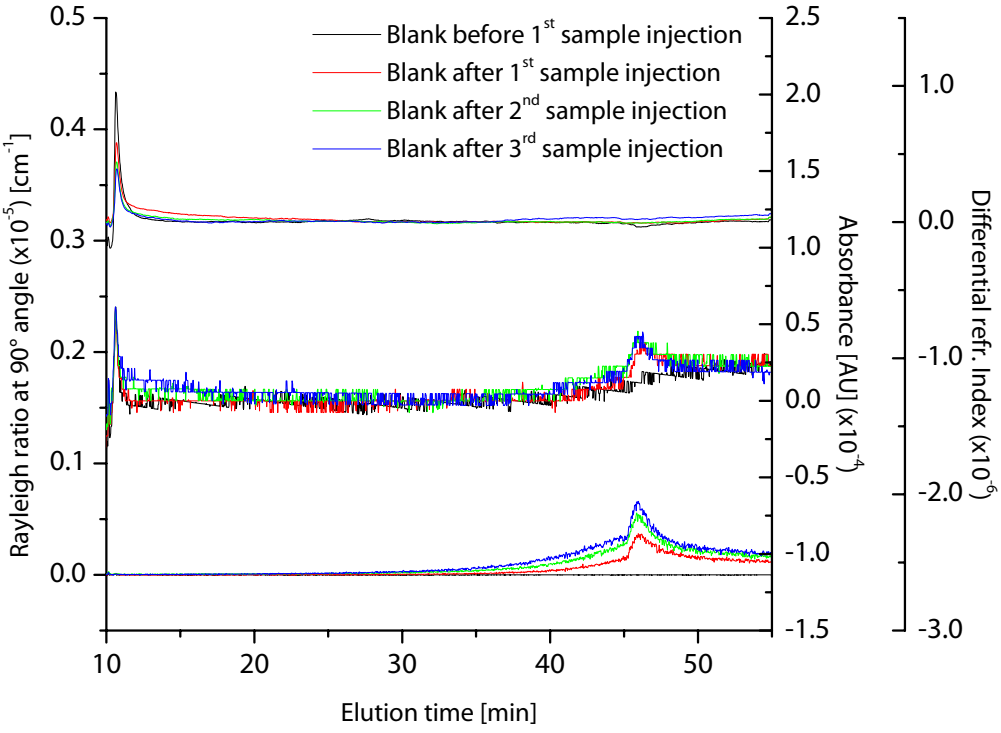

Figure 4.26: *AF4-MALS elugrams of intermittent carrier liquid-injections (before and in-between liposome injections). The lowest elugrams represent the Rayleigh ratio, the elugrams in the middle represent the UV-VIS signal and the uppermost elugrams the dRI signal.*

Only for the MALS detector increasing traces at the end of the fractionation could be detected indicating the elution of very small amounts of particles from the channel when the cross flow was turned off. Elugrams from the MALS detector of the intermittent injections of liposome sample are displayed in Figure 4.27. The first injections of liposomes yielded smaller peaks than the subsequent injections and it is obvious that saturation of the membrane happened, as observed before. The appearance of (minor amounts of) particles in intermittent blank runs indicates that carry-over from preceding sample runs did occur only to a very small degree. Thus adsorption to the membrane appears more likely to explain the lower recoveries seen

for the injections of liposomes onto fresh membranes, than the limited extent of carry-over that was observed here.

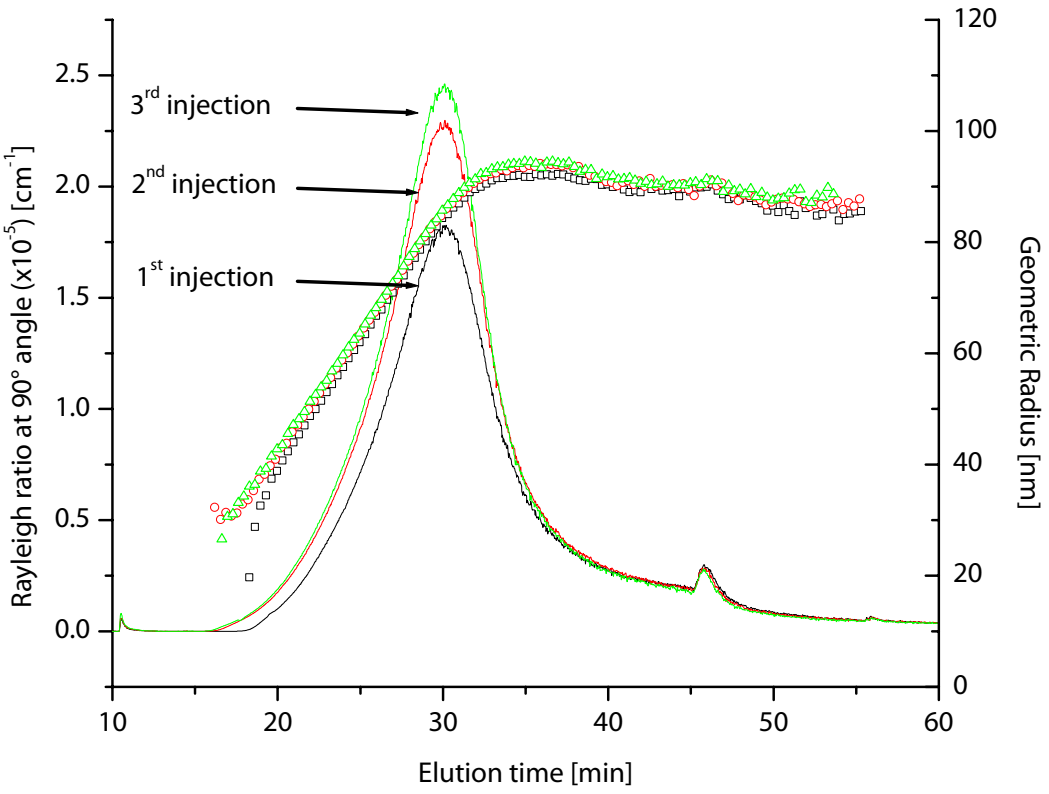

Figure 4.27: *AF4-MALS elugrams and geometric radii obtained from three consecutive injections of native liposome with a sample load mass of 10 µg.*

Finally, recoveries of two samples of 30 nm liposomes (coloured with Sudan Red and native) were determined for a sample load of 100 µg on a pre-saturated membrane. Recoveries were calculated from the AUC of both the UV-VIS - and the dRI detector-curve using the experimentally determined values of absorptivity and dn/dc, respectively. A relatively high sample load mass of 100 µg was injected in order to assure a detectable signal for the dRI detector. Injection volumes were 1 µL for the Sudan Red liposomes and 10 µl for the native liposomes. A correction for the too high injection volume described in chapter 4.1.3 was performed. For fractionation of the sample a channel flow rate of 1.00 mL·min^{-1} and a cross flow gradient of 2.00 to 0.15 mL·min^{-1} for 30 min were used. Recoveries fluctuating around 100 percent were achieved from the first injection on for detection with dRI, and around 85 percent for detection by UV-VIS absorbance (Figure 4.28). The injected mass was determined by the enzyme test and calibration of the injected volume was performed. The recoveries

determined here appeared reasonable and indicated complete elution from the channel. However, it must be stated that the sample load mass of 100 µg might cause overloading phenomena for larger liposomes. In summary, it can be stated that membrane effects such as sample losses or adsorption play a role only for small sample load masses while saturation of the membrane is achieved fast for higher sample loads.

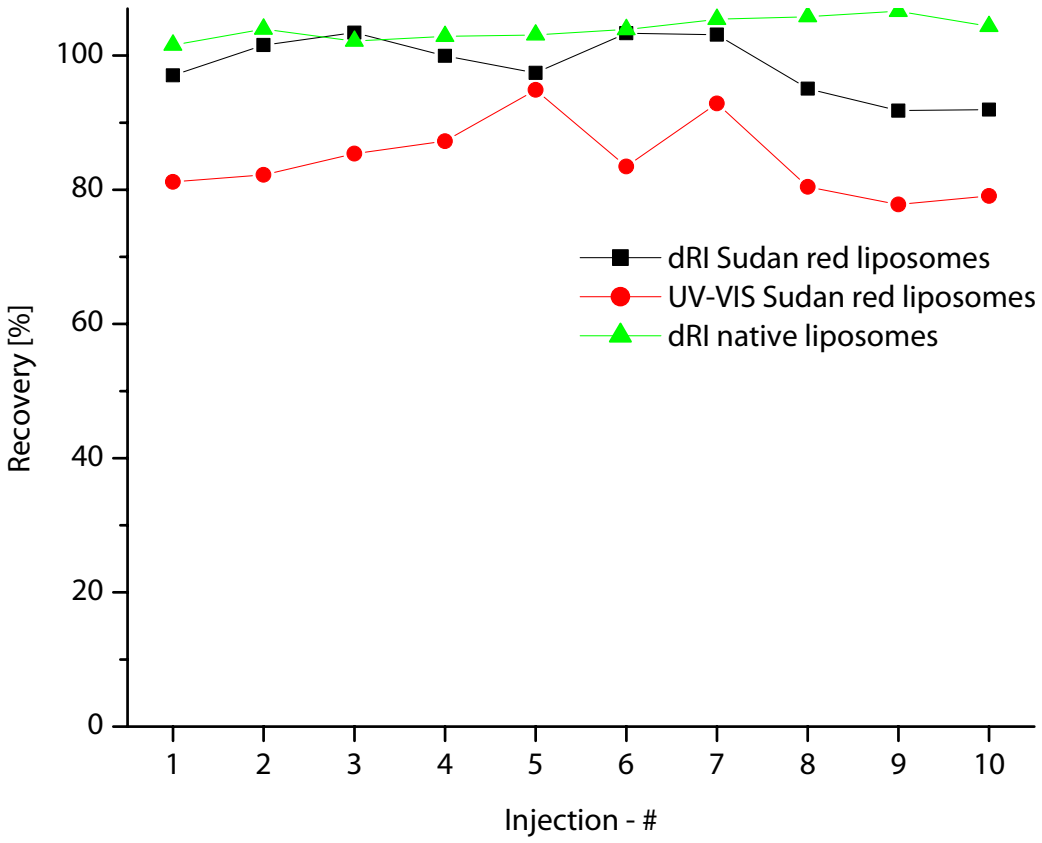

Figure 4.28: *Recovery rates obtained for consecutive injections of 10 µg Sudan Red liposomes and native liposomes, determined by UV-VIS and/or dRI detection.*

4.1.8 Choice of model for fitting MALS data

Liposome sizes may range over three orders of magnitude. Furthermore, liposome morphologies, although representing hollow spheres may vary in terms of core/shell-ratio and show large differences in their curvature. Both factors strongly influence light scattering properties such as the angular dependency of the scattered light. Three different fitting methods that are not taking account to particle shape (Zimm/Debye/Berry) were compared to the hollow sphere model in terms of

calculated particle sizes and quality of fit. Two model analytes were chosen: relatively large, unilamellar liposomes (LUV) prepared by detergent removal as described in chapter 3.2.1.4 having mean diameter of around 200 nm, and relatively small, unilamellar liposomes (SUV) prepared by filter extrusion through 30 nm filter pores after five freeze thaw cycles as described in chapter 3.2.1.2.

The SUVs were fractionated using channel flow rates of 1.00 $mL \cdot min^{-1}$ and a cross flow gradient of 1.00 to 0.10 $mL \cdot min^{-1}$ for 35 minutes. In order to get an impression of the performance of the fitting models over the whole range of particle size of the eluting sample, three slices at different positions of the elugram were selected. Particle sizes and quality of fit were determined with the different methods at the top of the peak and at the front and the end of the peak at ten percent peak height (Figure 4.29).

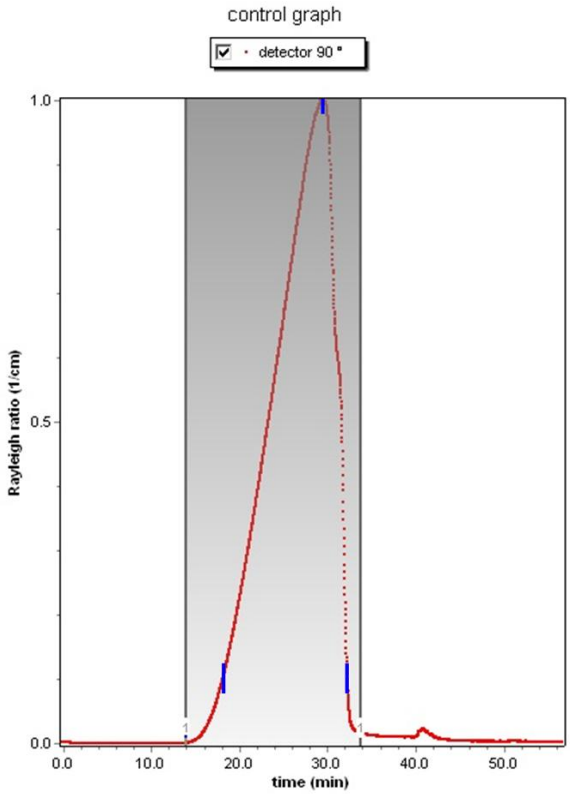

Figure 4.29: *Position of the slices chosen for testing the fit models with SUVs.*

The data for the two smallest angles were removed because they were deviating too strong from the behaviour seen from the other angles. Removing the smallest angles from the fitting procedure resulted in a significantly improved fit error and the fit based on the remaining angles was found sufficient for retrieving meaningful radii.

First, the SUVs were investigated. A typical Debye plot (coated sphere model) for the slice at the top of the peak is represented in Figure 4.30.

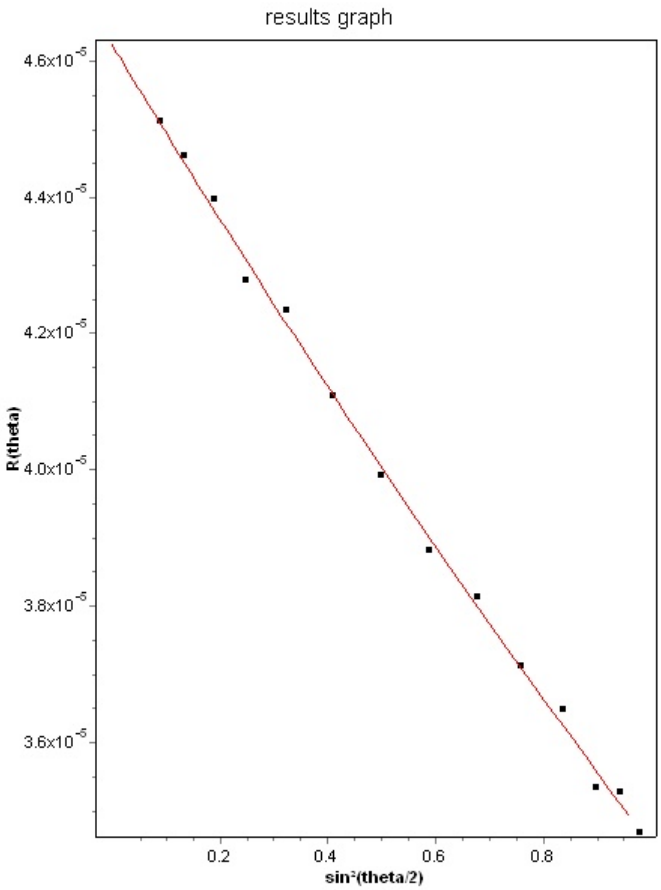

Figure 4.30: *Debye plot at the top of the peak from a fractionation of SUVs, determined with the coated sphere model.*

As it can be seen from the figure, a reasonable fit to the angular data was obtained for the coated sphere model. First, second and third order polynomials were chosen for the Zimm/Debye/Berry fit models. Absolute sizes and quality of fit at the three slices are summarised in Table 4.2, small error indicating good fit. The models with the best fit are highlighted in the table.

Table 4.2: Radii of SUVs for three slices determined by the different fit methods.

Polynomial fit order	Fit method	Radius* [nm]		
		Slice		
		Front	**Top**	**Tail**
First-order fit	Zimm	**19.3 ± 0.9**	43.5 ± 0.5	60.4 ± 0.5
	Debye	**18.5 ± 0.9**	**36.0 ± 0.3**	44.1 ± 0.6
	Berry	**19.1 ± 0.9**	41.3 ± 0.4	**55.2 ± 0.4**
Second order fit	Zimm	18.7 ± 5.1	37.2 ± 2.3	54.0 ± 2.4
	Debye	18.7 ± 4.9	37.8 ± 1.7	51.3 ± 1.7
	Berry	18.7 ± 5.1	37.6 ± 2.1	53.9 ± 2.2
Third order fit	Zimm	24.4 ± 13.8	43.5 ± 6.5	71.6 ± 4.2
	Debye	23.7 ± 13.3	41.6 ± 5.4	62.9 ± 3.0
	Berry	24.2 ± 13.7	43.0 ± 6.2	69.1 ± 3.8
None	Coated sphere	**20.5 ± 0.8**	**40.4 ± 0.3**	**51.0 ± 0.3**

** root mean square radius for Zimm/Debye/Berry; geometric radius for coated sphere*

For all three models the linear fit (first order polynomial) resulted in small errors in the same magnitude as for fitting with the coated sphere model. For particles smaller than 50 nm this is within expectation as it was demonstrated for spheres (Shortt et al., 1996) or random coils (Andersson et al., 2003). Therefore, it was not surprising that the errors became rather big, especially for the smallest liposomes at the first slice when higher polynomials were used, which increased the curvature of the fitting curve. As expected for particles smaller than 50 nm, the Zimm and Debye plot gave better fits whereas for larger particles the Berry approach seemed to work best. For the small particles investigated here, the quality of fit was found good irrespective of whether the three shape independent models (first order polynomial) or the coated sphere models were chosen.

In the next step the four models were applied for all slices within the whole peak and mean geometric radii were calculated. As it can be seen from Table 4.3, the uncertainties of the mean radii determined with the coated sphere model were smaller than for all the other fitting models. Only first order polynomials to the Zimm and Debye fit and second order polynomials to the Debye fit gave relatively small uncertainties. In summary, for such small vesicles the choice of the fit method has only a moderate influence onto the mean radii obtained.

Table 4.3: Geometric radius moments of the SUVs using the different fit methods.

Polynomial fit order	Fit method	Geometric radius moments [nm]*					
		Rn		Rw		Rz	
First-order fit	Zimm	29.4	(3.0 %)	34.8	(1.0 %)	38.6	(1.0 %)
	Debye	27.4	(2.0 %)	30.5	(1.0 %)	32.5	(1.0 %)
	Berry	23.9	(20.0 %)	31.7	(7.0 %)	34.2	(6.0 %)
Second order fit	Zimm	11.6	(148.0 %)	31.3	(9.0 %)	34.0	(7.0 %)
	Debye	28.9	(2.0 %)	33.6	(1.0 %)	36.8	(1.0 %)
	Berry	17.0	(58.0 %)	31.6	(8.0 %)	34.2	(7.0 %)
Third order fit	Zimm	31.6	(29.0 %)	36.1	(22.0 %)	39.0	(19.0 %)
	Debye	31.0	(27.0 %)	35.0	(20.0 %)	37.6	(17.0 %)
	Berry	31.5	(29.0 %)	35.8	(21.0 %)	38.6	(18.0 %)
None	Coated sphere	32.8	(1.0 %)	35.5	(1.0 %)	37.6	(0.9 %)

** The percentage values represent the uncertainties of the mean radii*

In order to see whether the fitting model influences particle sizes determined for larger vesicles to a greater extent, the study was repeated with LUVs. The LUVs were fractionated using a channel flow of 1.00 mL·min^{-1} and a cross flow gradient of 2.00 to 0.15 mL·min^{-1} for 30 minutes. Slices of the elugram were chosen as described before (Figure 4.31).

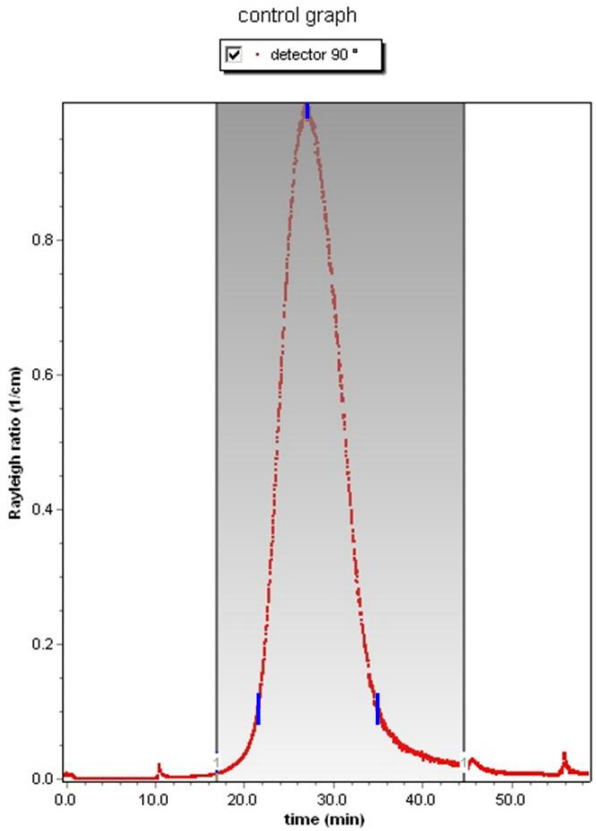

Figure 4.31: *Position of the slices chosen for testing the fit models with LUVs.*

Again, it was found appropriate to exclude the scattering data from the two smallest angles. The Debye plot of the light scattering data for the LUVs showed stronger curvature than for the SUVs (Figure 4.32) due to the increased size of the vesicles.

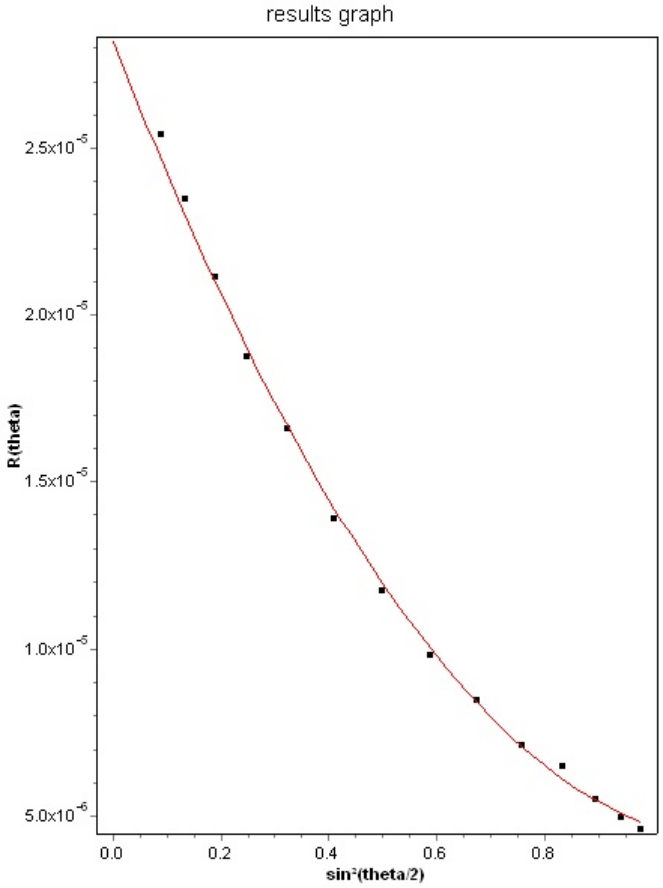

Figure 4.32: *Debye plot at the top of the peak from a fractionation of LUVs, determined with the coated sphere model.*

The radii determined for the different slices are summarised in Table 4.4. In general, much more pronounced differences were seen for the radii calculated for the different methods. In some cases at the tail of the peak the huge error for the Zimm fitting method made determination of radii impossible. The fitting methods with the smallest error are highlighted and it can be seen that three different methods were suggested for fitting the data for the different particle size of the peak.

Table 4.4: Radii of LUVs for three slices determined by the different fit methods.

Polynomial fit order	Fit method	Radius* [nm]		
		Slice		
		Front	Top	Tail
First-order fit	Zimm	84.6 ± 1.1	180.5 ± 6.2	n/a
	Debye	52.0 ± 1.5	65.4 ± 2.1	70.5 ± 8.2
	Berry	**72.8 ± 0.9**	124.0 ± 2.1	214.7 ± 3.9
Second order fit	Zimm	73.6 ± 5.3	57.5 ± 9.9	284.2 ± 28.2
	Debye	67.1 ± 2.5	**84.7 ± 1.6**	109.5 ± 6.4
	Berry	74.0 ± 4.3	86.3 ± 3.4	250.7 ± 10.3
Third order fit	Zimm	49.9 ± 21.7	109.6 ± 10.7	n/a
	Debye	62.4 ± 9.3	94.7 ± 2.5	**137.4 ± 3.8**
	Berry	54.6 ± 17.1	101.4 ± 7.5	150.1 ± 16.6
none	Coated sphere	**62.8 ± 0.8**	**88.6 ± 0.4**	**111.0 ± 3.8**

** root mean square radius for Zimm/Debye/Berry; geometric radius for coated sphere*
n/a = error too large for determination of radii

For the slice at the front of the peak the smallest fit error was achieved for the first order Berry fit method, for the top slice for the second order Debye fit and for the slice at the tail of the peak a third order Debye fit. The only fit method that resulted in good fits for all three slices was the coated sphere model. When the geometric radii moments for the whole peak were determined, it could also be seen that for most of the other fit methods the resulting mean radii were varying excessively and showed very high uncertainties (Table 4.5).

Table 4.5: Geometric radius moments of the LUVs using the different fit methods.

Polynomial fit order	Fit method	Geometric radius moments [nm]*					
		Rn		Rw		Rz	
First-order fit	Zimm	89.5	(7.0 %)	356.7	(5.0 %)	1861.5	(5.0 %)
	Debye	60.1	(7.0 %)	66.1	(5.0 %)	67.1	(5.0 %)
	Berry	19.2	(131.0 %)	147.0	(2.0 %)	174.3	(2.0 %)
Second order fit	Zimm	28.5	(119.0 %)	51.7	(35.0 %)	140.5	(12.0 %)
	Debye	88.2	(3.0 %)	91.5	(3.0 %)	94.6	(3.0 %)
	Berry	93.8	(4.0 %)	114.0	(4.0 %)	156.1	(4.0 %)
Third order fit	Zimm	15.0	(2255.0 %)	94.2	(36.0 %)	108.0	(15.0 %)
	Debye	66.2	(20.0 %)	104.0	(3.0 %)	112.2	(2.0 %)
	Berry	45.5	(113.0 %)	105.7	(11.0 %)	115.1	(10.0 %)
none	Coated sphere.	92.3	(1.0 %)	97.5	(1.0 %)	101.0	(1.0 %)

** The percentage values represent the uncertainties of the mean radii*

For the LUVs studied here, the importance of choosing the best model becomes obvious when looking at the variations in calculated mean particle sizes. In summary, the fitting with the coated sphere model appeared to be most universal for the range of liposomes sizes used in this study. All data presented elsewhere within this thesis were gained using the coated sphere model.

4.2 Comparison of techniques for size characterisation of liposomes

4.2.1 SEC-PCS vs. AF4-MALS

In publication 1 size characterisation of liposomes by PCS, SEC-PCS and AF4-MALS was compared. Liposomes in this study were produced by high pressure homogenisation, a technique that is known to generate very small liposomes. The PCS measurements of the unfractionated sample were performed by Merete Skar according to the method described in (Frantzen et al., 2003). From the valid results for ten parallels, fitting to the autocorrelation function resulted most frequently in bimodal distributions. The intensity weighted distributions are displayed in Figure 4.33. Two discrete peaks were obtained between 40 and 65 nm and between 110 and 200 nm.

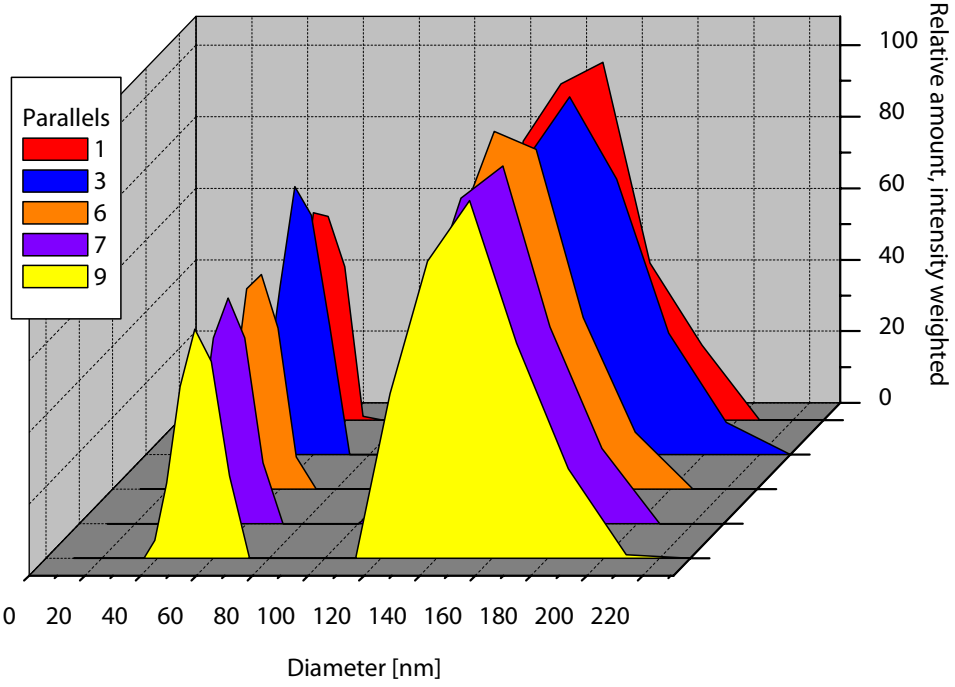

Figure 4.33: *Size distributions of homogenised egg-PC liposomes as obtained by PCS measurements.*

The SEC-PCS study was performed by Christer Bakke Frantzen. The liposomes were fractionated using size exclusion chromatography on a Sephacryl S-1000 column

with subsequent concentration determination and PCS size determination of the fractions as described in (Ingebrigtsen and Brandl, 2002). The resulting distribution is displayed by blue triangles in figure Figure 4.34. The size distribution showed only one peak which was rather steep to the left and had a broad tail towards larger liposome sizes. The peak ranged from 7 to 130 nm.

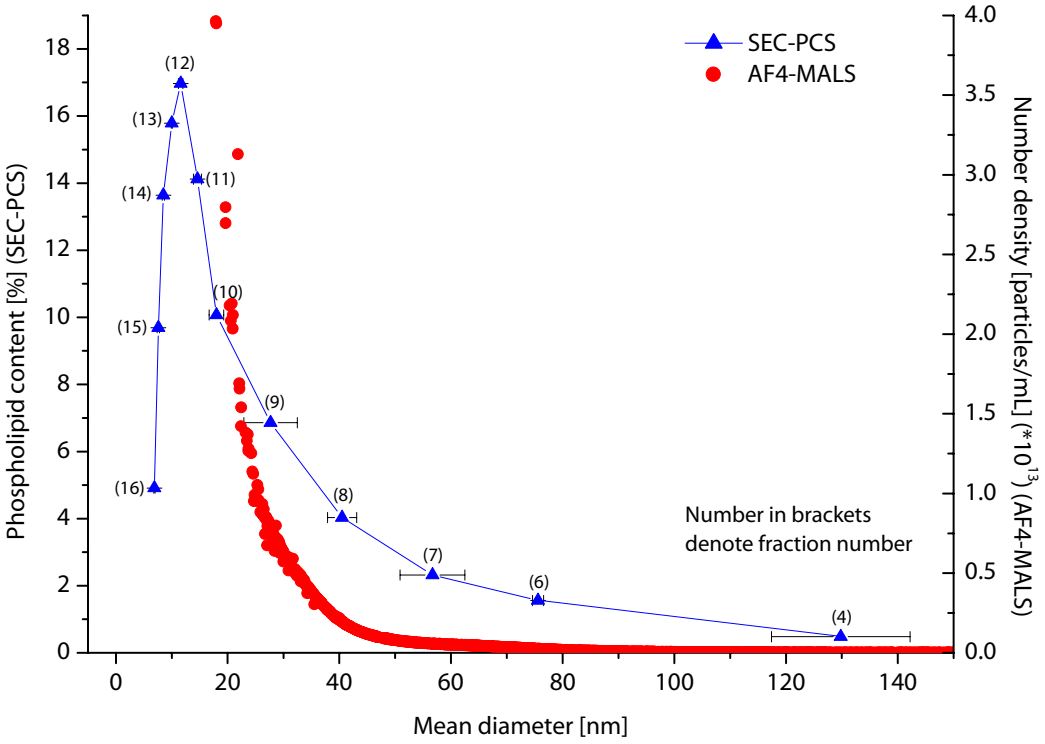

Figure 4.34: *Size distribution of homogenised egg-PC liposomes as obtained by SEC-PCS measurements (blue triangles; n = 3) and AF4-MALS (red circles).*

For the AF4 fractionation of the sample a channel flow of 1.00 mL·min^{-1} was applied along with a cross flow gradient of 0.80 to 0.15 mL·min^{-1} over 30 minutes. A spacer with a thickness of 350 nm was used in this study. Elugrams obtained from the MALS and dRI detectors are displayed in Figure 4.35 along with the geometric radii curve.

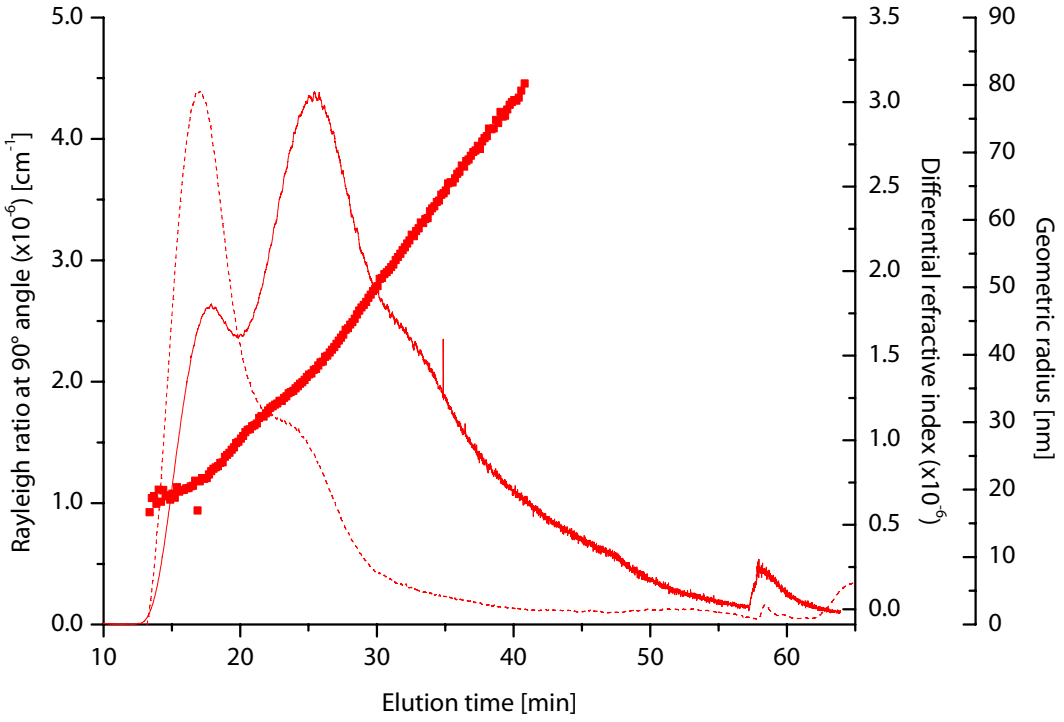

Figure 4.35: *AF4-MALS elugrams from Rayleigh ratio (solid line) and dRI detection (dashed line) along with geometric radii (scattered squares) of homogenized egg-PC liposomes.*

From the dRI trace it can be seen that the majority of the sample eluted at early elution times and showed low light scattering intensity which is also expressed by the small particle sizes in the geometric radii curve. A distribution plot of the number density (particles per mL) against geometric diameter is displayed by red circles in Figure 4.34. A long tail towards particle diameters of around 145 nm was obtained. Towards smaller particle sizes the curve becomes very steep down to diameters of around 20 nm where no more particle sizes are calculated by MALS. With the number density template in Astra the amount of particles at certain sizes can be calculated from the light scattering intensity based on the chosen form factor. For particles sizes that are too small to be calculated by MALS the calculated amount of particle per mL becomes both too high and too imprecise.

Liposome sizes determined by PCS are hydrodynamic diameters, while gyration radii or geometric radii in the case of the coated sphere model are determined by MALS. For vesicles the scattering mass is distributed on a thin shell surrounding the spherical core, and the three different diameters are almost identical (Jin et al., 1999).

Therefore, it is possible to compare the results directly. Both AF4-MALS and SEC-PCS gave a much better insight into the size distribution of the liposomes sample in this study. The bimodal size distribution obtained from the PCS analysis of the unfractionated sample could not be confirmed by any of the fractionation based methods and small particle sizes were clearly underestimated by PCS. Both the fractionation-based methods showed similar trends in particle size distribution with smaller diameters measured by SEC-PCS. This may be explained by the fact that PCS provides resolution of particle sizes down to 3 nm while the smallest measurable particle sizes that can be determined by MALS are in the range of 20–30 nm. It is arguable, however, whether number weighted mean particle diameters of around 7 nm are reliable, assuming the lipid bilayer thickness is around 4 nm. Intensity weighted mean particle sizes will on the other hand overestimate large particles. The results from a single weighting of the PCS cannot represent the real size distribution and a combination of the different weighting should be used. In summary, the AF4-MALS approach has slight advantages being less time consuming, having lower preparative effort and thus shows less sources of error than SEC-PCS. However, AF-MALS has limitations for very small liposomes such as the homogenised liposomes in this study. An additional online-coupling of PCS to the MALS detector might improve the detectability of very small liposomes.

4.2.2 Comparison of AF4-MALS with PCS

PCS is the most common used method for particle size determination of liposomes. It is a fast, non-invasive method that delivers particle size information in the range 3 nm up to 3 µm according to producer's information. However, heterogeneous samples or sample that contains a few larger particles along with a majority of small particles require fractionation prior to PCS measurement, as discussed in chapter 4.2.1. Here, the performance of PCS for liposome samples of narrow size distribution was investigated. Liposomes prepared by filter extrusion through 30 nm filter membranes after five freeze-thaw cycles as well as liposomes prepared by detergent removal were used.

The PCS measurements were performed following the standard protocol described in (Frantzen et al., 2003). For the 30 nm sample the run time was set to 43 minutes in order to achieve a count rate of above one million counts which assures statistical accuracy and the channel width was set to auto-set. The Gaussian distribution model was chosen for all ten parallels. Mean diameters of 71, 68 and 55 nm were calculated, weighted by intensity, volume and number, respectively and the sample had a low polydispersity index of 0.07 (Table 4.6).

Table 4.6: PCS - analysis of 30 nm liposomes with data collection times of 43 minutes.

	Weighted mean diameter [nm]*			
Run-#	**Intensity**	**Volume**	**Number**	**Polydispersity index**
1	71 ± 19	68 ± 18	55 ± 14	0.068
2	71 ± 19	68 ± 18	55 ± 14	0.070
3	72 ± 19	68 ± 18	55 ± 14	0.068
4	71 ± 19	68 ± 18	54 ± 15	0.072
5	71 ± 19	68 ± 18	54 ± 15	0.073
6	71 ± 18	68 ± 17	56 ± 14	0.063
7	71 ± 17	68 ± 17	57 ± 14	0.059
8	71 ± 18	68 ± 18	55 ± 14	0.065
9	71 ± 18	68 ± 18	55 ± 14	0,067
10	71 ± 19	68 ± 18	55 ± 14	0.069
Average mean diameter**	71 ± 0***	68 ± 0	55 ± 1	0.07 ± 0.00

**) the values following ± are the standard deviations of the different weighted mean diameters*
***) average of mean diameters was determined only for runs where Gaussian distribution was chosen (all)*
****) average of the mean diameters and standard deviation of the average of the mean diameters*

Collection times of 16 minutes were necessary for achieving count rates above one million for the 200 nm liposomes, the Gaussian fit method could be used for eight out of ten parallels as highlighted in Table 4.7. The polydispersity index was 0.06 in average.

Table 4.7: PCS - analysis of 200 nm liposomes with data collection times of 16 minutes.

	Weighted mean diameter [nm]*			
Run-#	**Intensity**	**Volume**	**Number**	**Polydispersity index**
1	212 ± 47	200 ± 44	168 ± 37	0.049
2	**211 ± 51**	**197 ± 47**	**159 ± 38**	**0.058**
3	212 ± 51	198 ± 48	160 ± 39	0.058
4	**211 ± 51**	**197 ± 48**	**158 ± 39**	**0.059**
5	**211 ± 55**	**195 ± 51**	**151 ± 39**	**0.068**
6	**210 ± 58**	**191 ± 53**	**142 ± 40**	**0.077**
7	**211 ± 48**	**199 ± 45**	**164 ± 37**	**0.052**
8	**213 ± 43**	**203 ± 41**	**175 ± 36**	**0.042**
9	**211 ± 48**	**199 ± 46**	**164 ± 38**	**0.052**
10	**212 ± 49**	**199 ± 46**	**164 ± 38**	**0.052**
Average mean diameter**	211 ± 1***	197 ± 3	160 ± 9	0.06 ± 0.01

**) the values following ± are the standard deviations of the different weighted mean diameters*
***) average of mean diameters was determined only for runs where Gaussian distribution was chosen (bold)*
****) average of the mean diameters and standard deviation of the average of the mean diameters*

Both samples were fractionated by AF4 and geometric radii were determined by MALS. The fractionation method was a channel flow rate of 1.00 $mL \cdot min^{-1}$ and cross flow gradients of 2.00 to 0.15 $mL \cdot min^{-1}$ for 30 minutes and 1.00 to 0.15 $mL \cdot min^{-1}$ for 30 minutes for the 30 nm and 200 nm liposomes, respectively. The resulting elugrams for the MALS detector and the geometric radii curves are displayed in Figure 4.36 and Figure 4.37. Both samples were almost completely eluted within the given experience time. In Table 4.8 and Table 4.9 the mean geometric diameters (calculated from the radii determined by AF4-MALS) are given.

Table 4.8: Mean geometric diameters derived from AF4-MALS analysis of 30 nm liposomes.

	Mean geometric diameter [nm]*		
Run-#	**z-average**	**Weight-average**	**Number-average**
1	76 (2 %)	71 (2 %)	66 (2 %)
2	75 (2 %)	71 (2 %)	66 (2 %)
3	75 (2 %)	71 (2 %)	65 (2 %)
4	75 (2 %)	71 (2 %)	65 (2 %)
5	75 (2 %)	71 (2 %)	66 (2 %)
6	75 (2 %)	71 (2 %)	66 (2 %)
7	75 (2 %)	71 (2 %)	66 (2 %)
8	75 (2 %)	71 (2 %)	66 (2 %)
9	75 (2 %)	71 (2 %)	66 (2 %)
10	75 (2 %)	71 (2 %)	66 (2 %)
Average mean diameter**	75 ± 0	71 ± 0	66 ± 0

** The percentage values represent the uncertainties of the mean diameters*
***) average of the mean diameters and standard deviation of the average of the mean diameters*

The mean geometric diameters for the 30 nm liposomes were very good reproducible for the whole sequence of fractionations while for the 200 nm liposomes only the elution behaviour showed a very homogeneous behaviour for the three fractionations but the determined diameters were varying. The different mean geometric diameter might be explained by the differences that are seen in the geometric radius curves at the beginning of the peak. The particle sizes determined at those early elution times are differing and might have an impact on the calculated mean diameters.

Table 4.9: Mean geometric diameters derived from AF4-MALS analysis of 200 nm liposomes.

	Mean geometric diameter [nm]*		
Run-#	**z-average**	**Weight-average**	**Number-average**
1	217 (4 %)	207 (2 %)	195 (2 %)
2	206 (4 %)	198 (2 %)	187 (2 %)
3	207 (4 %)	199 (2 %)	189 (2 %)
Average mean diameter**	210 ± 5	201 ± 4	190 ± 3

**) the percentage values represent the uncertainties of mean diameters*
***) average of the mean diameters and standard deviation of the average of the mean diameters*

It can be concluded that for both samples very similar particle sizes were obtained by the two methods. Particle sizes were slightly smaller for the PCS measurements which might be explained by the aforementioned higher sensitivity of dynamic light scattering for very small particles. Both methods were relatively time-consuming when the protocols suggested were used. In summary, for liposomes of very narrow size distribution as seen here, PCS size determination of the unfractionated sample is a good alternative to AF4-MALS. PCS is a good tool for the fast assessment of polydispersity indices and giving a first idea of the particle sizes. However, it has to be stated that the assumption of e.g. a normal distribution of the particle sizes does only represent the size distributions of liposomes in ideal cases and only mean diameters can be determined.

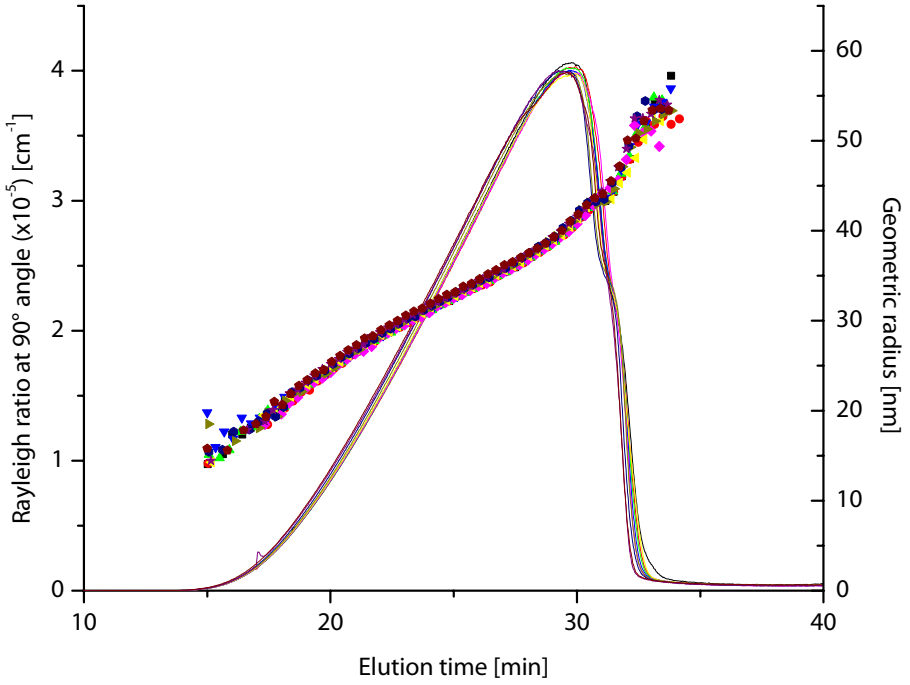

Figure 4.36: *A sequence of AF4-MALS elugrams of 30 nm liposomes. Lines show Rayleigh ratios, scattered symbols the geometric radii.*

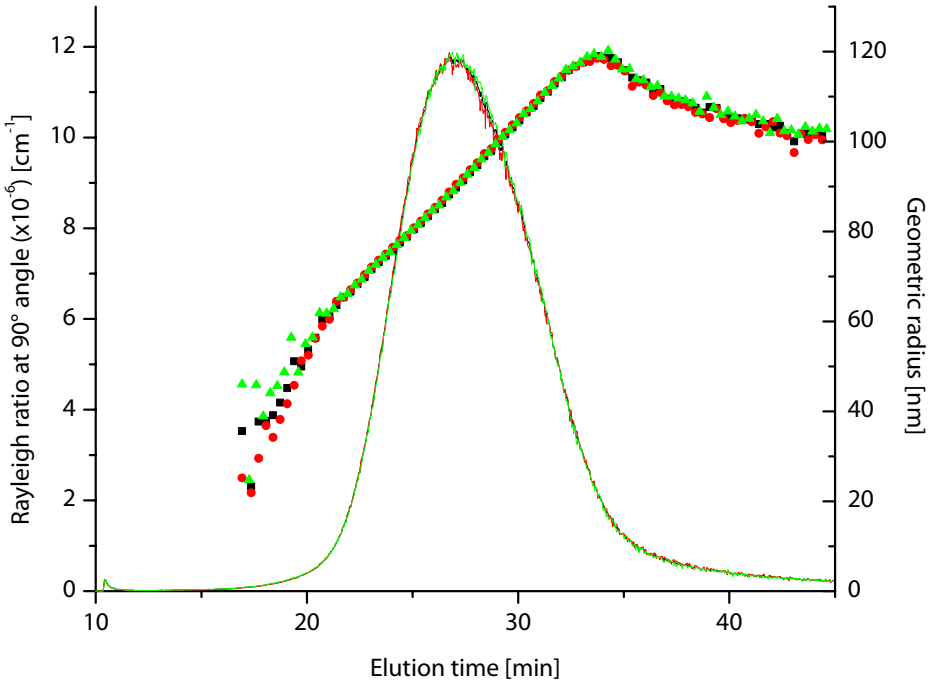

Figure 4.37: *A sequence of AF4-MALS elugrams of 200 nm liposomes. Lines show Rayleigh ratios, scattered symbols the geometric radii.*

4.2.3 Comparison of AF4-MALS with cryo-TEM

In order to compare the liposome size distribution obtained from AF4-MALS with another independent method of size characterisation, egg-PC liposomes prepared by high-pressure homogenisation were visualised using cryo-TEM. Vesicle diameters were measured after magnification of electron micrographs. Sections for counting were randomly selected taking care not to include area where liposomes were arranged according to their size due to limited water layer thickness. In Figure 4.38 a typical section of a cryo-TEM micrograph is displayed.

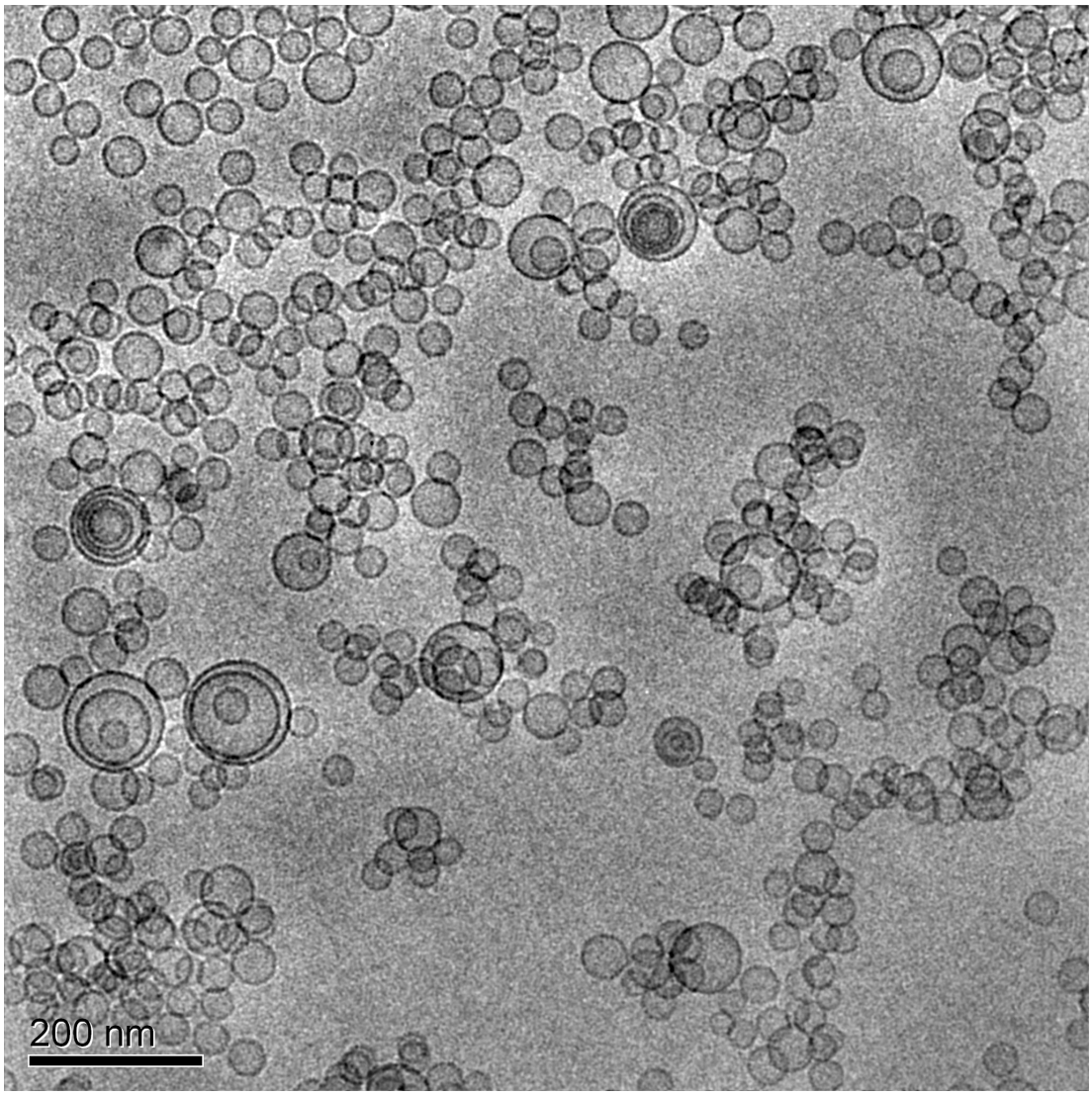

Figure 4.38: *Cryo-TEM micrograph on the homogenized egg-PC liposomes.*

The micrograph shows spherical, mostly unilamellar vesicles apart from very few oligolamellar and multivesicular structures. A number weighted histogram is displayed in Figure 4.39 in comparison to a number density plot of the very same

sample upon AF4 fractionation using a long cross flow gradient of 1.00 to 0.15 mL·min^{-1} over 75 min (Figure 4.40).

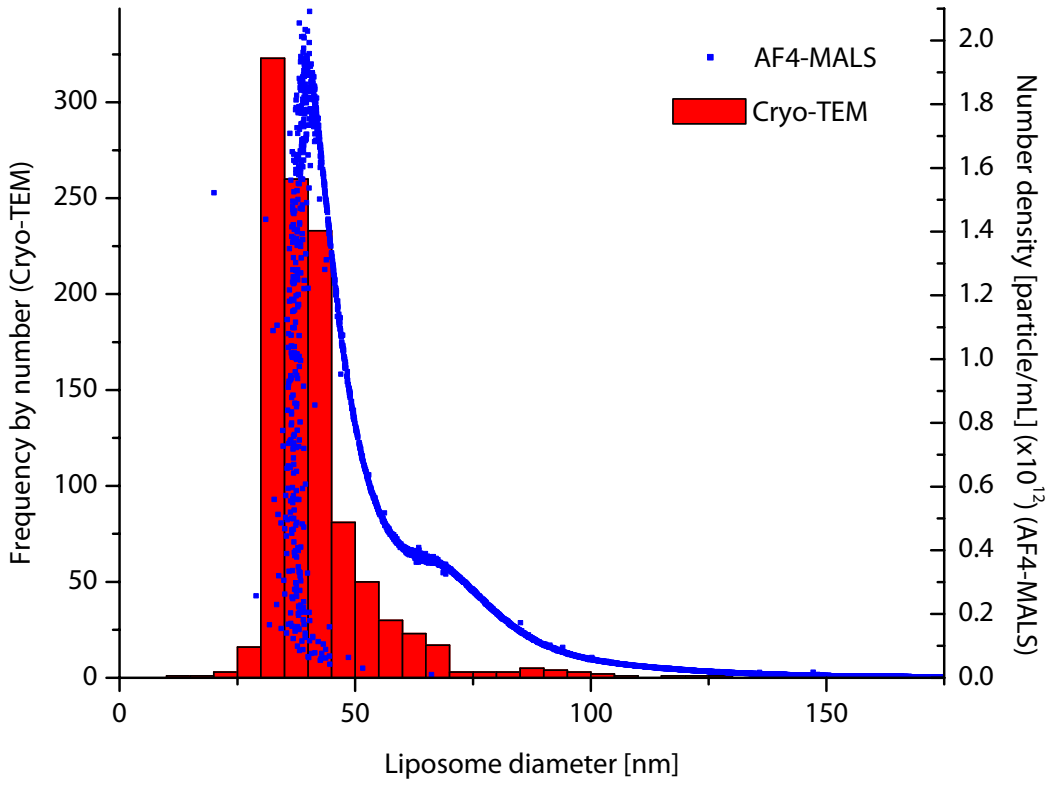

Figure 4.39: *Size distribution per number of the homogenised liposomes determined by cryo-TEM (red bars; n = 1063), and number density size distribution determined by AF4-MALS (blue squares).*

The particle size distribution for the MALS detector was prepared using the number density template. The particle size distributions derived from both techniques are steep to the left and show a pronounced shoulder at the larger particle size end. Liposome sizes measured from cryo-TEM electrographs range from about 25 nm to approximately 100 nm in diameter. The lower limit of particle diameters derived from AF4-MALS was found at 35 nm. This difference may be explained by the aforementioned fact that light scattered from particles smaller than $\lambda/20$ of the wavelength of the light source (λ = 690 nm) used in MALS does not show angular dependency.

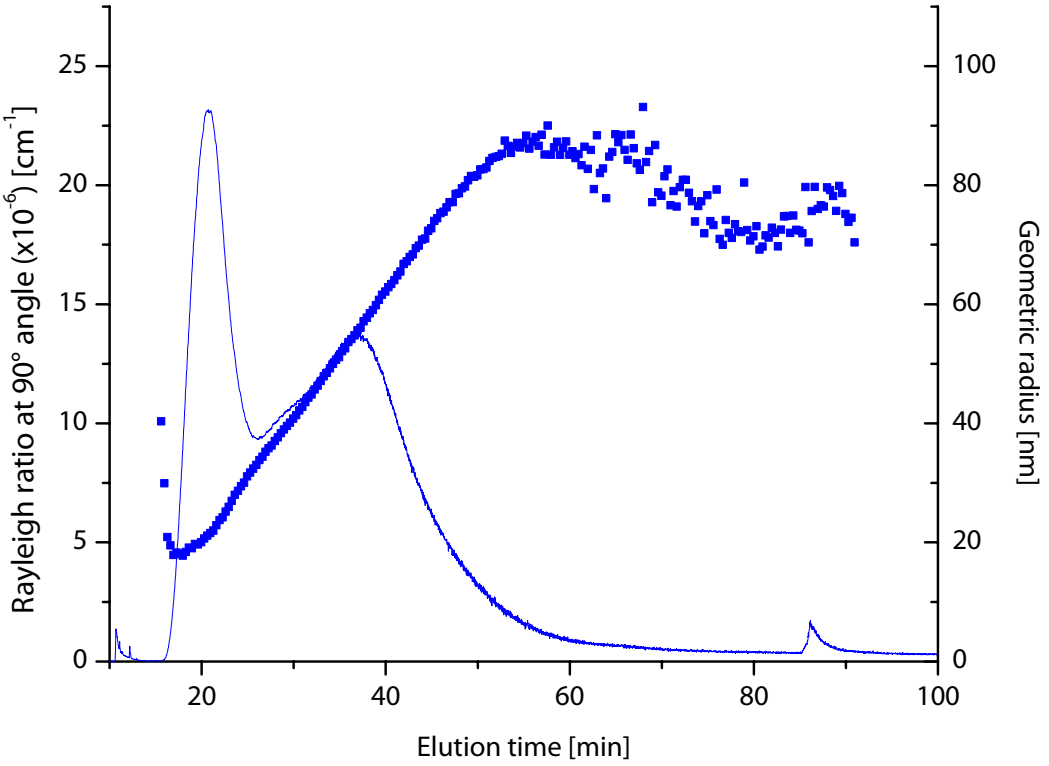

Figure 4.40: *AF4-MALS elugram of homogenized liposomes. Lines show Rayleigh ratios, scattered symbols the geometric radii.*

Obviously, both cryo-TEM and AF4-MALS lead to similar particle size distributions, at least for liposomes larger than 35 nm. The effort for preparing cryo-TEM electrographs and counting a statistically significant number of particles, however, is by far higher than that for AF4-MALS analysis. Measuring of 1000 particles is the smallest possible number in order to identify particles sizes differing by only one order of magnitude in a statistically reliable manner. For comparison, by light scattering techniques amounts of particles in the order of 10^9–10^{12} are analysed. In addition, even though having advantages compared to other EM specimen preparation methods, sample preparation by shock-vitrification still may lead to artefacts such as liposomes arranging according to their size in areas of limited water layer thickness or deformation of the vesicles.

5 CONCLUSION

An experimental setup for particle size characterisation of liposome dispersions has been established based on the combination of AF4 and MALS. The setup appears appropriate to gain a detailed and complete quantitative overview over particle diameters in the range of 30 to 300 nm.
More specifically our experimental data allowed drawing the following conclusions:

- The cross flow is the primary factor governing the performance of AF4 of liposomes. AF4 methods using cross flow gradients were found superior to isocratic methods in terms of resolution of a broad range of particle sizes within reasonable analysis times.

- Ionic strength of the carrier liquid was found to influence retention time via two different mechanisms: firstly, too low ionic strengths of the carrier medium increase repulsive effects between the liposomes themselves and liposomes and accumulation wall leading to pre-mature elution from the channel. Secondly, ionic strengths different from the medium in which the liposomes were formed do readily cause osmotic shrinking and swelling of the liposomes and thus influence the elution behaviour and should be prevented.

- Sample load masses between ten and 100 µg of total lipid were found feasible. Sample load masses of 100 µg, however, may lead to overloading especially for large liposomes of narrow size distribution. Sample load masses of one µg are close to the LOD for UV-VIS turbidity - and differential refractive index detection. The LOD may be lowered for liposomes carrying a membrane standing dye. For such small sample load masses, however, considerate adsorptive losses onto the accumulation wall were observed.

- It was demonstrated that online coupling of AF4 with MALS renders particle size analysis widely independent of erratic retention times. The coated sphere model was found superior compared to Zimm/Debye/Berry fits in terms of fit errors and applicability over the whole range of liposome diameters studied.

- Comparable particle sizes were obtained for AF4-MALS, SEC-PCS and cryo-TEM particle counting. Heterogeneous liposome samples could be fractionated satisfactorily by AF4 with the limitation that MALS does not calculate particle sizes below a diameter of 30 nm.

6 FUTURE PERSPECTIVES

- The experience gained through this thesis may serve as a starting point for a straightforward method development for size characterisation by AF4-MALS of other liposome samples in the future.

- Alternative semi-permeable membranes should be checked for their applicability in AF4 in order to increase the versatility of AF4 and to decrease carry-over and sample loss phenomena.

- A combination of PCS and MALS may decrease the lower size detection limit for liposomes. The simultaneous determination of geometric and hydrodynamic radii of the eluting liposomes might in addition give important information about liposomal shape.

- Size distributions obtained from size characterisation by AF4-MALS should be used for comparison with size-dependent biodistribution behaviour of liposomes used as drug carriers.

7 ACKNOWLEDGEMENTS

This work was carried out at the "Drug Transport and Delivery Group" (former "Section for Pharmaceutics and Biopharmaceutics"), Department of Pharmacy, University of Tromsø from June 2005 to August 2009. During this period I have received great help in various ways that I wish to acknowledge here.

First, I would like to express my gratitude to my supervisor Prof. Dr. Martin Brandl for giving me the opportunity performing this work. Thanks for the help and guidance I received through this project and for introducing me to the world of liposomes. Also thank you, for initiating numerous social events and gatherings together with Annette, which made the stay in Tromsø very much appreciable.

I also wish to thank the University of Tromsø for providing excellent working conditions with laboratory equipment, the Norwegian research council for financing the AF4 instrument and Wyatt Technology for funding my trip to the Particles conference 2008 in Orlando.

For countless discussions about technical and theoretical problems during this work I wish to thank Dr. Michelle Chen, Alge Kaltenborn and Dr. Dierk Roessner from Wyatt Technology. Without their help my patience would have been exhausted a long time ago!

Further, I would like to thank Dr. Markus Drechsler, University of Bayreuth, for taking the cryo-TEM micrographs presented in this work.

I wish to thank Prof. Dr. Regine Süss, University of Freiburg and Dr. Christian Schifter for providing me with the detergent removal liposomes and for the interesting discussions we had during this work.

I would like to thank Dr. Heinrich Haas and Ursula Fattler for their commitment during the collaboration with Medigene AG and for providing liposome samples.

Special thanks go to Tove Larsen, Pharmaceutical Institute, University of Oslo, for helping me with measuring zeta potentials.

Cheers to Rod Wolstenholme for creating beautiful posters and for philosophical discussions about graphical design, font types and sizes as well as about Microsoft.

Thanks to Lars Småbrekke for such diverse advice as writing an article or preparing a trial lecture in Norwegian, showing how to skate on skis and explaining routes on some of the most beautiful mountains around Tromsø.

Further, I would like to express my deep gratitude to Prof. Dr. Purusotam Basnet and Prof. Dr. Richard Engh for proof reading this work and for valuable comments on it.

Especially, I would like to thank the two master students, Helene Helgesen Moen and Dominik Ausbacher. They have not only delivered very nice theses and big contributions to my work, but it was always a pleasure to work and spend time together with them in the lab.

Sincere thanks go to my colleague Wenche S. Schei for her great help with finding my way through the jungle of Norwegian administration when I came to Tromsø and for support during teaching.

Without the help of Merete L. Skar it would not have been possible to perform this work. Having a person like her that you can ask any kind of questions at almost any time, that never has bad mood, and always is there when you need someone to discuss or just talk to is just priceless!

Many heartfelt thanks go to Natasa Skalko-Basnet and Ingunn Tho. Even in the most turbulent times I could always drop in and talk to you, discuss any kind of problems or worries and receive great advice. I am really grateful for this experience and wish you the very best for your future!

I also would like to thank my fellow PhD students and colleagues for creating such a great working environment and I will always remember the familiar atmosphere we had together, the uncounted gatherings in Skarven and at Martin and Annette's place for baking Christmas cookies (and occasional drinking of Schnapps when kindly asked to).

Especially, I would like to thank Johanna Kanzer, Dominik Ausbacher, Rahul V. Haware and Daniel Zeiss for listening, discussing, laughing, playing epic squash battles, skiing, hiking, going out, listening to music or just hanging out together. I hope our friendship will outlast the past four years in Tromsø and I wish you good luck with your future projects and jobs!

A really important role played all my friends at home, who always were backing me up, cheering me up, being there for me, and making me remember where I am coming from.

A big thank you to Hilde's parents, Bente and Finn Gravem, for supporting me in various ways and always making me feel at home at their place in Kolbotn.

There is no way I can thank my family for 31 years of support and love. I am deeply grateful for your support in any possible way, for your eager interest in my work, for taking part in happy moments and for comforting me in sad moments.

At last, I would like to express my deep gratitude to my girlfriend Hilde. Your proof-reading of numerous documents, your patient listening to my complaints, your strong believe in me and your love have given me the strength to finish this work. Tusen takk!!

8 REFERENCES

Abra, R. M. & Hunt, C. A. (1981) Liposome disposition in vivo. III. Dose and vesicle-size effects. *Biochimica et Biophysica Acta, Lipids and Lipid Metabolism,* 666, 493-503.

Allen, T. M. & Stuart, D. D. (1999) Liposome Pharmacokinetics. Classical, Sterically Stabilized, Cationic Liposomes and Immnuoliposomes. In Janoff, A. S. (Ed.) *Liposomes : rational design.* 63-88, New York, Marcel Dekker.

Almgren, M., Edwards, K. & Karlsson, G. (2000) Cryo transmission electron microscopy of liposomes and related structures. *Colloids and Surfaces, A: Physicochemical and Engineering Aspects,* 174, 3-21.

Andersson, M., Wittgren, B. & Wahlund, K.-G. (2003) Accuracy in Multiangle Light Scattering Measurements for Molar Mass and Radius Estimations. Model Calculations and Experiments. *Analytical Chemistry,* 75, 4279-4291.

Arfvidsson, C. & Wahlund, K.-G. (2003) Mass overloading in the flow field-flow fractionation channel studied by the behavior of the ultra-large wheat protein glutenin. *Journal of Chromatography, A,* 1011, 99-109.

Arifin, D. R. & Palmer, A. F. (2003) Determination of size distribution and encapsulation efficiency of liposome-encapsulated hemoglobin blood substitutes using asymmetric flow field-flow fractionation coupled with multi-angle static light scattering. *Biotechnology Progress,* 19, 1798-1811.

Bangham, A. D., De Gier, J. & Greville, G. D. (1967) Osmotic properties and water permeability of phospholipid liquid crystals. *Chemistry and Physics of Lipids,* 1, 225-246.

Bangham, A. D., Standish, M. M. & Watkins, J. C. (1965) Diffusion of univalent ions across the lamellae of swollen phospholipids. *Journal of Molecular Biology,* 13, 238-252.

Benincasa, M. A., Cartoni, G. & Imperia, N. (2002) Effects of ionic strength and electrolyte composition on the aggregation of fractionated humic substances studied by flow field-flow fractionation. *Journal of Separation Science,* 25, 405-415.

Benincasa, M. A. & Giddings, J. C. (1997) Separation and characterization of cationic, anionic, and nonionic water-soluble polymers by flow FFF: sample recovery, overloading, and ionic strength effects. *Journal of Microcolumn Separations,* 9, 479-495.

Berger, N., Sachse, A., Bender, J., Schubert, R. & Brandl, M. (2001) Filter extrusion of liposomes using different devices: comparison of liposome size, encapsulation efficiency, and process characteristics. *International Journal of Pharmaceutics,* 223, 55-68.

Berry, G. C. (1966) Thermodynamic and conformational properties of polystyrene. I. Light-scattering studies on dilute solutions of linear polystyrenes. *Journal of Chemical Physics,* 44, 4550-4564.

Blessing, T., Remy, J.-S. & Behr, J.-P. (1998) Monomolecular collapse of plasmid DNA into stable virus-like particles. *Proceedings of the National Academy of Sciences of the United States of America,* 95, 1427-1431.

Brandl, M., Bachmann, D., Drechsler, M. & Bauer, K. H. (1990) Liposome preparation by a new high pressure homogenizer Gaulin Micron LAB 40. *Drug Development and Industrial Pharmacy,* 16, 2167-2191.

Baalousha, M., Kammer, F. V. D., Motelica-Heino, M., Hilal, H. S. & Le Coustumer, P. (2006) Size fractionation and characterization of natural colloids by flow-field flow fractionation coupled to multi-angle laser light scattering. *Journal of Chromatography, A,* 1104, 272-281.

Chuan, Y. P., Fan, Y. Y., Lua, L. & Middelberg, A. P. J. (2008) Quantitative analysis of virus-like particle size and distribution by field-flow fractionation. *Biotechnology and Bioengineering,* 99, 1425-1433.

Claassen, E. (1992) Post-formation fluorescent labelling of liposomal membranes. In vivo detection, localisation and kinetics. *Journal of immunological methods,* 147, 231-240.
Colfen, H. & Antonietti, M. (2000) Field-flow fractionation techniques for polymer and colloid analysis. *Advances in Polymer Science,* 150, 67-187.
Debye, P. (1947) Molecular-weight determination by light scattering. *Journal of Physical and Colloid Chemistry,* 51, 18-32.
Edwards, K. A. & Baeumner, A. J. (2006) Analysis of liposomes. *Talanta,* 68, 1432-1441.
Egelhaaf, S. U., Wehrli, E., Muller, M., Adrian, M. & Schurtenberger, P. (1996) Determination of the size distribution of lecithin liposomes: A comparative study using freeze fracture, cryoelectron microscopy and dynamic light scattering. *Journal of Microscopy (Oxford),* 184, 214-228.
Frantzen, C. B., Ingebrigtsen, L., Skar, M. & Brandl, M. (2003) Assessing the accuracy of routine photon correlation spectroscopy analysis of heterogeneous size distributions. *AAPS PharmSciTech,* 4, 295-303.
Giddings, C. J. (1966) New separation concept based on a coupling of concentration and flow nonuniformities. *Separation Science and Technology,* 1, 123-125.
Giddings, J. C. (1993) Field-flow fractionation: analysis of macromolecular, colloidal, and particulate materials. *Science,* 260, 1456-1465.
Giddings, J. C. (1997) Factors Influencing Accuracy of Colloidal and Macromolecular Properties Measured by Field-Flow Fractionation. *Analytical Chemistry,* 69, 552-557.
Giddings, J. C., Yang, F. J. & Myers, M. N. (1976) Theoretical and experimental characterization of flow field-flow fractionation. *Analytical Chemistry,* 48, 1126-1132.
Gregoriadis, G. (1978) Liposomes in therapeutic and preventive medicine: the development of the drug-carrier concept. *Annals of the New York Academy of Sciences,* 308, 343-370.
Grohganz, H., Ziroli, V., Massing, U. & Brandl, M. (2003) Quantification of various phosphatidylcholines in liposomes by enzymatic assay. *AAPS PharmSciTech,* 4, Article 63.
Hansen, M. E., Giddings, J. C. & Beckett, R. (1989) Colloid characterization by sedimentation field-flow fractionation. VI. Perturbations due to overloading and electrostatic repulsion. *Journal of Colloid and Interface Science,* 132, 300-312.
Hope, M. J., Bally, M. B., Webb, G. & Cullis, P. R. (1985) Production of large unilamellar vesicles by a rapid extrusion procedure. Characterization of size distribution, trapped volume and ability to maintain a membrane potential. *Biochimica et Biophysica Acta, Biomembranes,* 812, 55-65.
Ingebrigtsen, L. & Brandl, M. (2002) Determination of the size distribution of liposomes by SEC fractionation, and PCS analysis and enzymatic assay of lipid content. *AAPS PharmSciTech,* 3, Article 07.
Jin, A. J., Huster, D., Gawrisch, K. & Nossal, R. (1999) Light scattering characterization of extruded lipid vesicles. *European Biophysics Journal,* 28, 187-199.
Kanno, T., Yamada, T., Iwabuki, H., Tanaka, H., Kuroda, S. I., Tanizawa, K. & Kawai, T. (2002) Size distribution measurement of vesicles by atomic force microscopy. *Analytical Biochemistry,* 309, 196-199.
Korgel, B. A., Van Zanten, J. H. & Monbouquette, H. G. (1998) Vesicle size distributions measured by flow field-flow fractionation coupled with multiangle light scattering. *Biophysical Journal,* 74, 3264-3272.
Kowalkowski, T., Buszewski, B., Cantado, C. & Dondi, F. (2006) Field-flow fractionation: theory, techniques, applications and the challenges. *Critical Reviews in Analytical Chemistry,* 36, 129-135.

Lasic, D. (1993) *Liposomes : from physics to applications,* Amsterdam, Elsevier.
Lee, H., Williams, S. K. R., Wahl, K. L. & Valentine, N. B. (2003a) Analysis of whole bacterial cells by flow field-flow fractionation and matrix-assisted laser desorption/ionization time-of-flight mass spectrometry. *Analytical Chemistry,* 75, 2746-2752.
Lee, S., Nilsson, P.-O., Nilsson, G. S. & Wahlund, K.-G. (2003b) Development of asymmetrical flow field-flow fractionation-multi angle laser light scattering analysis for molecular mass characterization of cationic potato amylopectin. *Journal of Chromatography, A,* 1011, 111-123.
Li, P., Hansen, M. & Giddings, J. C. (1997) Separation of lipoproteins from human plasma by flow field-flow fractionation. *Journal of Liquid Chromatography & Related Technologies,* 20, 2777-2802.
Litzen, A. (1993) Separation speed, retention, and dispersion in asymmetrical flow field-flow fractionation as functions of channel dimensions and flow rates. *Analytical Chemistry,* 65, 461-470.
Litzen, A. & Wahlund, K.-G. (1989) Improved separation speed and efficiency for proteins, nucleic acids and viruses in asymmetrical flow field flow fractionation. *Journal of Chromatography,* 476, 413-421.
Litzen, A. & Wahlund, K.-G. (1991a) Effects of temperature, carrier composition and sample load in asymmetrical flow field-flow fractionation. *Journal of Chromatography,* 548, 393-406.
Litzen, A. & Wahlund, K.-G. (1991b) Zone broadening and dilution in rectangular and trapezoidal asymmetrical flow field-flow fractionation channels. *Analytical Chemistry,* 63, 1001-1007.
Liu, D. & Huang, L. (1992) Size homogeneity of a liposome preparation is crucial for liposome biodistribution in vivo. *Journal of Liposome Research,* 2, 57-66.
Liu, D., Mori, A. & Huang, L. (1992) Role of liposome size and RES blockade in controlling biodistribution and tumor uptake of GM1-containing liposomes. *Biochimica et biophysica acta,* 1104, 95-101.
Makino, K., Yamada, T., Kimura, M., Oka, T., Ohshima, H. & Kondo, T. (1991) Temperature- and ionic strength-induced conformational changes in the lipid head group region of liposomes as suggested by zeta potential data. *Biophysical Chemistry,* 41, 175-183.
Martin, M. (1998) Theory of Field Flow Fractionation. In Grushka, E. & Brown, P. R. (Eds.) *Advances in chromatography: A tribute to J. Calvin Giddings.* 3-138, New York, Marcel Dekker.
Matsumura, Y. & Maeda, H. (1986) A new concept for macromolecular therapeutics in cancer chemotherapy: mechanism of tumoritropic accumulation of proteins and the antitumor agent smancs. *Cancer Research,* 46, 6387-6392.
Mayer, L. D., Tai, L. C. L., Ko, D. S. C., Masin, D., Ginsberg, R. S., Cullis, P. R. & Bally, M. B. (1989) Influence of vesicle size, lipid composition, and drug-to-lipid ratio on the biological activity of liposomal doxorubicin in mice. *Cancer Research,* 49, 5922-5930.
Mayhew, E., Conroy, S., King, J., Lazo, R., Nikolopoulus, G., Siciliano, A. & Vail, W. J. (1987) High-pressure continuous-flow system for drug entrapment in liposomes. *Methods in Enzymology,* 149, 64-77.
Milsmann, M. H. W., Schwendener, R. A. & Weder, H. G. (1978) The preparation of large single bilayer liposomes by a fast and controlled dialysis. *Biochimica et Biophysica Acta, Biomembranes,* 512, 147-155.
Moon, M. H. & Giddings, J. C. (1993) Size distribution of liposomes by flow field-flow fractionation. *Journal of Pharmaceutical and Biomedical Analysis,* 11, 911-920.
Moon, M. H., Park, I. & Kim, Y. (1998) Size characterization of liposomes by flow field-flow fractionation and photon correlation spectroscopy: Effect of ionic strength and pH of carrier solutions. *Journal of Chromatography, A,* 813, 91-100.

Mori, Y., Kimura, K. & Tanigaki, M. (1990) Influence of particle-wall and particle-particle interactions on retention behavior in sedimentation field-flow fractionation. *Analytical Chemistry,* 62, 2668-2672.
Mui, B. B. L., Cullis, P. P. R., Evans, E. E. A. & Madden, T. T. D. (1993) Osmotic properties of large unilamellar vesicles prepared by extrusion. *Biophysical Journal,* 64, 443-453.
New, R. R. C. (1990) *Liposomes : a practical approach,* Oxford, IRL Press.
Nozaki, Y., Lasic, D. D. & Tanford, J. A. (1982) Size analysis of phospholipid vesicle preparations. *Science,* 217, 366-367.
Olson, F., Hunt, C. A., Szoka, F. C., Vail, W. J. & Papahadjopoulos, D. (1979) Preparation of liposomes of defined size distribution by extrusion through polycarbonate membranes. *Biochimica et biophysica acta,* 557, 9-23.
Papahadjopoulos, D. & Watkins, J. C. (1967) Phospholipid model membranes. II. Permeability properties of hydrated liquid crystals. *Biochimica et Biophysica Acta, Biomembranes,* 135, 639-652.
Pecora, R. & Aragon, S. R. (1974) Theory of light scattering from hollow spheres. *Chemistry and Physics of Lipids,* 13, 1-10.
Reviakine, I. & Brisson, A. (2000) Formation of Supported Phospholipid Bilayers from Unilamellar Vesicles Investigated by Atomic Force Microscopy. *Langmuir,* 16, 1806-1815.
Roessner, D. & Kulicke, W.-M. (1994) Online coupling of flow field-flow fractionation and multi-angle laser light scattering. *Journal of Chromatography, A,* 687, 249-258.
Ruysschaert, T., Marque, A., Duteyrat, J.-L., Lesieur, S., Winterhalter, M. & Fournier, D. (2005) Liposome retention in size exclusion chromatography. *BMC Biotechnology,* 5, Article 11.
Schifter, C.-R. (2008) Investigations on the influence of liposomal size on their endocytosis in different cell lines. *Fakultät für Chemie, Pharmazie und Geowissenschaften.* Freiburg i. Br., Albert-Ludwigs-Universität.
Schimpf, M. E., Caldwell, K. & Giddings, J. C. (2000) *Field flow fractionation handbook,* New York, Wiley-Interscience.
Schimpf, M. E. & Wahlund, K.-G. (1997) Asymmetrical flow field-flow fractionation as a method to study the behavior of humic acids in solution. *Journal of Microcolumn Separations,* 9, 535-543.
Schneider, T., Sachse, A., Roessling, G. & Brandl, M. (1995) Generation of contrast-carrying liposomes of defined size with a new continuous high pressure extrusion method. *International Journal of Pharmaceutics,* 117, 1-12.
Setala Niko, L., Holopainen Juha, M., Metso, J., Wiedmer Susanne, K., Yohannes, G., Kinnunen Paavo, K. J., Ehnholm, C. & Jauhiainen, M. (2007) Interfacial and lipid transfer properties of human phospholipid transfer protein: implications for the transfer mechanism of phospholipids. *Biochemistry,* 46, 1312-1319.
Seymour, L. W. (1992) Passive tumor targeting of soluble macromolecules and drug conjugates. *Critical Reviews in Therapeutic Drug Carrier Systems,* 9, 135-187.
Shortt, D. W., Roessner, D. & Wyatt, P. J. (1996) Absolute measurement of diameter distributions of particles using a multiangle light scattering photometer coupled with flow field-flow fractionation. *American Laboratory,* 28, 21-28.
Stauch, O., Schubert, R., Savin, G. & Burchard, W. (2002) Structure of artificial cytoskeleton containing liposomes in aqueous solution studied by static and dynamic light scattering. *Biomacromolecules,* 3, 565-578.
Szoka, F., Jr. & Papahadjopoulos, D. (1978) Procedure for preparation of liposomes with large internal aqueous space and high capture by reverse-phase evaporation. *Proceedings of the National Academy of Sciences of the United States of America,* 75, 4194-4198.

Tardi, C., Drechsler, M., Bauer, K. H. & Brandl, M. (2001) Steam sterilization of vesicular phospholipid gels. *International Journal of Pharmaceutics,* 217, 161-172.
Van Zanten, J. H. (1996) Characterization of vesicles and vesicular dispersions via scattering techniques. In Rosoff, M. (Ed.) *Vesicles.* 239-294, New York, Marcel Dekker.
Van Zanten, J. H. & Monbouquette, H. G. (1991) Characterization of vesicles by classical light scattering. *Journal of Colloid and Interface Science,* 146, 330-336.
Vinson, P. K., Bellare, J. R., Davis, H. T., Miller, W. G. & Scriven, L. E. (1991) Direct imaging of surfactant micelles, vesicles, disks, and ripple phase structures by cryo-transmission electron microscopy. *Journal of Colloid and Interface Science,* 142, 74-91.
Wahlund, K.-G. & Giddings, J. C. (1987) Properties of an asymmetrical flow field-flow fractionation channel having one permeable wall. *Analytical Chemistry,* 59, 1332-1339.
Wahlund, K.-G. & Litzen, A. (1989) Application of an asymmetrical flow field-flow fractionation channel to the separation and characterization of proteins, plasmids, plasmid fragments, polysaccharides and unicellular algae. *Journal of Chromatography,* 461, 73-87.
Wei, Z., Mcevoy, M., Razinkov, V., Polozova, A., Li, E., Casas-Finet, J., Tous, G. I., Balu, P., Pan, A. A., Mehta, H. & Schenerman, M. A. (2007) Biophysical characterization of influenza virus subpopulations using field flow fractionation and multiangle light scattering: Correlation of particle counts, size distribution and infectivity. *Journal of Virological Methods,* 144, 122-132.
Wittemann, A., Drechsler, M., Talmon, Y. & Ballauff, M. (2005) High elongation of polyelectrolyte chains in the osmotic limit of spherical polyelectrolyte brushes: a study by cryogenic transmission electron microscopy. *Journal of the American Chemical Society,* 127, 9688-9689.
Wittgren, B. & Wahlund, K.-G. (1997a) Effects of flow-rates and sample concentration on the molar mass characterization of modified celluloses using asymmetrical flow field-flow fractionation-multi-angle light scattering. *Journal of Chromatography, A,* 791, 135-149.
Wittgren, B. & Wahlund, K.-G. (1997b) Fast molecular mass and size characterization of polysaccharides using asymmetrical flow field-flow fractionation-multiangle light scattering. *Journal of Chromatography, A,* 760, 205-218.
Woodle, M. C. & Papahadjopoulos, D. (1989) Liposome preparation and size characterization. *Methods in Enzymology,* 171, 193-217.
Wyatt, P. J. (1993) Light scattering and the absolute characterization of macromolecules. *Analytica Chimica Acta,* 272, 1-40.
Yohannes, G., Pystynen, K.-H., Riekkola, M.-L. & Wiedmer, S. K. (2006a) Stability of phospholipid vesicles studied by asymmetrical flow field-flow fractionation and capillary electrophoresis. *Analytica Chimica Acta,* 560, 50-56.
Yohannes, G., Sneck, M., Varjo, S. J. O., Jussila, M., Wiedmer, S. K., Kovanen, P. T., Oeoerni, K. & Riekkola, M.-L. (2006b) Miniaturization of asymmetrical flow field-flow fractionation and application to studies on lipoprotein aggregation and fusion. *Analytical Biochemistry,* 354, 255-265.
Yuan, F., Dellian, M., Fukumura, D., Leunig, M., Berk, D. A., Torchilin, V. P. & Jain, R. K. (1995) Vascular permeability in a human tumor xenograft: molecular size dependence and cutoff size. *Cancer Research,* 55, 3752-3756.
Zillies, J. C., Zwiorek, K., Winter, G. & Coester, C. (2007) Method for quantifying the PEGylation of gelatin nanoparticle drug carrier systems using asymmetrical flow field-flow fractionation and refractive index detection. *Analytical Chemistry,* 79, 4574-4580.
Zimm, B. H. (1948) The scattering of light and the radial distribution function of high-polymer solutions. *Journal of Chemical Physics,* 16, 1093-1099.

ISBN 978-82-7589-242-1